Numerical Simulation of Continuous Countercurrent Adsorption Systems

by

A. K. M. Shamsur Rahman

A Thesis Presented to the

FACULTY OF THE COLLEGE OF GRADUATE STUDIES

KING FAHD UNIVERSITY OF PETROLEUM & MINERALS

DHAHRAN, SAUDI ARABIA

In Partial Fulfillment of the
Requirements for the Degree of

MASTER OF SCIENCE

In

CHEMICAL ENGINEERING

June, 1992

INFORMATION TO USERS

This manuscript has been reproduced from the microfilm master. UMI films the text directly from the original or copy submitted. Thus, some thesis and dissertation copies are in typewriter face, while others may be from any type of computer printer.

The quality of this reproduction is dependent upon the quality of the copy submitted. Broken or indistinct print, colored or poor quality illustrations and photographs, print bleedthrough, substandard margins, and improper alignment can adversely affect reproduction.

In the unlikely event that the author did not send UMI a complete manuscript and there are missing pages, these will be noted. Also, if unauthorized copyright material had to be removed, a note will indicate the deletion.

Oversize materials (e.g., maps, drawings, charts) are reproduced by sectioning the original, beginning at the upper left-hand corner and continuing from left to right in equal sections with small overlaps. Each original is also photographed in one exposure and is included in reduced form at the back of the book.

Photographs included in the original manuscript have been reproduced xerographically in this copy. Higher quality 6" x 9" black and white photographic prints are available for any photographs or illustrations appearing in this copy for an additional charge. Contact UMI directly to order.

U·M·I
University Microfilms International
A Bell & Howell Information Company
300 North Zeeb Road, Ann Arbor, MI 48106-1346 USA
313/761-4700 800/521-0600

Numerical simulation of continuous countercurrent adsorption systems

Rahman, A. K. M. Shamsur, M.S.

King Fahd University of Petroleum and Minerals (Saudi Arabia), 1992

U·M·I
300 N. Zeeb Rd.
Ann Arbor, MI 48106

NUMERICAL SIMULATION OF CONTINUOUS COUNTERCURRENT ADSORPTION SYSTEMS

BY

A. K. M. SHAMSUR RAHMAN

A Thesis Presented to the
FACULTY OF THE COLLEGE OF GRADUATE STUDIES
KING FAHD UNIVERSITY OF PETROLEUM & MINERALS
DHAHRAN, SAUDI ARABIA

In Partial Fulfillment of the
Requirements for the Degree of

MASTER OF SCIENCE
In

CHEMICAL ENGINEERING

JUNE 1992

KING FAHD UNIVERSITY OF PETROLEUM & MINERALS
DHAHRAN 31261,SAUDI ARABIA.

COLLEGE OF GRADUATE STUDIES

This thesis, written by **A.K.M. SHAMSUR RAHMAN** under the direction of his Thesis Advisors and approved by his Thesis Committee, has been presented to and accepted by the Dean of the College of Graduate Studies, in partial fulfillment of the requirements for the degree of

MASTER OF SCIENCE IN CHEMICAL ENGINEERING

Thesis Committee

Mirza Manirul Hassan

Dr. Mirza M. Hassan
Chairman

Kevin F. Loughlin

Dr. Kevin F. Loughlin
Member

Shafkat Ali Beg.

Dr. Shafkat A. Beg
Member

Mazen Shalabi

Dr. Mazen A. Shalabi
Chairman
Department of Chemical Engineering

Dr. Ala H. Al-Rabeh
Dean
College of Graduate Studies

Date : 4-7-92

TO MY PARENTS

ACKNOWLEDGEMENTS

I would like to express my extremely profound thanks and praise to **ALLAH**, the Almighty, the most Gracious, the most Merciful and peace be upon His Prophet.

I am greatly indebted to my supervisor Dr. Mirza M. Hassan for his careful guidance, encouragement and help during the course of this work. Appreciation is extended to Dr. Kevin F. Loughlin and to Dr. Shafkat A. Beg for their constant help and encouragement and for valuable suggestions and significant contributions.

I am grateful to the chemical engineering department of King Fahd University of Petroleum & Minerals, for providing me with a challenging atmosphere and continuous support. The cooperation and help from the Data Processing Centre (DPC) at KFUPM are also greatly appreciated.

I would also like to express my profound gratitude to my mother and brothers for all their love and affection, and for enduring the geographical distance from me during my graduate studies. Their sacrifices and foresightedness made this work possible.

Last, but not the least, I would like to thank all of my friends, here at KFUPM and those who are staying at different parts of the world for their moral support in different phases of this investigation.

CONTENTS

APPENDICES

LIST OF FIGURES

LIST OF TABLES

THESIS ABSTRACT

FULL NAME OF STUDENT : **A.K.M. SHAMSUR RAHMAN**

TITLE OF STUDY : **NUMERICAL SIMULATION OF CONTINUOUS COUNTERCURRENT ADSORPTION SYSTEMS**

MAJOR FIELD : **CHEMICAL ENGINEERING**

DATE OF DEGREE : **June 1992.**

Theoretical models for unsteady state continuous countercurrent adsorption systems are developed both for two section and four section (SORBEX) equivalent countercurrent processes having nonlinear equilibria. Further, a detailed model representing the actual system is developed by writing appropriate differential equations for each adsorption column.

An axially dispersed plug flow model with linear driving force rate expression for mass transfer and Langmuir equilibria are considered. For the equivalent models, an equivalent solid phase velocity was assumed and for the detailed model, time dependent boundary conditions for each column are formulated and related to the switching time. Computations are performed for several cycles till the cyclic steady state is obtained.

The results obtained from the equivalent and detailed models for the limiting cases of linear and nonlinear isotherms are compared with available experimental data and are found to agree well. The effect of various process parameters on the *performance of the systems are investigated for all models. There exists a set of optimum values of all the process parameters which can be evaluated from the present simulation.*

King Fahd University of Petroleum & Minerals
Department of Chemical Engineering

MASTER OF SCIENCE

الخلاصة

اسم الطالب : أ . ك . م . شمس الرحمن
عنوان الرسالة : محاكاة رقمية لأنظمة الإمتزاز المستمر .
التخصص : هندسة كيميائية .
التاريخ : يونيو ١٩٩٢م .

في هذا البحث طورت نماذج نظرية لحالة الإتزان غير المستقر في أنظمة الإمتزاز ذات القطاعين والأربعة قطاعات (SORBEX) وغير خطية وذلك بعد كتابة المعادلات التفاضلية الملائمة لتمثيل الأنظمة .

تم إعتبار نموذج الإنسياب المحوري بقوة دافعة خطية تمثل معدل التفاعل وإنتقال المادة وتم إجراء حسابات لكل دورة حتى الوصول لحالة الإتزان المستقر . تمت مقارنة النتائج التي تم الحصول عليها من النموذج المكافئ والنموذج التفصيلي لحالة النهايات لكل من الـ (isotherm) الخطي وغير الخطي مع النتائج المعملية المتوفرة وقد وجد الإتفاق بينهما .

تمت دراسة تأثير عدة عوامل لكل النماذج . وجد أن هنالك قيمة مثلى لكل عامل تمت دراسته في عملية المحاكاة .

درجة ماجستير العلوم
جامعة الملك فهد للبترول والمعادن
قسم الهندسة الكيميائية
الظهران ، المملكة العربية السعودية

CHAPTER 1

INTRODUCTION

1.1 INTRODUCTION

Adsorption is a physical phenomena where molecules of various fluids get attached due to the presence of vanDer Waal's force and/or electrostatic force on to the active surfaces of some solids. Because of the difference in polarity and molecule size between fluid and solid, molecules of gas or liquid, as soon as they come into contact with the solid surface, adhere to it. Because of the above mentioned phenomena and because of its reversibility, particular solids can be utilized to separate gases or liquids from a homogeneous mixture.

1.2 ADSORPTION AS A SEPARATION TECHNIQUE

Perhaps, the most familiar example of such a process is the use of an adsorption column, packed with a suitable hydrophilic adsorbent, as a drier for the removal of traces of moisture from either gas or liquid streams. Similar processes are also in common use on a large scale for the removal of undesirable impurities such as H_2S and mercaptans from natural gas and organic pollutants from water. Such processes are conveniently classified as purification processes since the adsorbable components are present at low concentrations and have little or no economic value, and therefore are not frequently recovered. The economic benefit of the process is derived entirely from the increase in the purity and value of the stream containing the major component.

The application of adsorption as a means of separating mixtures into two or more streams, each enriched in a valuable component which is to be recovered, is a more recent development. Early examples include the arosorb process for recovery of aromatic hydrocarbons which was introduced in the early 1950s and a variety of processes, first introduced in the early 1960s, for the separation of linear paraffins from branched and cyclic isomers. During the 1970s there has been a significant increase in both the range and scale of such processes. The economic incentive has been the escalation of energy prices, which has made the separation of close boiling components by distillation a costly and uneconomic process. For such mixtures it is generally possible to find an adsorbent for which the adsorption separation factor is much greater than the relative volatility, so that a more economic adsorptive separation is in principle possible. However for an adsorption process to be developed on a commercial scale,the availability of a suitable adsorbent in tonnage quantities at economic cost is required. This has stimulated fundamental research in adsorption and led to the development of new adsorbents [6].

1.3 SELECTIVITY

The primary requirement for an economic separation process is an adsorbent with sufficiently high selectivity, capacity and life. The selectivity may depend on a difference in either adsorption kinetics or adsorption equilibrium. The equilibrium separation factor is defined as

$$\alpha_{AB} = \frac{x_A/y_A}{x_B/y_B} \tag{1.1}$$

where x_A and y_A are, respectively, the mole fractions of component A in adsorbed and fluid phases at equilibrium.

The search for a suitable adsorbent is generally the first step in the development of an adsorption process. Since the separation factor generally varies with temperature and often also with composition, the choice of suitable conditions to maximize the separation factor is a major consideration in process design.

Kinetic separations are in general possible only with molecular sieve adsorbents such as zeolites or carbon molecular sieves. The kinetic selectivity is measured by the ratio of the micropore or intracrystalline diffusivities for the components considered. Differences in diffusion rates between molecules of comparable molecular weight become large enough to provide a useful separation only when diffusion is hindered by steric effects. This requires that the diameter of the micropore be comparable with the dimensions of the diffusing molecule. Molecular sieve separations, which depend on the virtually complete exclusion of the larger molecule from the micropores, as in the separation of linear from branched and cyclic hydrocarbons on 5A zeolite, may be regarded as the extreme limit of a kinetic separation in which the rate of adsorption of one component is essentially zero. Because the geometric requirements for a molecular sieve separation are stringent, such separations are less common than separations based on differences in adsorption equilibrium or on moderate differences in intracrystalline diffusivity [6].

1.4 PRACTICAL ADSORBENTS

The requirement for adequate adsorptive capacity restricts the choice of adsorbents for practical separation processes to microporous adsorbents with pore diameters ranging from a few Angstroms to few tens of Angstroms. This includes both the traditional microporous adsorbents such as silica gel, activated alumina, and activated carbon as well as the more recently developed crystalline aluminosilicates or zeolites.

1.4.1 Silica Gel

Silica gel is a partially dehydrated form of polymeric colloidal silicic acid. The chemical composition can be expressed as $SiO_2.nH_2O$. The water content, which is present mainly in the form of chemically bound hydroxyl groups, amounts typically to about 5 wt%.

The presence of hydroxyl groups imparts a degree of polarity to the surface so that molecules such as water, alcohols, phenols, and amines (which can form hydrogen bonds) and unsaturated hydrocarbons (which can from π -complexes) are adsorbed in preference to nonpolar molecules such as saturated hydrocarbons.

1.4.2 Activated Alumina

Activated alumina is a porous high-area form of aluminum oxide, prepared either from bauxite ($Al_2O_3.3H_2O$) or from the monohydrate by dehydration and recrystallization at elevated temperature. The surface is more strongly polar than that of silica gel and has both acidic and basic characteristic, reflecting the amphoteric nature of the sorbent.

1.4.3 Activated Carbon

Activated carbon is normally made by thermal decomposition of carbonacous material followed by activation with steam or carbon dioxide at elevated temperature (700-1100°C). The activation process involves essentially the removal of tarry carbonization products formed during the pyrolysis, thereby opening the pores.

1.4.4 Carbon Molecular Sieves

Activated carbon adsorbents generally show very little selectivity in the adsorption of molecules of different sizes. However, by special activation procedures it is possible to prepare carbon adsorbents with a very narrow distribution of micropore size and which therefore behave as molecular sieves.

1.4.5 Zeolites

Zeolites are porous crystalline aluminosilicates. The zeolite framework consists of an assemblage of SiO_4 and AlO_4 tetrahedra, joined together in various regular arrangements through shared oxygen atoms, to form an open crystal lattice containing pores of molecular dimensions into which guest molecules can penetrate. Since the micropore structure is determined by the crystal lattice, it is precisely uniform with no distribution of pore size. It is this feature which distinguishes the zeolites from the traditional microporous adsorbents.

1.4.6 Ion Exchange Resins

Ion exchange is the reversible interchange of ions between a liquid and solid, in which there are no permanent changes in the structure of the solid. Since the transfer of ions between phases occurs at a solid surface, ion exchange can be considered as a sorption process and has many similarities with adsorption.

Ion exchange materials consist of an organic or inorganic network structure with attached functional groups. Most ion exchange materials used in adsorption are synthetic resins made by the polymerization of organic compounds into a porous three-dimensional structure. Ion exchange resins are called cationic if they exchange positive ions and anionic if they exchange negative ions. Cation exchange resins have acidic functional groups, such as sulfonic, whereas anion exchange resins contain basic functional groups, such as amine. Ion exchange resins act as adsorbents for many chemicals such as phenol, methanol etc.

1.5 THEORY OF ADSORPTION

In the literature the isotherms of physical adsorption are divided into five classes, as shown in Figure 1.1.

The isotherms for true microporous adsorbents, in which the pore size is not very much greater than the molecular diameter of the sorbate molecule, are normally of type I. This result arises in such adsorbents because there is a definite saturation limit corresponding to complete filling of the micropores. If there is any intermolecular attraction effects, an isotherm of type V is observed. In the case of formation of two surface layers either on a plane surface or on the wall of a pore very much wider than the molecular diameter of sorbate, an isotherm of type IV is seen. Isotherms type II and III are generally observed only in adsorbents in which there is a wide range of pore sizes.

Although there are five different classes of isotherms, normally only two types of isotherms, type I and II, are encountered in most practical situations.

1.5.1 Linear Isotherm

This type of relationship is valid only for the dilute system, where the fluid and solid phase concentration follow Henry's law. The equilibrium relationship is given by

$$q^* = Kc \tag{1.2}$$

1.5.2 The Langmuir Isotherm

This is the simplest theoretical model for monolayer adsorption. According to this model, the equilibrium relationship is given by

$$\frac{q^*}{q_s} = \frac{bc}{1+bc} \tag{1.3}$$

1.5.3. Other Nonlinear Adsorption Isotherms - Langmuir-Freundlich

Because of the limited success of the Langmuir model in predicting mixture equilibria, several authors have modified the equations by the introduction of a power law expression of Freundlich :

$$\frac{q^*}{q_s} = \frac{bc^n}{1 + bc^n} \tag{1.4}$$

Besides these, many other isotherm models exist such as, Statistical Model isotherm, BET isotherm etc.

1.6 ADSORPTION SEPARATION PROCESSES

Adsorption, as a separation technique is a popular mode of operation since early 50's. Since then, adsorption processes have been employed to separate a particular gas from a gas mixture, and in the purification of some liquids where distillation and other methods are inapplicable.

Adsorption separation processes depend on the preferential adsorption of a component or a family of similar components from a bulk feed. The selectivity of the adsorbent, which may depend on differences in sorption equilibrium, or, less commonly on a difference in sorption kinetics, is therefore an important factor in determining the viability of any such process.

Adsorption separation processes can be divided into two broad classes: cyclic batch and countercurrent operation. A useful and comprehensive review of adsorption technology has been given by Wankat [9]. The traditional mode of operation of an adsorption separation process (cyclic batch operation) is shown schematically in Figure 1.2(a). As an alternative, an equivalent countercurrent system can be considered, which is shown in Figure 1.2(b). The main advantage of the countercurrent arrangement is that, as in a heat exchanger, countercurrent flow maximizes the average driving force, thus increasing the efficiency of utilizing adsorbent [4]. Countercurrent operation requires circulation of solid, which is obviously more difficult than circulating adsorbing liquid. However, from early 50's researchers have contributed a great deal of work in the field of countercurrent adsorption systems resulting in the development of a wide range of industrially important continuous countercurrent adsorption separation processes.

1.6.1. Continuous Countercurrent Systems

Countercurrent contact maximizes the driving force for mass transfer and therefore provides, in principle, more efficient utilization of the adsorbent capacity than is possible in a simple batch-contacting system. However, for countercurrent contact it is necessary to either circulate the adsorbent, as shown in Figure 1.2(b), or appropriately design a countercurrent process which is complex and reduces operational flexibility. It is evident that for relatively easy separations (high separation factor and adequate mass transfer rates) the balance of advantage will lie with a simple batch system; but for difficult separations in which selectivity is limited or mass transfer is slow, the advantage of a continuous countercurrent system in reducing the required inventory of adsorbent must eventually outweigh the disadvantages of the more complex engineering.

Simulated countercurrent adsorption processes, in which fluid inlet and outlet points are switched at intervals through a fixed adsorbent bed in order to simulate the effect of continuous countercurrent contact, have been developed for a number of industrially important separations including the separation of glucose and fructose (the Sarex process).

1.7. DESCRIPTION OF SIMULATED MOVING BED AND CONTINUOUS COUNTERCURRENT ADSORPTION PROCESSES

1.7.1 Continuous Countercurrent Adsorption

Mass transfer operations are commonly carried out in continuous counter current systems since this mode of contact maximizes the driving force and therefore the efficiency of the process. To achieve continuous countercurrent contact in an adsorption system requires circulation of the solid adsorbent. The circulation of the solid adsorbent can be achieved either by mechanically moving the solid phase countercurrently with respect to the fluid phase or by simulating the countercurrent movement.

It has proved generally more economic to use a simulated countercurrent system in which countercurrent flow is simulated by moving feed and draw off points at fixed time intervals, sequentially through the adsorbent bed in the direction of the fluid flow. Processes based on this principle have been developed for a number of commercially important separations (paraxylene from mixed C_8 aromatics, fructose from an aqueous fructose-glucose mixture, olefins from paraffins etc.)

1.7.2 Simulated Moving Bed Adsorption

Most of the benefit of countercurrent operation can be achieved without the problems associated with moving the solid adsorbent by using a multiple column (or multiple section) fixed-bed system, with an appropriate sequence of column switching designed to simulate a counter flow system. The basic principle is illustrated in Figure 1.3, although obviously many variants are possible. At each switch a fully regenerated column is added at the outlet of the adsorption side which is approaching breakthrough while the fully loaded column at the feed end of the adsorption side is switched to the outlet end of the regeneration train. In this way the adsorbent is seen to be in effect moving counter current to the fluid flow direction in both adsorption and regeneration trains. With sufficiently small elemental beds switched with appropriate frequency, such a system becomes a perfect analog of a countercurrent flow system.

In this process the adsorbent is contained in a number of identical columns connected in series through pneumatically controlled switch valves which allow the introduction of feed or eluent or withdrawal of product between any pair of columns. The cascade is divided into four sections; section I between desorbent inlet and extract withdrawal, section II between extract withdrawal and feed inlet, section III between the feed inlet and raffinate withdrawal points and section IV between raffinate withdrawal and the desorbent recirculation point. The countercurrent flow is simulated by advancing the desorbent, extract, feed, raffinate and recirculation points at specified time intervals by one column in the direction of fluid flow. The system is thus formally equivalent to the true counter current system sketched in Fig. 1.4. Every time the feed location will be advanced by one column, and when the feed location appears again in its initial point, the whole system is considered to have completed one cycle. Depending upon the number of columns we will have different cycle times. It is evident that a steady state simulated moving bed process can be approximated by a continuous countercurrent process.

1.8 SCOPE OF CONTINUOUS COUNTERCURRENT ADSORPTION PROCESSES

The simplest type of adsorptive separation process involves sorption of a single component or a family of similar species from a solvent or carrier which is itself not significantly adsorbed. This requires a highly selective adsorbent so that a clean separation can be achieved in a few theoretical equilibrium stages. Examples of such processes, which include the recovery of small concentration of organic solvents from air, removal of impurities such as moisture and NO_2 from air or organics from waste water, sugar decolorization and some simple ion exchange processes such as water softening, are given in Table 1.1. Brief detail of two representative systems are shown in Figure 1.5.

Such processes differ in the mode of solid transport, the manner of fluid-solid contacting (fixed bed/fluidized bed), the number of stages in the contactor and the nature of the desorption or regeneration step, which may involve either near-isothermal displacement or thermal swing operation in which the desorption section runs at elevated temperature. In the latter case the temperature of the adsorbent is higher in the regeneration section of the bed. The necessary heating and cooling is commonly achieved using a few stages of the sectioned bed as a heat exchanger.

Steam stripping, which is commonly used in solvent recovery systems, may be regarded as a hybrid process since desorption is achieved by both the elevated temperature and the displacing action of the steam. Despite these important differences, the principle of operation of all these processes is in essence as sketched in Figure 1.2(b) [7,8].

1.9 INDUSTRIAL SCALE CONTINUOUS COUNTERCURRENT ADSORPTION FRACTIONATION PROCESSES

Because of some useful and economic features, continuous counter current adsorption processes are now-a-days being used widely as an important industrial separation technique. A summary of some important countercurrent adsorption fractionation processes which have been operated commercially is given in Table 1.2. Except for the hypersorption process, which is no longer in operation, all these processes operate on the simulated moving bed principle using either the cascade arrangement shown in Figure 1.4 or the simplified three section unit shown in Figure 1.6. All these processes operate in the liquid phase although in principle, either liquid or vapor phase operation is possible [1,2,5].

1.9.1 "Sorbex" processes

The Sorbex family of processes which have been developed by UOP for a variety of industrially important separations operate on the same principle as the simulated moving bed system as shown in Figure 1.7. The actual configuration is however somewhat different. This arrangement is shown in Figure 1.8 . Instead of being contained in discrete beds separated by switch valves the adsorbent is contained in a single bed which is divided into a number of sections. Specially designed flow distributors [3] allow fluid to be introduced (or withdrawn) at each section. The flow circuit is completed by a pump which recirculates fluid from the bottom to the top of the column. At any time only four of the connections to the column are utilized. Switching of the flows is accomplished by a single complex rotary valve which, at each switch, advances the desorbent extract, feed and raffinate points by one section in the direction fluid flow and at the same time passes the extract and raffinate streams to the ancillary distillation column.

A summary of other important commercial processes which operate under the same principle as 'SORBEX' system are included in Table 1.2 and brief details of some of these systems are discussed below. The economic advantages of the sorbex type of process is greatest for the separation of similar sorbates, often isomers, where differences in physical properties are too small to permit the economic application of more conventional processes such as distillation.

1.9.2 Parex and Ebex Processes

The xylene isomers (including ethylbenzene) have very similar volatilities making distillation uneconomic, except perhaps for production of o-xylene. The Parex process which produces high purity p-xylene from a mixed feed has been one of the most successful applications of this type of process. The Ebex process for ethylbenzene recovery was developed more recently.

1.9.3 Sarex Process

The Sarex process uses the Sorbex principle with a CaY adsorbent to separate aqueous mixtures of fructose and glucose using water as both solvent and eluent.

1.9.4 Molex Process

In the Molex process the Sorbex system is used to separate linear from branched and cyclic hydrocarbon isomers using a 5A zeolite as the size selective adsorbent.

1.10 SCOPE AND OBJECTIVES OF PRESENT STUDY

1.10.1 Scope of Present Study

From an extensive literature survey, it is evident that though extensive work has been done in the area of continuous countercurrent adsorption, there is scope to contribute to this vast growing field of separation science. It is clear that despite much work, very little has been done so far on unsteady continuous countercurrent operation along with nonlinear equilibrium adsorption.

Complications arise due to the coupling of various process parameters especially the nonlinear equilibrium relationship between the components. And it is very difficult to predict the effect of process parameters from a simplified model of the continuous countercurrent adsorption system. Numerical solution of the countercurrent and detailed model can be satisfactorily handled by the method of orthogonal collocation to get a complete picture of the system for process dynamics as well as the steady state profile of a complicated and generalized system. Also, the effect of various operating parameters on the performance of the system can be studied and the accuracy of the theoretical results obtained from the developed model can be compared with available experimental data.

1.10.2 Objectives of Present study

1.10.2.1 Objectives of Continuous Countercurrent Modeling

1) Development of a theoretical model for unsteady state continuous countercurrent adsorption using a nonlinear equilibrium isotherm.

2) Solution of that model for dispersed plug flow and Danckwert boundary conditions for processes with two and four sections.

3) Evaluation of the effect of various process parameters on the performance of the system.

4) Comparison of the results of the theoretical model with available experimental data.

1.10.2.1 Objectives of Detailed Modeling

1) Development and solution of the detailed model for Simulated Moving Bed (SMB) for various cases.

3) Comparison of numerical solutions for continuous countercurrent and simulated moving bed modelling.

4) Comparison of the results of the theoretical model with that of the published experimental data.

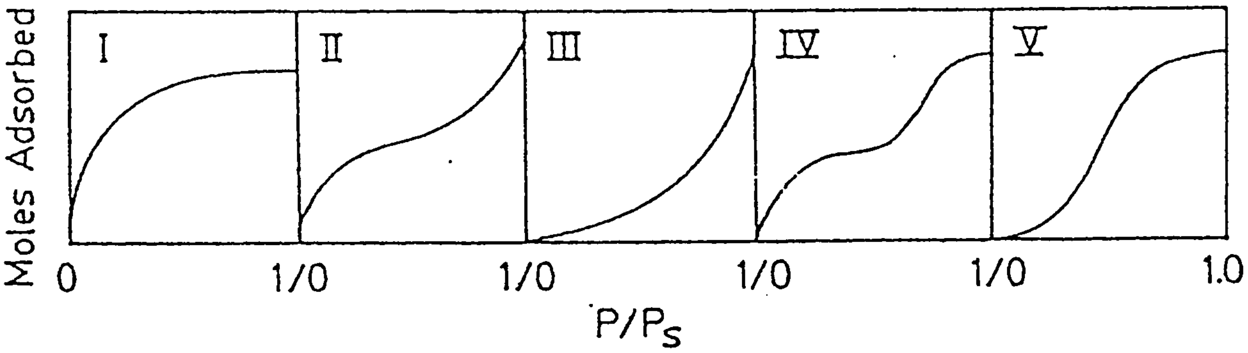

Figure 1.1 The Brunauer classification of isotherms.

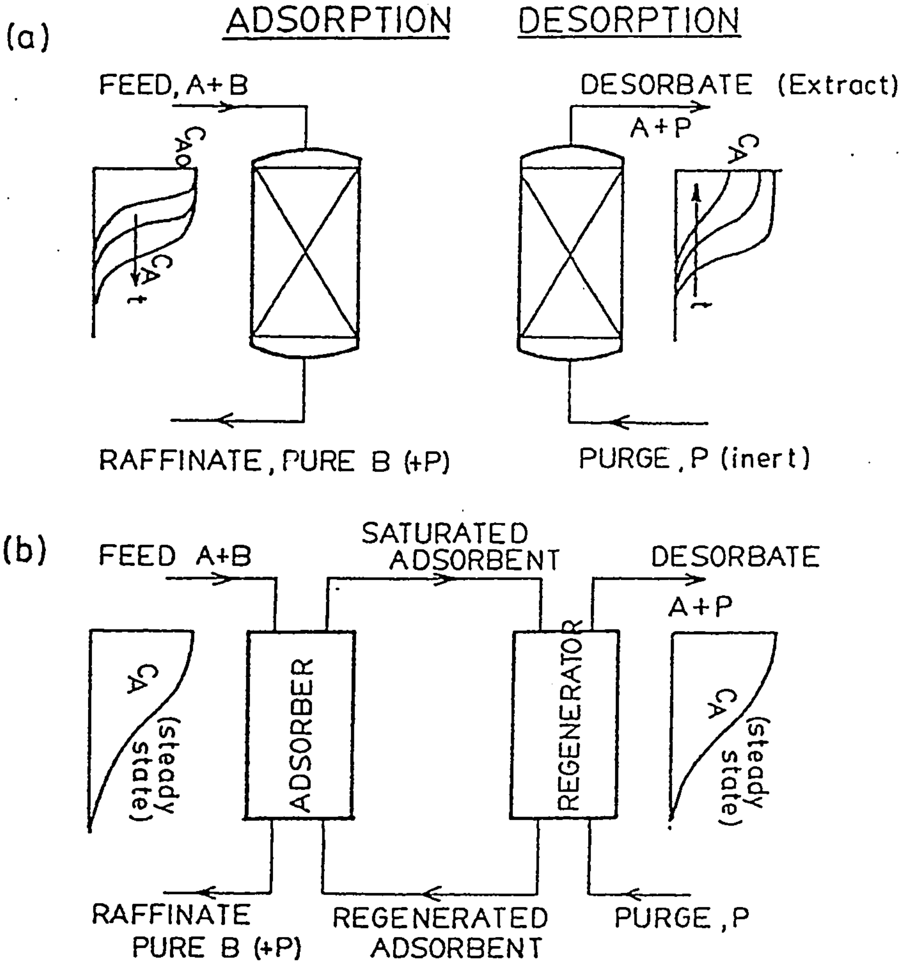

Figure 1.2 Schematic diagram showing two basic mode of operation a) Cyclic batch b) continuous countercurrent.

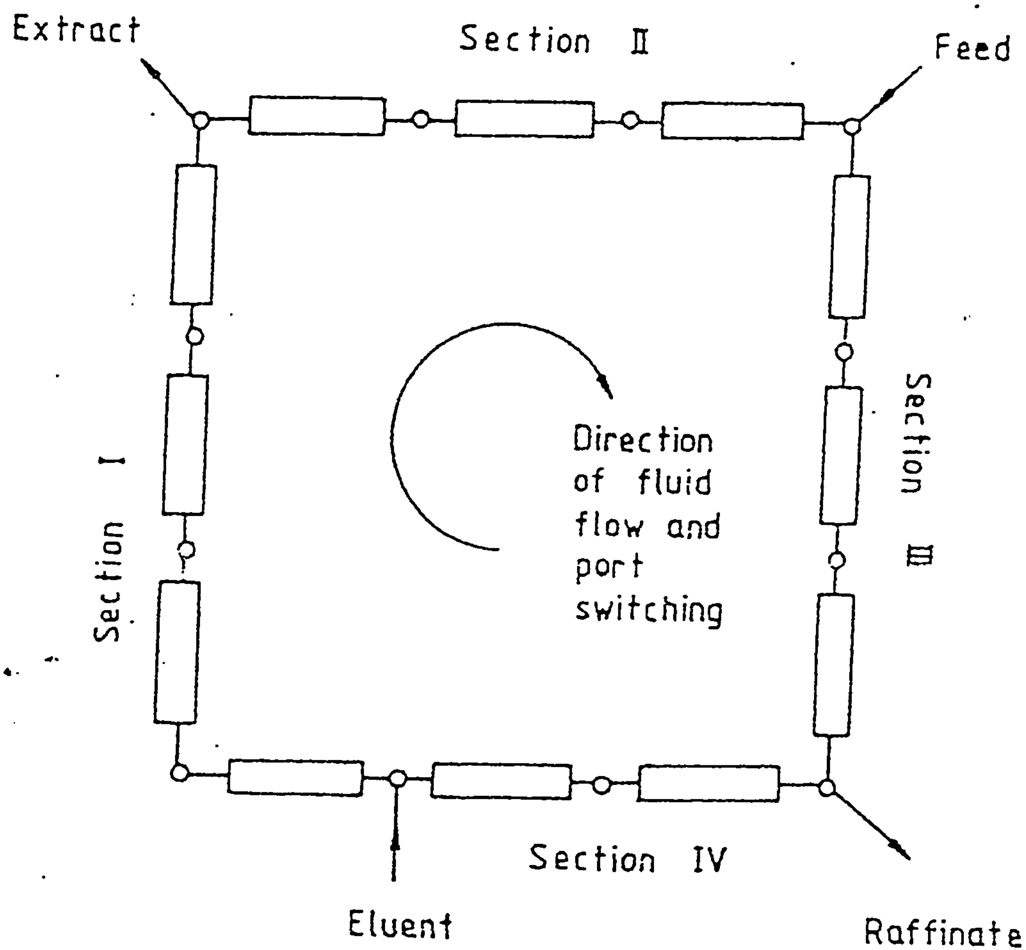

Figure 1.3 Schematic diagram of the physical arrangement of columns and switch valves.

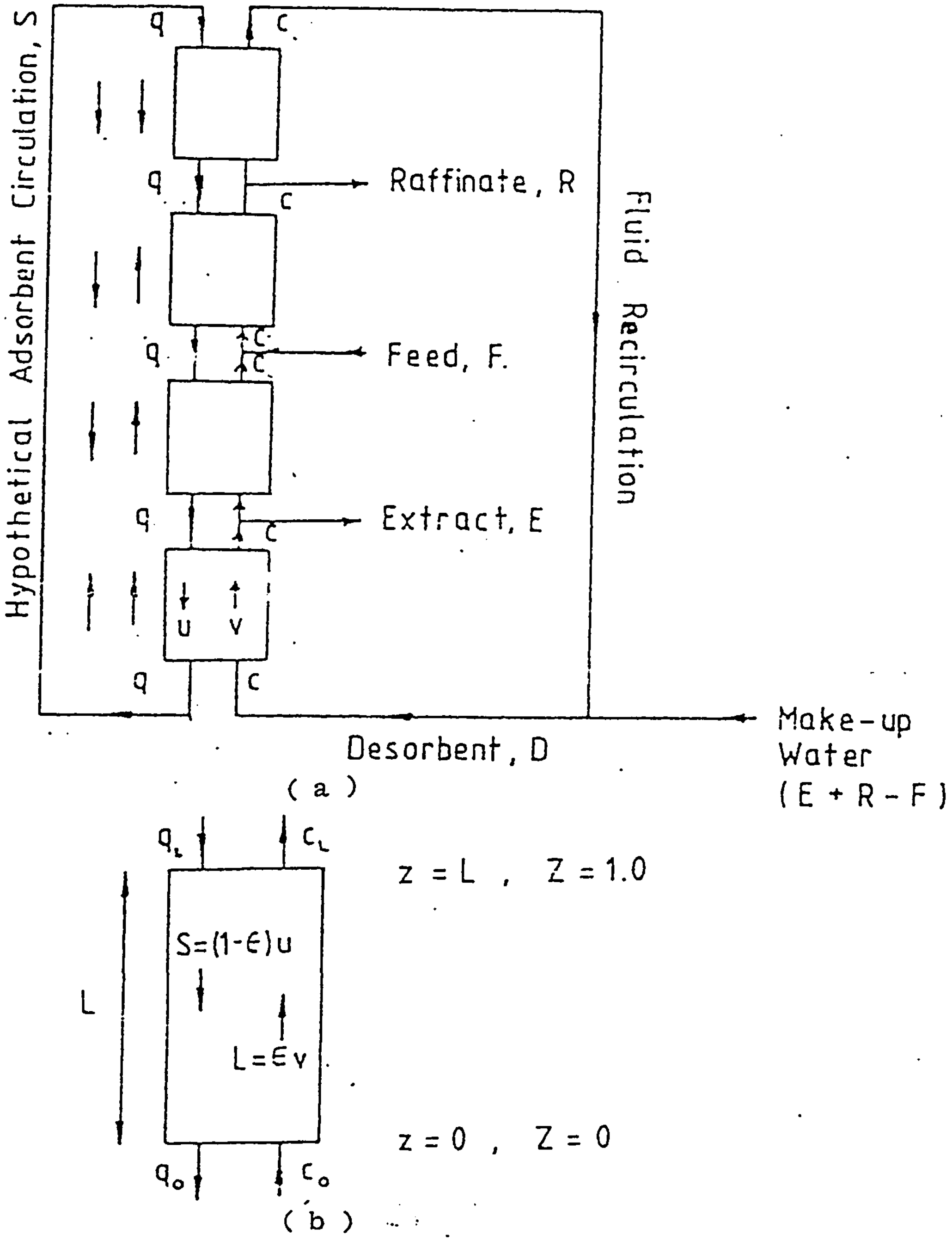

Figure 1.4 Schematic diagram of a) the equivalent countercurrent system b) the notation used in describing the profile within an individual section.

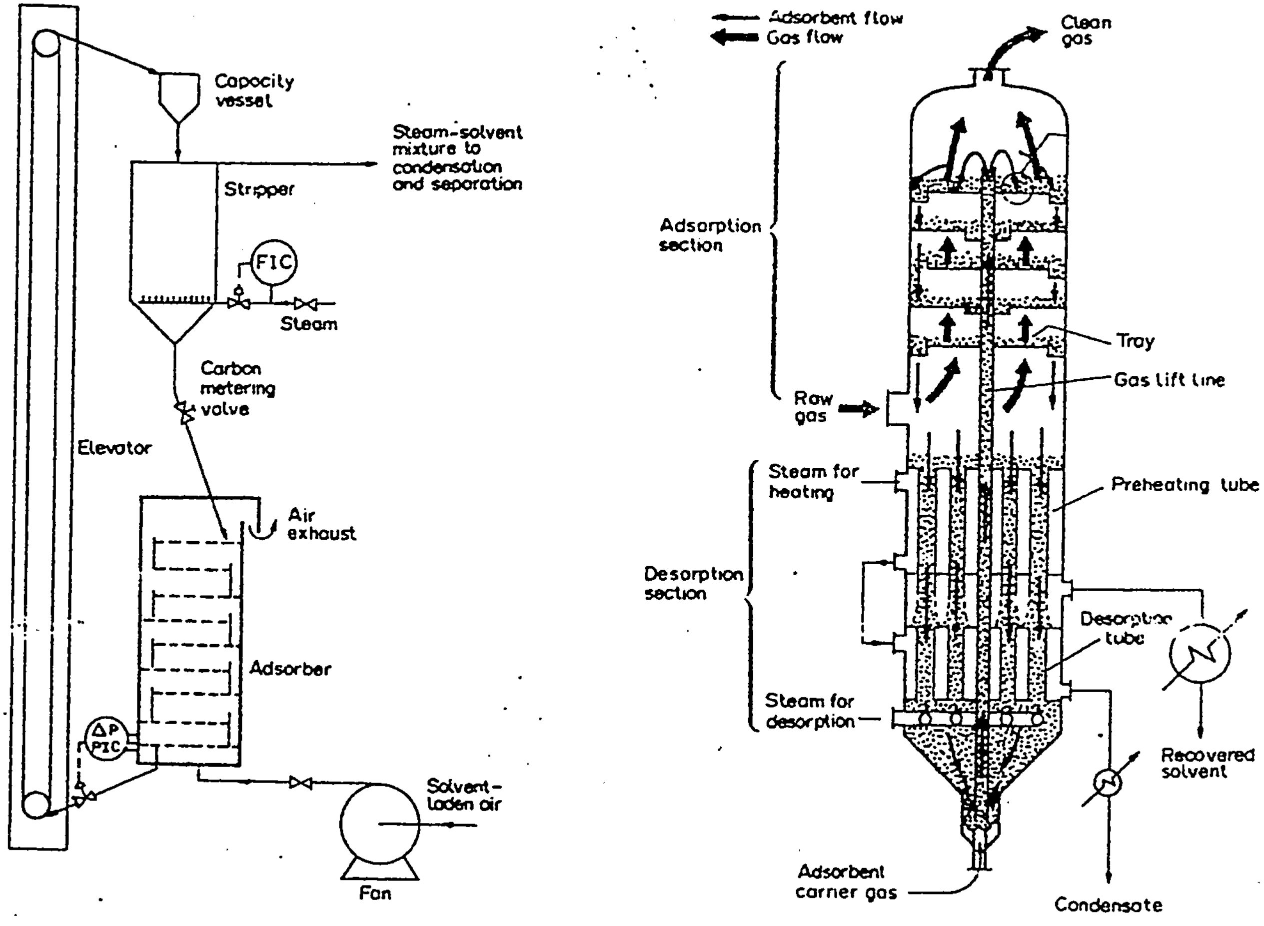

(a)

(b)

Figure 1.5 Schematic diagram of two representative continuous countercurrent adsorption system.

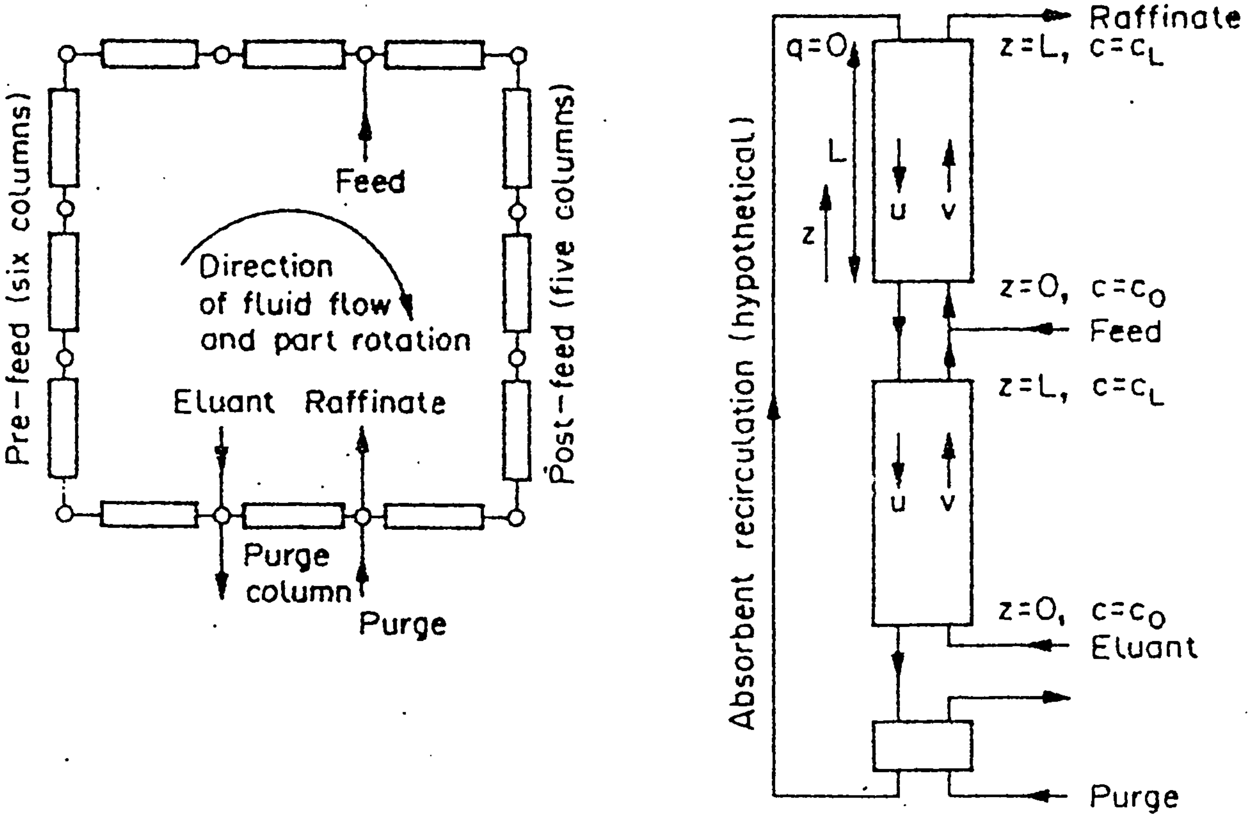

Figure 1.6 Two-section equivalent countercurrent arrangement.

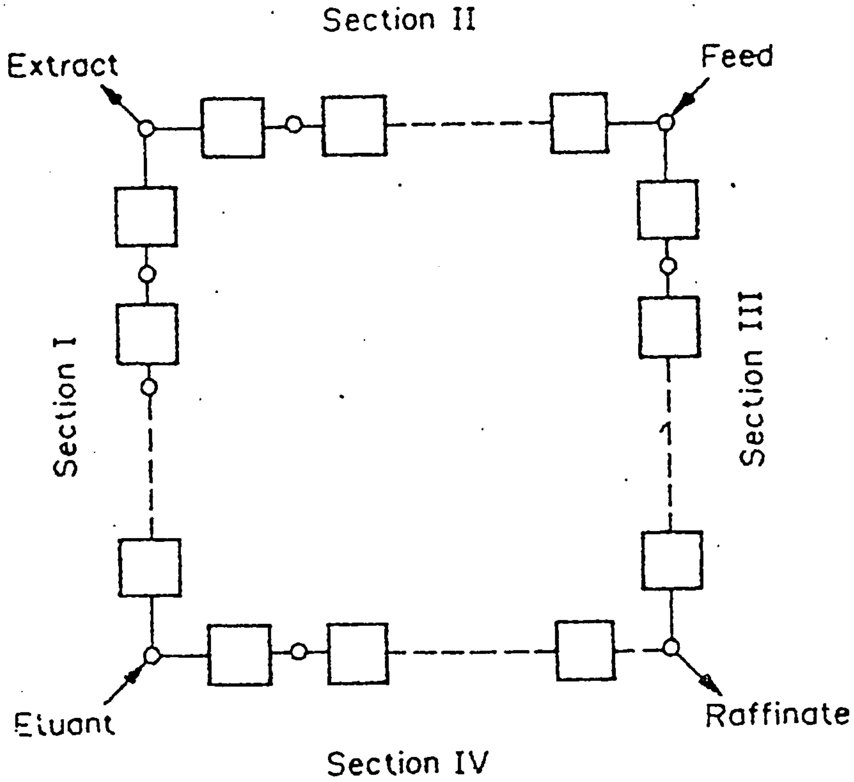

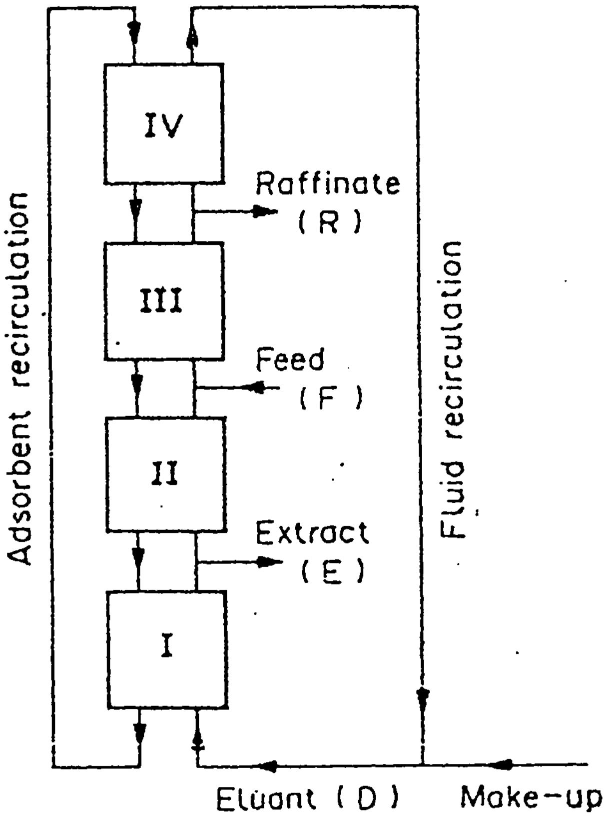

Figure 1.7 Four-section equivalent countercurrent arrangement.

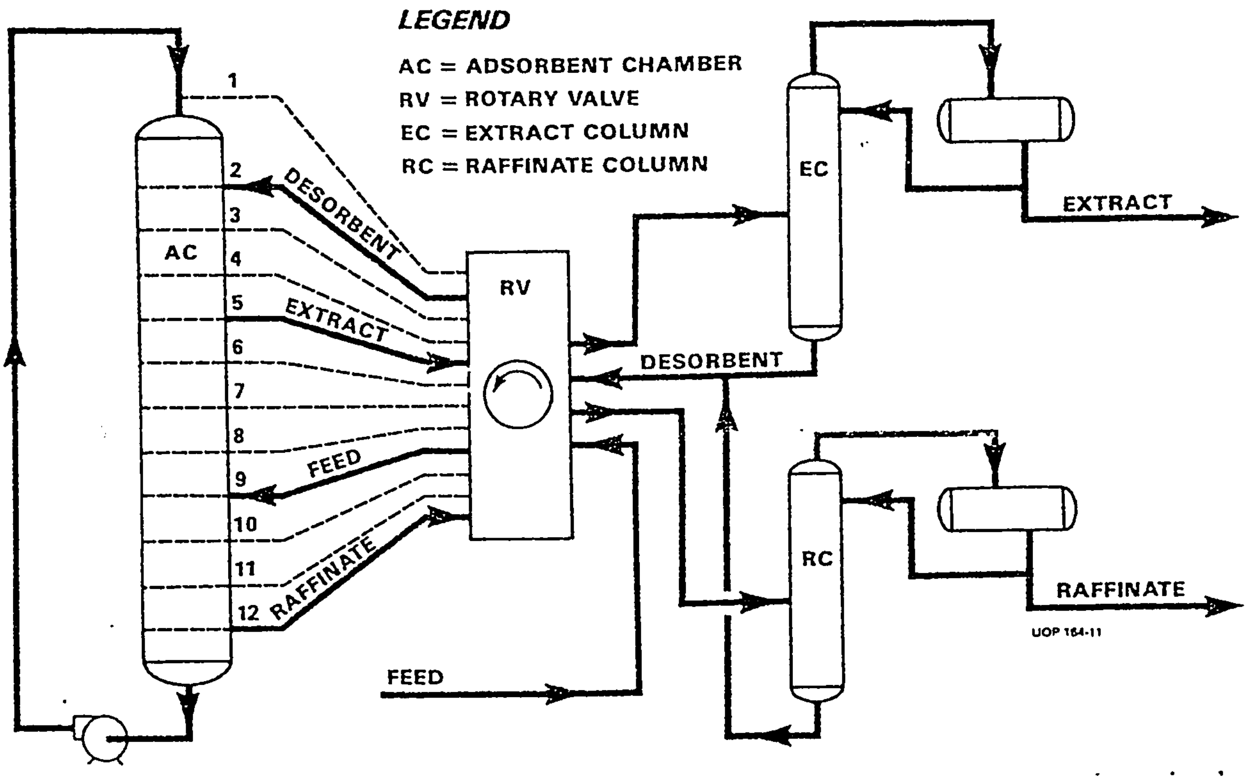

Figure 1.8 Schematic diagram of an industrial scale 'SORβEX' system.

Table 1.1 Simple countercurrent adsorption processes

Process	Gas/ liquid	Adsorbent	Contactor	Regeneration	Adsorbent circulation
Air/gas drying	G	Silica gel	Staged fluidized bed	Thermal	Gas lift
Solvent recovery	G	Activated carbon	Staged fluidized bed	Thermal	Bucket elevator
Solvent recovery (Purasiv)	G	Activated carbon	Staged fluidized bed	Thermal	Gas lift
Wastewater treatment	L	Activated carbon	Fluidized bed or pulsed bed	Thermal	Slurry
Wastewater treatment	L	Activated carbon	"Merry-go-round" SMB	Thermal	Slurry
Ion exchange	L	Ion exchange resins	Pulsed bed	Displacement	Slurry
Ion exchange	L	Ion exchange resins	Staged fluidized bed	Displacement	Slurry
Ion exchange	L	Magnetic resin	Staged fluidized bed(magnetically stabilized	Displacement	Slurry
Ion exchange	L	Ion exchange resins	"Merry-go-round" SMB	Displacement	Slurry

Table 1.2 Countercurrent adsorption fractionation processes

Process	Separation	Adsorbent	Contacting system	Regeneration
Hypersorption	C_2H_4 from refinery gas	Activated carbon	Dense moving bed	Steam stripping
Arosorb	Separation of aromatics and saturates from cracked naphtha	Silica gel	SMB(eight-column)	Displacement (pentane desorbent)
Aromax	p-Xylene from C_8 aromatics	X or Y zeolite	Three section SMB cascade	Heavy aromatic desorbent
Adsep(IWT)	Fructose from fructose-glucose	Ca^+ resin	Eight column four section SMB	Water desorbent
Molex	Linear/branched paraffins	5A zeolite	Sorbex	Light naphtha desorbent
Olex	Olefins from saturated isomers	CaX or SrX	Sorbex	Heavy naphtha
Parex	p-Xylene from C_8 aromatics	Sr-BaY K-BaX	Sorbex	p-Diethyl-benzene Toluene
Ebex	Ethylbenzene from C_8 aromatics	NaY	Sorbex	Tolune
Sarex	Fructose from fructose-glucose	CaY	Sorbex	Water
SCCR4	Fructose from fructose-glucose	Ca^+ resin	Three-section SMB	Water
SCCR5	Clinical dextran	Ca^+ resin	Three-section SMB	Water

REFERENCES

(1) Broughton, D. B., and Berg, R. C., Hydrocarbon Processing, 48(6), 115-120 (1969).

(2) Broughton, D. B., and Gembicki, S. A., Fundamentals of Adsorption, pp. 115-124, Engineering Foundation, New York (1984).

(3) Hesse, M. E., Multiple zone fluid-solid contacting apparatus, European Patent No. 0074815 (1982).

(4) Lerch, R. G., and Ratowsky, D. A., Optimum allocation of adsorbent in stage wise adsorption applications, Ind. Eng. Chem. Fundam. 6, 308-310 and 408 (1967).

(5) de Rosset, A. J., Neuzil, R. W., and Broughton, D. B., Percolation Processes, NATO ASI No. 33, 249-281, Noordhoff, Holland (1981).

(6) Ruthven, D. M., Principles of Adsorption and Adsorption Processes, John Willey, New York (1984).

(7) Ruthven, D. M., and Ching, C. B., Chem. Eng. Sci., 44(5), 1011-1038 (1989).

(8) Tondeur, D., Percolation Processes, NATO ASI No. 33, 517-538, Noordhoff, Holland (1981).

(9) Wankat, P. C., Large Scale Adsorption and Chromatography, CRC Press, Boca Raton, Florida(1986).

CHAPTER 2

LITERATURE REVIEW

2.1 INTRODUCTION

From early 1950's to date researchers have contributed a great deal of work in the field of continuous countercurrent adsorption systems. Various models are available regarding this special adsorption separation process. These models were developed considering different types of physical phenomena that can be encountered in adsorption separations.

Modelling in continuous countercurrent adsorption can be divided into two broad groups; graphical and numerical simulation. In graphical methods, a McCabe-Thiele approach to separating components is adopted. Though this procedure is very simple and quick, the scope of this method is limited. This analysis is possible for very simple systems viz., linear equilibrium isotherm with plug flow model. When systems become complex, a more practical, numerical simulation is the only choice. In numerical simulation, various models are possible depending upon the system complexity.

2.2 McCABE-THIELE ANALYSIS

Design procedures for countercurrent systems are basically similar to the elementary procedures used to design any steady state countercurrent mass transfer operation such as gas absorption. The main difference is that in adsorption systems the equilibrium isotherm is generally curved whereas for many gas absorption systems, at least at low concentration levels, the isotherm is essentially linear. That is why it is possible to represent these adsorption systems using a McCabe-Thiele diagram.

The McCabe-Thiele operating diagram for a simple system with isothermal purge regeneration is shown in Figure 2.1. The equilibrium line is shown as straight line to avoid complexity, though in most real adsorption systems the isotherms are curved except at very low concentrations. The equations of the operating lines can be obtained simply by mass balance;

$$x = x_F + \left(\frac{F}{S}\right)(y - y_F) \qquad \text{(adsorption)}$$

$$x = x_D + \left(\frac{D}{S}\right)(y - y_D) \qquad \text{(desorption)} \qquad (2.1)$$

If both adsorption and desorption sections operate under the same thermodynamic conditions (same pressure and temperature) , the equilibrium lines will be the same. For an operable process the net flow of solute must be up in the desorption section and down in the adsorption section. This requires $D/S > K$, $F/S < K$, implying that the desorbent flowrate must be higher than the feed flowrate. To achieve the required directions of mass transfer the operating lines in the adsorption and desorption sections must lie on opposite sides of the equilibrium line. It follows that $y_D < y_E$, and $y_E < y_F$, i.e. the concentration of the adsorbable species in the purge stream must be lower than in the raffinate product and the concentration in the extract must be lower than that of the feed. Such a process would only be economic in exceptional circumstances, e.g. for removal of an undesirable impurity, without recovery, when a plentiful supply of cheap purge is available.

The McCabe-Thiele analysis of a more commonly used Sorbex system is shown in Figure 2.2. This type of system is used in most commercial adsorptive fractionation processes. An additional component which is competitively adsorbed (the eluent or desorbent) is introduced into the system. The flowrates in each section are adjusted so that, for both components A and B, desorption occurs in sections I and II and adsorption in sections III and IV. The net flow of A (the more strongly adsorbed component) should be downwards in sections II, III and IV and upwards in section I, so that this species moves continuously to the extract point. Similarly the net flow of B should be downwards in section IV and upwards in sections I, II and III, so that it moves towards the raffinate withdrawal point.

Since the system operates isothermally or near isothermally, the equilibrium lines are the same throughout. The operating lines, in the

McCabe-Thiele representation can cross the equilibrium lines only at the feed point and at the eluent recirculation point where there are sudden changes in liquid composition as a result of the introduction of feed or eluent. To achieve a satisfactory separation, the operating diagrams for the two components must lie as sketched in Figure 2.2 so that the extract product contains a high concentration of A and a low concentration of B while the raffinate product contains a high concentration of B and a low concentration of A. The flow constraints referred to above require that the slope of the operating line in section I is greater than that for section II while the slope of the operating line for section III must be greater than for section IV.

The system sketched in Figure 1.6 has also been used but the efficiency of this system is quite low because more desorbent is required and the extract product is recovered in very dilute form.

2.3 MODELLING AND SIMULATION OF COUNTERCURRENT ADSORPTION PROCESSES

The problem of modelling a simulated countercurrent adsorption separation process has attracted a great deal of attention in recent years. The approaches which have been followed may be classified according to whether the system is simulated directly or represented in terms of an equivalent true countercurrent system and whether the bed elements are represented by a continuous flow model (plug flow or axial dispersed plug flow) or as a cascade of mixing cells. The classification of models for simulated moving bed (SMB) countercurrent processes is given in Table 2.1.

Each of these four models may be treated either according to equilibrium theory (I) or by including an appropriate rate expression to account for mass transfer resistance, generally in terms of a linear driving force model (II). The application of these models are given in Table 2.2.

For linear equilibrium systems all four modelling approaches are viable. The simplest representation of the fundamental theory of continuous countercurrent "Sorbex" system was developed from the basic principle of McCabe-Thiele analysis (a.1.I) for plug flow and constant separation factor. The equivalent countercurrent model with linearized mass transfer rate expression (model a.1.II) leads to fairly simple expressions for the steady state concentration profile. The linear driving force model together with the simple McCabe-Thiele analysis of the overall process provides all that is needed to design and optimize the system. The same general approach may be extended to nonlinear binary systems though an analytical solution of the equivalent countercurrent model equation can no longer be obtained. Alternatively one may choose to use the mixing cell model with either the equivalent countercurrent representation (model a.2.I) or with direct simulation of the SMB system (b.2.I). For either linear systems or nonlinear binaries these approaches are computationally straightforward.

For more complex nonlinear systems with coupling between the components (ternary and higher order) a more sophisticated approach is needed. The equivalent countercurrent mixing cell model (a.2.I) may still be used but it is now necessary to solve simultaneously the the mass balance equations for all components for each theoretical stage, in order to allow for the coupling of the equilibrium relationships. A similar computational approach is commonly used in modern multicomponent distillation design codes in order to allow for variation of volatility with composition. Initial estimates of appropriate flowrates and switch times may still be obtained from the McCabe-Thiele approach but this is no longer quite so straightforward since a trial and error solution using the full numerical simulation is needed in order to establish the appropriate equilibrium curves (which depend on the concentrations of all components in the system). Alternatively, initial estimates of the appropriate flow parameters may be derived from the equivalent countercurrent model using equilibrium theory, followed by detailed numerical simulation according to any of the models a.1, a.2, b.1 or b.2. This approach, which is particularly useful when the multicomponent equilibria can be represented in terms of the constant separation factor (multicomponent Langmuir) model, has been developed by Storti et al. [37] and applied to the optimization of a multicomponent "Sorbex" separation system.

2.4 SUMMARY OF PREVIOUS WORK

Some of the earliest work is due to Amundson and Kasten [1]. They developed the analytical solution for single-component adsorption and for a linear isotherm with film resistance.

The continuous countercurrent arrangement has long been used in industry as a series of discrete bed stages, and the use of a single pulsed bed has also been described (Perry and Chilton [31]; Winkler and Kaempf, [42]). In these applications, a spent section of carbon is removed from the end where the fluid enters and replaced by fresh carbon at the other end. For the pulsed bed, typical discharges at each replacement of carbon are 5 to 10% of the carbon, while serial beds each commonly contain 25 to 50% of the total amount of carbon (i.e. two to four beds). The limit of an infinite number of infinitesimal pulses or, equivalently, an infinite number of infinitesimal beds in series is the continuous countercurrent mode.

Analytical solutions of continuous countercurrent adsorption are available for single component and for linear equilibrium relationship with film plus pore resistance (Neretnieks [27]) and for an irreversible isotherm with film plus pore resistance (Neretnieks [28]). Neretnieks [29] also compares the performance of the continuous countercurrent operation with single-column periodic operation for linear and irreversible isotherms with film plus pore resistance.

Fornwalt and Hutchins [16] and Erskine and Schuliger [15] suggest a simplified graphical procedure to assess the effectiveness of multiple beds;

Chen et al. [4] used a tanks-in series model with linear mass transfer driving force.

Asymptotic solutions to moving-bed exchange equations are discussed by Rhee and Amundson [32] considering the effect of axial dispersion and interphase mass transfer. They derived the existence conditions by using perturbation theory in a properly defined moving coordinate system. They illustrated the application of their solution by using Langmuir isotherm.

Although there may be serious difficulties in implementing the continuous countercurrent adsorber (Westermark [41]), it nevertheless provides a convenient theoretical upper limit to the attainable separation.

There are very few reports in the literature of the theoretical examination of the serial bed arrangement. Svedberg [39] compares it numerically with continuous countercurrent operation for linear isotherms with film plus pore diffusion. His formulation also includes axial dispersion, but results are presented only for cases for which the latter is negligible. The ideal performance is quite closely approached with only one or a few divisions of the bed.

Liapis and Rippin [24] simulated binary adsorption in continuous countercurrent operation and also compared with other operation modes. Simulation studies were presented of three different modes of operating a two-component adsorption system. The efficiency with which an activated carbon adsorbent is utilized was compared for a single fixed bed, a periodic countercurrent system in which the adsorbent was equally distributed over two, four and six beds and a continuous countercurrent system.

The mathematical model of continuous countercurrent adsorbers was derived by Ruthven [33,34]. The model was developed for steady state and axially dispersed plug flow system. The linear relation for equilibrium isotherm was considered. By solving the dimensionless model analytically, a theoretical expression was derived for the Height Equivalent of a Theoretical Plate (HETP). That expression was compared with the expression found from chromatographic system. The ratio of these quantities was found to be 0.5 under practical operating conditions but the precise relationship was found to be a function of Peclet and Stanton numbers as well as of the countercurrent flow ratio.

Nemeth et al. [26] developed mathematical models of steady state countercurrent vapour adsorption and compared them for various assumptions of the shape of the isotherm. They studied both linear and non-linear isotherms for a dispersed plug flow model. They solved their model by the integral equation technique.

Ortlieb et al.[30] calculated the separation efficiency for systems having a Langmuir isotherm in countercurrent adsorption using a dynamic model and taking into account internal diffusion resistance.

Ching and Ruthven [11] have presented a theoretical and experimental study for the separation of glucose-fructose mixture at steady state. They assumed isothermal conditions, linear equilibrium and the dispersed plug flow model for their work. The dispersion coefficient was calculated from a pulse chromatographic measurement. An equilibrium stage model and McCabe-Thiele diagram has also been drawn to describe the behavior. They reported that the overall countercurrent HETP was of order 8-12 cm so that each column was equivalent to 10 theoretical stages.

The theoretical and experimental study of the transient response of the separation of glucose-fructose mixture by continuous countercurrent adsorption was produced by Ching and Ruthven [12]. They developed their theoretical model considering linear isotherm and dispersed plug flow. From experiment it was found that 27 hour of operation were required to approach steady state for the fructose profile and 12 hours for the glucose profile.

Ching and Ruthven [10] have reported a theoretical and experimental study of the "Sorbex" operation for the linear isotherm and dispersed plug flow model. They reported that under properly selected conditions product purities and recoveries of 85-95% could obtained.

Ching and Ruthven [13] published a theoretical and experimental study of a simulated countercurrent adsorption system for non-isothermal operation. They used a glucose-fructose mixture as their system. They reported their results for a steady state dispersed plug flow model, using a linear equilibrium relation. By comparing the results from previous work which was done under isothermal condition, the authors reported that the separation performance was significantly better.

The transient and steady state numerical and experimental study of a semi-continuous countercurrent adsorption unit for fructose glucose separation was done by Hidajat et al. [19]. They adopted the linear isotherm and axial dispersed plug flow model for their study. For HETP, a chromatographic method was used. Under the experimental conditions 60 hours of operation was required for fructose and about 37 hours for glucose to reach steady state. The theoretical predictions were in good agreement with the experimental results under the limiting operating conditions.

The theoretical analysis of the effect of subdivision of the adsorbent bed was studied by Hidajat et al. [20]. The unsteady state model and the linear equilibrium relation was chosen to develop the relationship. The authors suggested that subdivision of each section into more than two subsections will be economically justified only if product purity requirements are stringent.

Ching et al. [8] developed an improved adsorption process for the production of high fructose syrup. The experiment was carried out at steady state for a linear isotherm. It was shown that by applying a temperature profile to the system, the concentration of the extract product in a counter-current adsorption separation process might be increased relative to the maximum concentration attainable under isothermal conditions. To achieve the required temperature profile in a simulated countercurrent system it was necessary to heat and cool the columns in sequence as the feed and product draw-off points were switched through the bed. By maintaining a temperature difference of 30-35° C across the bed, an extract product containing 28% fructose and about 1% glucose was obtained, at steady state, from a feed containing 25 wt% of each sugar.

A study of a simulated countercurrent adsorption system for nonlinear equilibrium relationship was carried out by Ching et al. [7]. They used monoethanolamine(MEA) and methanol mixture for their system. It was found that the non-linearity of the MEA isotherm imposed significant constraints on the allowable operating conditions.

A thorough review of countercurrent and simulated countercurrent adsorption separation processes was done by Ruthven and Ching [35]. The authors have reviewed the various aspects of the SCC processes emphasising industrial-scale operation and mathematical modeling.

A simple model, based on equilibrium theory, for simulating countercurrent adsorption separation processes involving multicomponent and nonlinear equilibria was developed by Storti et al. [36]. The reliability of the model was tested by comparison with a detailed model in the context of the separation of the aromatic isomers of C_8 by adsorption on zeolites. Based on that model, a simple and accurate procedure was developed for designing optimal separation units, where adsorbent and desorbent requirements were minimized while enrichment of both the extract and the raffinate were maximized.

A theoretical model of a simulated countercurrent adsorption system for non-linear equilibrium relationship was developed and solved by the method of orthogonal collocation (Hidajat and Ching [21]). They used monoethanolamine(MEA)- methanol mixture as their system. They also reported a comparison between their theoretical and experimental results. It was found that the nonlinearity of the MEA isotherm imposed significant constraints on the allowable operating conditions. A summary of these studies is given in Table 2.3.

2.5 DISCUSSION OF EARLIER MODELS

2.5.1 Equivalent Countercurrent Model: Dispersed Plugflow with Linear Isotherm

Assuming plug flow of the solid and axially dispersed plug flow of the fluid, the basic differential equation describing the system dynamics is

$$D_L\frac{\partial^2 c}{\partial z^2} - V\frac{\partial c}{\partial z} + \left(\frac{1-\varepsilon}{\varepsilon}\right)u\frac{\partial q}{\partial z} = \frac{\partial c}{\partial t} + \left(\frac{1-\varepsilon}{\varepsilon}\right)\frac{\partial q}{\partial t} \qquad (2.2)$$

If a linear equilibrium relationship ($q^* = Kc$) and a linear driving force mass transfer rate expression are assumed, at steady state:

$$\frac{dq}{dt} = k(q^* - q) = k(Kc - q) = -u\frac{dq}{dz} \tag{2.3}$$

and equation (2.2) becomes

$$D_L\frac{d^2c}{dz^2} - V\frac{dc}{dz} - (\frac{1-\varepsilon}{\varepsilon})k(Kc - q) = 0 \tag{2.4}$$

with the Danckwerts boundary conditions:

$$z=0, \quad c_o = c_o{}^1 - \frac{D_L}{V}\frac{dc}{dz}|_{z=0}$$

(liquid inlet)

$$z=L, \quad \frac{dc}{dz}|_{z=L} = 0 \tag{2.5}$$

(liquid outlet)

where $c_o{}^1$ is the sorbate concentration in the fluid phase just inside the bed. These equations may be expressed in dimensionless form. After some rearrangement (utilizing a mass balance between z=0 and z=L) one obtains

$$\frac{d^2\varphi}{dZ^2} - (Pe + St)\frac{d\varphi}{dZ} + PeSt(1-\gamma)\varphi = PeSt(1 - \frac{\gamma q_o}{KC_o}) \tag{2.6}$$

$$\varphi|_{Z=0} = 1 - Pe^{-1}\frac{d\varphi}{dZ}|_{Z=0}\,; \quad \frac{d\varphi}{dZ}|_{Z=1} = 0 \tag{2.7}$$

The solution of equations (2.6) and (2.7) giving the concentration profile is

$$\frac{\varphi(1-1/\gamma)+1/\gamma-q_o/Kc_o}{1-q_o/Kc_o} = \frac{m_1 e^{m_1+m_2 Z} - m_2 e^{m_2+m_1 Z}}{m_1 e^{m_1}(1-m_2/Pe) - m_2 e^{m_2}(1-m_1/Pe)} \tag{2.8}$$

where $m_1(+)$ and $m_2(-)$ are given by

$$m = \frac{1}{2}\{(Pe+St) \pm [(Pe+St)^2 + 4PeSt(\gamma-1)]^{1/2}\} \tag{2.9}$$

The concentration ratio over the bed (or section of bed) ($\varphi_L = c_L/c_o$) is given by

$$\frac{\varphi_L(1-1/\gamma)+1/\gamma-q_o/Kc_o}{1-q_o/Kc_o} = \frac{m_1 - m_2}{m_1 e^{-m_2}(1-m_2/Pe) - m_2 e^{-m_1}(1-m_1/Pe)}$$

$$= A(Pe, St) \tag{2.10}$$

In the plug flow limit, $Pe \rightarrow \infty$, m_1 and A reduces to $e^{St(1-\gamma)}$. In the equilibrium limit where mass transfer resistance is small and dispersion is due entirely to axial mixing, $St \rightarrow \infty$ and A reduces to $1/\gamma e^{Pe(1-\gamma)}$. The concentration ratio across any section of the bed is therefore given by

$$\frac{c_L}{c_o} = \frac{1}{\gamma - 1}[(1 - q_o/Kc_o)\gamma A(Pe, St) + \gamma q_o/Kc_o - 1] \tag{2.11}$$

2.5.2 Equivalent Countercurrent Model: Equilibrium Stage Model

Alternatively one may choose to represent the bed as equivalent to a certain number (n) of ideal equilibrium stages. For a linear system the fluid phase concentration ratio will then be given by the Kremser equation (Kremser [23], Souders and Brown [38]) :

$$\frac{c_0 - c_L}{c_0 - c_L/K} = \frac{\gamma^{n+1} - \gamma}{\gamma^{n+1} - 1} \tag{2.12}$$

or

$$\frac{c_0}{c_L} = \frac{1}{\gamma - 1}[\gamma^{n+1}(1 - 1/K) + \gamma/K - 1] \tag{2.12}$$

A simple mass balance over the section gives

$$q_L = q_0 + (\frac{L}{S})(c_L - c_0) \tag{2.13}$$

For each section of the unit there is one equation of the form of equation (2.10) or (2.12) and one equation of the form of equation (2.13) relating the inlet and outlet concentrations. This gives in all a set of eight equations relating the 10 concentrations $q_0, q_I, q_{II}, q_{III}, c_0, c_I, c_{II}, c_{III}, c_{III}'$, and C_{IV}. Two additional equations are obtained from the mass balances over the feed point and for the recirculating stream :

$$
\begin{aligned}
&(D-E)c_{II} = (D-E+F)c_{II}' \\
&(D-E+F-R)c_{IV} = Dc_0 \qquad (2.14)
\end{aligned}
$$

With the flowrates, Peclet and Stanton numbers and equilibrium constants all defined the solution to this set of equations gives the steady state concentration profile through the system. Since all equations are linear and equilibrium for each component is assumed independent, solution of the equations is straightforward.

The relationship between the two models may be derived by considering the HETP (height equivalent to a theoretical plate) (Ruthven [33]). Setting $q_0 = Kc_L$ in equation (2.10) gives the number of theoretical stages in bed length L, and hence the HETP :

$$\frac{1}{n} = \frac{H}{L} = \frac{\ln\gamma}{\gamma-1}\left(\frac{1}{Pe} + \frac{1}{St}\right) \qquad (2.15)$$

2.5.3 Numerical simulation: Linear Systems

As an alternative to the equivalent countercurrent representation one may simulate the SMB system numerically. Each section of volume V is considered as equivalent to a certain number of theoretical stages (n) with each stage considered as an ideal mixing cell of volume V/n, distributed between the fluid phase and the adsorbed phase in accordance with the bed voidage :

$$V_s = (1-\varepsilon)V/n \; V_l = \varepsilon V/n \tag{2.16}$$

a differential mass balance for the ith stage gives

$$QC_{i-1} = Qc_i + V_l\frac{dc_i}{dt} + V_s\frac{dq_i}{dt} \tag{2.17}$$

assuming that equilibrium is achieved in each stage and that the isotherm is linear equation (2.17) may be written as :

$$\frac{dc_i}{dt} = \frac{Q}{V_l+KV_s}(c_{i-1}-c_i) \tag{2.18}$$

Q is the actual flowrate which is constant for all stages within a section but varies between sections as a result of the introduction of feed or withdrawal of product :

$$\begin{aligned} Q_{II} &= Q_I - E \\ Q_{III} &= Q_I - E + F \\ Q_{IV} &= Q_I - E + F - R \end{aligned} \tag{2.19}$$

the fluid concentration remains constant between sections I and II and between sections III and IV but changes between sections II-III and IV-I as a result of introduction of feed or make up eluent :

$$\begin{aligned} &(c_{nI})_I = (c_1)_{II} \\ &(c_{nII})_{II}Q_{II} + c_F F = (c_1)_{III}Q_{III} \\ &(c_{nIII})_{III} = (c_1)_{IV} \\ &(c_{nIV})_{IV}Q_{IV} + c_D D = (c_1)_I Q_I \end{aligned} \tag{2.20}$$

With D, E, F and R defined, for each component, there is a set of $n_I+n_{II}+n_{III}+n_{IV}$ simple linear first order equations defining the concentration at each theoretical plate as a function of time.

2.5.4 Numerical Simulation : Nonlinear Systems

The approaches described in the previous sections are limited to the limiting case in which the equilibria for both components are linear and uncoupled. For nonlinear systems and coupled equilibria an alternative approach is needed (Ching et al [6,7]). The unit is represented in terms of the equivalent countercurrent system (Figure 1.4) with each section considered as equivalent to a number of equilibrium stages and the equivalent countercurrent velocities of solid (u) and fluid (V) given by

$$u = \frac{l}{\tau}, \quad u + V = \frac{L}{\varepsilon A} \tag{2.20}$$

At steady state the mass balance for the ith stage gives

$$S(q_{1,i+1} - q_{1,i}) = L(c_{1,i} - c_{1,i-1}) \tag{2.21}$$

with a similar expression for component 2, where $S = uA(1-\varepsilon)$ and $L = VA\varepsilon$. The equilibria are represented by expressions of the general form

$$\frac{q_1^*}{c_1} = K_1(c_{1,}\, c_2); \frac{q_2^*}{c_2} = K_2(c_{1,}\, c_2) \tag{2.22}$$

in which K_1 and K_2 are no longer constants but any convenient functional forms. Substitution into equation (2.21) yields a steady state mass balance equation for each component on each theoretical plate. The flowrate in each section are related by the usual overall balances. Thus for a two component system with N theoretical plates there is a set of 2N nonlinear simultaneous algebraic equations giving the concentration of each component through the system.

2.6 CONCLUSIONS

The objective of this review has been on the numerical simulation of continuous countercurrent adsorptive fractionation processes which depend on equilibrium rather than on kinetic selectivity. It has been found that despite vast work in this area, very little work is accomplished in the modelling of unsteady nonlinear systems. Further, nothing has so far been done on the modelling and simulation of the actual system. All the existing models are developed on the principle of the "SORBEX" arrangement.

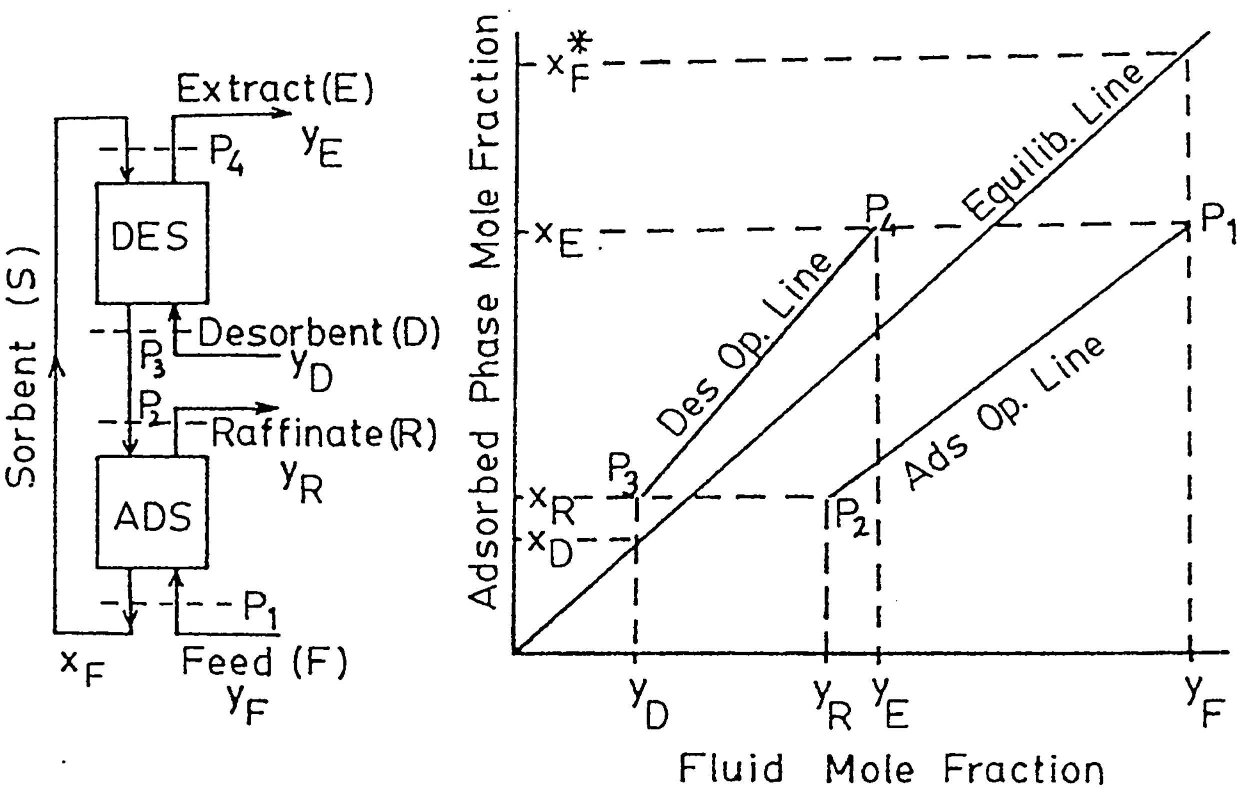

Figure 2.1 McCabe-Thiele analysis of a countercurrent system.

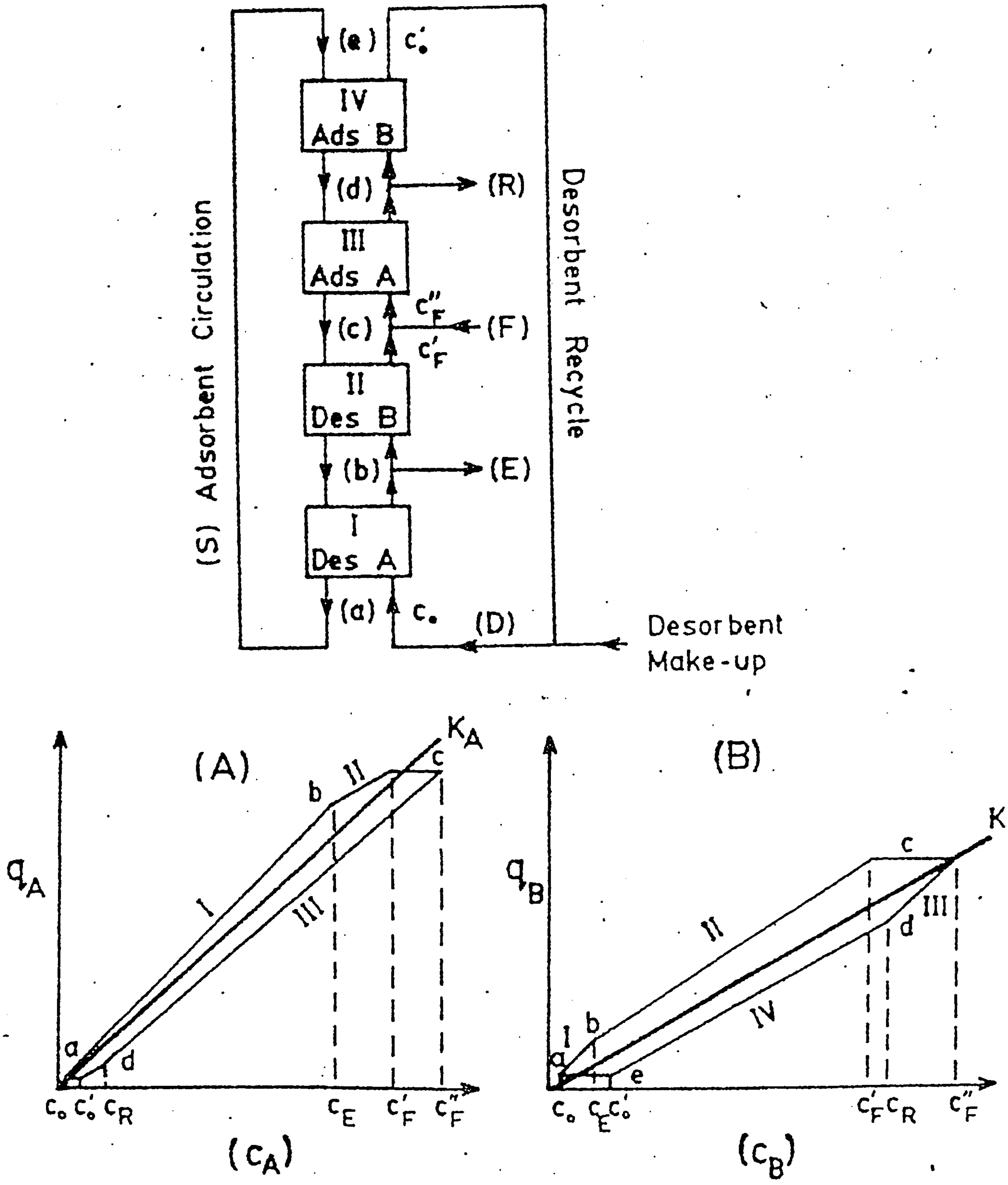

Figure 2.2 McCabe-Thiele analysis of 'SORBEX' system.

Table 2.1 Classification of models for countercurrent processes

Representation of system	Representation of bed elements
(a)Continuous countercurrent	(a.1) Continuous
	(a.2) Mixing cell
(b) SMB (direct simulation of port switching)	(b.1) Continuous
	(b.2) Mixing cell

Table 2.2 Examples of the application of various countercurrent models

Model No.	Comments	References
a.1.I	Equilibrium theory for 'Sorbex' unit-constant separation factor, plug flow	Storti et al. [37]
a.1.II	Equivalent countercurrent model-linear system, plug flow	Hashimoto et al. [17,18]
	Equivalent countercurrent model-linear system, dispersed plug flow (analytical solution)	Ching and Ruthven [10,11]
	Extension of this model to 'Sorbex' system	Ching et al. [14]
	Axial dispersed plug flow model applied to sorbitol-glucose separation	Kubota et al. [22]
	Equivalent countercurrent model with intraparticle diffusion (linear system)	Liu and Pigford [25]
a.2.I	Comparison of equilibrium and continuous models for SMB system	Ching and Ruthven [10,11] Ching et al. [14]
b.1.II	Numerical simulation of SMB using continuous model for bed elements	Hashimoto et al. [17,18]
	Numerical simulation of SMB using continuous model for bed elements	Storti et al. [37]
	Numerical simulation of SMB using mixing cell model-linear system	Carta and Pigford. [3]
b.2.I	Numerical simulation of SMB using mixing cell model-linear system	Barker and Thawait[2]
	Numerical simulation of SMB using mixing cell model-linear system	Hidajat et al. [19,20]
	Numerical simulation of SMB using mixing cell model-linear system	Ching et al. [5]
	Numerical simulation of SMB using mixing cell model-nonlinear system	Ching et al. [6,7]

Table 2.3 Summary of Literature Survey

Authors	Year	Isotherm	Flow model	Temp profile	Data
Amundson and Kasten[1]	1952	Linear	Plug flow	Isothermal	Theoretical
Neretnicks[27,28,29]	1974	Linear	Plug Flow	Isothermal	Theoretical
Svedberg[40]	1976	Linear	D. Plug flow	Isothermal	Theoretical
Liapis and Rippin[24]	1979	Linear	Plug flow	Isothermal	Experimental
Ruthven[34]	1983	Linear	D. Plug flow	Isothermal	Theoretical
Ching and Ruthven[10]	1985	Linear	D. Plug flow	Isothermal	Experimental
Ching and Ruthven[11]	1985	Linear	D. Plug flow	Isothermal	Experimental
Ching and Ruthven[12]	1985	Linear	D. Plug flow	Isothermal	Experimental
Ching et al.[14]	1985	Linear	D. Plug flow	Isothermal	Experimental
Nemeth et al.[26]	1985	Both	D. Plug flow	Isothermal	Theoretical
Ching et al.[13]	1986	Linear	D. Plug flow	Nonisothermal	Experimental
Hidajat et al.[19,20]	1986	Linear	D. Plug flow	Isothermal	Experimental
Ching et al.[8]	1986	Linear	D. Plug flow	Nonisothermal	Experimental
Ching et al.[7]	1988	Nonlinear	D. Plug flow	Isothermal	Experimental
Ruthven & Ching[35]	1989	Both	D. Plug flow	Isothermal	Both
Storti et al.[37]	1988	Nonlinear	D. Plug flow	Isothermal	Theoretical
Hidajat et al.[21]	1990	Nonlinear	D. Plug flow	Isothermal	Both

REFERENCES

(1) Amundson, N. R., and Kasten, P. R., Ind. Eng. Chem., 44, 1704 (1952).

(2) Barker, P.E., and Thawait, S., Chem. Ind., 7 November, 817-821 (1983).

(3) Carta, G., and Pigford, R. L., Ind. Eng. Chem. Fundam, 25,677-685 (1986)

(4) Chen, J. W., Cunningham, R. L., and Buege, J. A., Ind. Eng. Chem., Proc. Design Develop., 11, 430 (1972)

(5) Ching, C. B., Hidajat, K., Ho, C., and Ruthven, D. M., Reactive Polym., 6, 15-20 (1987a).

(6) Ching, C. B., Hidajat, K., Ho, C., and Ruthven, D. M., Chem. Eng. Sci., 42, 2547-2555 (1987b).

(7) Ching, C. B., Ho, C., and Ruthven, D. M., Chem. Eng. Sci., 43, 703-711 (1988).

(8) Ching, C. B., Ho, C., and Ruthven, D. M., AICHE J. 32, 1876-1880 (1986).

(9) Ching, C. B., and Ruthven, D. M., Can. J. Chem. Eng., 62, 398-403 (1984).

(10) Ching, C. B., and Ruthven, D. M., AICHE Symp. Ser., 81(242), 1-8 (1985a).

(11) Ching, C. B., and Ruthven, D. M., Chem. Eng. Sci., 40(6), 877-885 (1985b).

(12) Ching, C. B., and Ruthven, D. M., Chem. Eng. Sci., 40(6), 887-891(1985).

(13) Ching, C. B., and Ruthven, D. M., Chem. Eng. Sci., 41, 3063-3071 (1986).

(14) Ching, C. B., Ruthven, D. M., and Hidajat, R., Chem. Eng. Sci., 40, 1411-1417 (1985).

(15) Erskine, D. B., and Schuliger, W. G., Chem. Eng. Progr., 67, 41 (1971)

(16) Fornwalt, H.J., and Hutchins, R.A., Chem. Eng., 73, 155-164, (1968).

(17) Hashimoto, K., Adachi, S., Noujima, H., and Maruyama, A., Bitechnol. Bioeng., 25, 2371-2393, (1983).

(18) Hashimoto, K., Adachi, S., Noujima, H., and Maruyama, A., J. Chem. Eng. Japan, 16, 400-406, (1983).

(19) Hidajat, K., Ching, C. B., and Ruthven, D. M., Chem. Eng. J., 33, B55-B61 (1986a).

(20) Hidajat, K., Ching, C. B., and Ruthven, D. M., Chem. Eng. Sci., 41, 2953-2956 (1986b).

(21) Hidajat, K., and Ching, C. B., Trans I Chem. Eng., 68, 104-108 (1990).

(22) Kubota, R., Hata, C., and Shinya, H., Can. J. Chem. Eng., 66, (1988).

(23) Kremser, A., Natn. Petrol. News, 22 (21), 42 (1930)

(24) Liapis, A. I., and Rippin, D. W. T., AICHE J., 25, 455-460 (1979).

(25) Liu, P.D., and Pigford, R. L., AICHE National Meeting, Houston, (1987).

(26) Nemeth, J.,Vasanits, E. V., and Virag, T., Int. J. Heat & Mass Transfer, 28(4), 859-866 (1985).

(27) Neretnieks, I., The Swedish Paper Journal, 77, 407 (1974a).

(28) Neretnieks, I., Chem. Eng., Tech, 46, 781 (1974b).

(29) Neretnieks, I., report DECHEMA, Frankfurt/M., (Oct.,1974c)

(30) Ortlieb, H. J., Bunke, G., and Gelbin, D., Chem. Eng. Sci., 36, 1009-1016 (1981).

(31) Perry, J. H., and Chilton, C. H., Chemical Engineers' Handbook, McGraw-Hill Book Company, 5th ed., 16-20 (1973).

(32) Rhee, H. K., and Amundson, N. R., Chem. Eng. Sci., 28, 55-62 (1973).

(33) Ruthven, D. M., Principles of Adsorption and Adsorptive Processes, John Wiley, New York (1984).

(34) Ruthven, D. M., Can. J. Chem. Eng., 61, 881-883 (1983).

(35) Ruthven, D. M., and Ching, C. B., Chem. Eng. Sci., 44(5), 1011-1038 (1989).

(36) Storti, G., Santacesaria, E., Morbidelli, M., and Carra, S., Ind. Eng. Chem. Proc. Des. Dev., 24, 89-92 (1985).

(37) Storti, G., Masi, M., and Morbidelli, M., NATO ASI Vimeiro, Portugal, Elsevier (1988).

(38) Souders, M., and Brown, G. C., Ind. Eng. Chem. 24, 519-527 (1932)

(39) Svedberg, V. G., Can. J. Chem. Eng., 61, 881-883 (1983).

(40) Svedberg, V. G., Chem. Eng. Sci., 31, 345-353 (1976)

(41) Westermark, M., Doctoral thesis, Dept. of Chem. Eng., Royal Inst. of Technology, Stockholm, Sweden (1975)

(42) Winkler, H. E., and Kaempf, H. J., Wassar, Luft und Betrieb, 16, June, (1972)

CHAPTER 3

NUMERICAL SIMULATION OF UNSTEADY CONTINUOUS COUNTERCURRENT ADSORPTION SYSTEM WITH NON-LINEAR ADSORPTION ISOTHERM

3.1 INTRODUCTION

Large scale adsorptive separation processes may be conveniently divided into two broad classes; batch systems, in which the adsorbent beds are regenerated in a cyclic manner, and continuous flow systems involving continuous countercurrent contact between feed and adsorbent. Continuous countercurrent systems maximize mass transfer driving force and reduces adsorbent requirements. However, in continuous countercurrent systems, adsorbent recirculation is a difficult operation. In reality, continuous countercurrent contact is achieved by keeping the solid beds fixed while moving the fluid inlet and outlet points simultaneously at set time intervals in the direction of flow of the fluid phase as shown in Figure 3.1.

The effects of various parameters e.g. bed length, feed and eluent rates, and switch time are strongly coupled making it difficult to predict a priori the outcome of a parameter change. An efficient mathematical model is therefore necessary to visualize the effects of these various parameters.

The first generation of continuous countercurrent adsorption processes [1,10] proved uneconomic, largely as a result of practical difficulties associated with circulation of the solid adsorbents. Such problems are eliminated in the simulated moving bed system (Sorbex) [2,6,8,13], developed by U.O.P. Even though continuous countercurrent processes are now in extensive industrial use for several hydrocarbon separations [14], in the separation of glucose and fructose in the production of high fructose syrup [12], and in the separation of MEA and methanol [8,9], only limited efforts have been directed towards modelling and experimental investigation of such systems. The transient behavior of countercurrent staged processes has been investigated theoretically by Lapidus and Amundson [11]. A general review of countercurrent systems has been reported by Ruthven and Ching [15]. The simplest theoretical model assuming steady state operation with linear isotherm was derived by Ching and Ruthven [4] to explain their experimental data on the glucose-fructose system. A cell model for unsteady state operation with linear isotherm was developed by Ching and Ruthven [5]. However, the model results are limited to systems with a linear isotherm and therefore to low concentrations of adsorbable components. Recently, steady state models with nonlinear isotherm have been developed by both Ching et al. [3] and Hidajat et al. [9]. For most practical systems the concentrations of adsorbable species are large and therefore the effect of non-linearity of the isotherm is critical in optimizing the operating parameters. The more general case of solving the unsteady state operation with nonlinear isotherm has not yet been solved. An investigation of the effects of various operating parameters on both the dynamics and steady state in case of nonlinear isotherm is of great practical significance.

In this paper, a general mathematical model of continuous countercurrent adsorption system is developed for components which follow a nonlinear Langmuir equilibrium isotherm. The model equations are solved from transient to steady state, and the effects of various process parameters on separation have been investigated. A comparison of the theoretical results obtained for the limiting case of the present model are in agreement with the experimental data of Ching and Ruthven [4,5].

3.2 THEORETICAL MODEL

The model is developed with five columns in the pre-feed section (section 1) and six columns in the post feed section (section 2) which is the configuration reported by Ching and Ruthven [4]. A 12th column is used to totally remove the adsorbed phase component under a high liquid water flow.This system may be considered as approximately equivalent to the hypothetical continuous countercurrent arrangement shown in Figure 3.2a.

The equivalent solid velocity (u) is given by the ratio of individual column length to switch time.

The theoretical model for an equivalent continuous countercurrent system can be obtained from an overall mass balance around a differential volume of adsorber shown in Figure 3.2(b). The following assumptions are adopted to formulate the model.

1) Plug flow of solid.
2) Axially dispersed plug flow of fluid.
3) Isothermal operating conditions.
4) Linear driving force expression for mass transfer rate.
5) Isotherms are of nonlinear Langmuir form.

Adsorbent is considered to be flowing with a downward velocity $u = L/t_{switch}$ where L is the individual column length and t_{switch} is the switch time, while the liquid is flowing upwards with a velocity V.

The basic differential equation describing the system dynamics for ith component and jth section can be written as

$$D_{L_j}\frac{\partial^2 c_{ij}}{\partial z^2_j} - V_j\frac{\partial c_{ij}}{\partial z_j} + (\frac{1-\varepsilon}{\varepsilon})u\frac{\partial q_{ij}}{\partial z_j} = \frac{\partial c_{ij}}{\partial t} + (\frac{1-\varepsilon}{\varepsilon})\frac{\partial q_{ij}}{\partial t} \qquad (3.1)$$

For a Langmuir type of equilibrium isotherms, the rate equation is

$$\frac{\partial q_{ij}}{\partial t} = k_i\left[\frac{b_i q_s c_{ij}}{1 + \sum_{i=1}^{k} b_i c_{ij}} - q_{ij}\right] \tag{3.2}$$

Initial Conditions **:**

$$c_{ij} = 0.0, \tag{3.3}$$

Boundary Conditions **:**

at $z_j = 0$,

$$D_{L_j}\frac{\partial c_{ij}}{\partial z_j}\Big|_{z_j=0^+} = -V_j\left(c_{ij}\big|_{z_j=0^-} - c_{ij}\big|_{z_j=0^+}\right) \tag{3.4}$$

at $z_j = L_{s_j}$,

$$\frac{\partial c_{ij}}{\partial z_j} = 0.0 \tag{3.5}$$

Using the following dimensionless variables

$$C' = \frac{c}{c_f}; \quad Q' = \frac{q}{q_f}; \quad \tau = \frac{t}{L_{s_1}/V_1}; \quad Z_j = \frac{z_j}{L_{s_1}}$$

equations 1 to 5 can be written as

$$\frac{\partial C'_{ij}}{\partial \tau} = F_j\left[\frac{1}{Pe_j}\frac{\partial^2 C'_{ij}}{\partial^2 Z_j} - \frac{\partial C'_{ij}}{\partial Z_j} + \gamma_j \Phi \frac{\partial Q'_{ij}}{\partial Z_j} - \Psi K_i \Phi \frac{\partial Q'_{ij}}{\partial \tau}\right] \tag{3.6}$$

$$\frac{\partial Q'_{ij}}{\partial \tau} = \alpha_j [\frac{C'_{ij}}{1 + \sum_{i=1}^{k} \lambda_i (C'_{ij} - 1.0)} - Q'_{ij}] \tag{3.7}$$

***Initial Conditions* :**

$$C_{ij} = 0.0 \tag{3.8}$$

***Boundary Conditions* :**

at $Z_j = 0.0$

$$C'_{ij_o} = Cf'_{ij} + \frac{1}{Pe_j} \frac{dC'_{ij}}{dZ_j}\Big|_{Z_j = 0^+} \tag{3.9}$$

at $Z_j = \frac{z_j}{L_{s_j}} = 1.0$

$$\frac{dC'_{ij}}{dZ_j} = 0.0 \tag{3.10}$$

where Cf'_{ij} is the inlet concentration of i for section 1 which can be obtained from the material balance equation at the mixing point of feed and outlet of section 2.

The system of coupled differential equations described by equations (3.6) - (3.10) has been solved from transient to steady state conditions by the method of orthogonal collocation. Equations (3.6) and (3.7) with boundary conditions represented by Equations (3.9) and (3.10) may be expressed in collocation form as

$$\frac{dC'_{A,1,j}}{d\tau} = F_1[(\frac{1}{Pe_1}B_{j,1} - A_{j,1})C'_{A,1,1} + \gamma_1 A_{j,1}Q'_{A,1,1} + (\frac{1}{Pe_1}B_{j,M2} - A_{j,M2})C'_{A,1,M2}$$

$$+ \gamma_1 \Phi A_{j,M2}Q'_{A,1,M2} + \sum_{i=2}^{M1}(\frac{1}{Pe_1}B_{j,i} - A_{j,i})C'_{A,1,i} + \gamma\Phi\sum_{i=2}^{M1}A_{j,i}Q'_{A,1,i}$$

$$- \Psi K \Phi \alpha_1 \{\frac{C'}{1 + \lambda_A(C'_{A,1,i} - 1) + \lambda_B(C'_{B,1,i} - 1)} - Q'_{A,1,i}\}] \tag{3.11}$$

Boundary conditions can be written as

$$(C'_{A,1,i} - CHZ) = \frac{1}{Pe_1}(A_{1,1}C'_{1,i} + A_{1,M2}C'_{1,M2} + \sum_{i=2}^{M1}A_{1,i}C'_{1,i}) \tag{3.12}$$

and

$$A_{M2,1}C'_{A,1,1} + \sum_{i=2}^{M1}A_{M2,i}C'_{A,1,i} + A_{M2,M2}C'_{A,1,M2} = 0 \tag{3.13}$$

where CHZ = $Cl'_{A,1}$

For the system in the present study, six equivalent countercurrent beds of length L are in the pre feed section and five beds of length L are in the post feed section. Sixteen collocation points were used for both sections which requires the solution of 128 simultaneous nonlinear ordinary differential equations. This set of differential equations has been solved using the functional iteration method.

3.3 METHOD OF SOLUTION

In the present study the orthogonal collocation method was used to solve the above system of partial differential equations. The method orthogonal collocation which uses polynomial approximation techniques for solving partial differential equations was developed a decade ago or so, mainly by Villadsen [16] and Finlayson [7]. The method has been found to require less computer time than standard finite difference techniques in the simulation of the performance of continuous countercurrent adsorption systems to obtain a solution of given accuracy since the finite difference method needed a large number of segments to approximate the system which results in large dimensionality of equations. On the other hand one main advantage to the polynomial approximation method is that it requires far fewer spatial discritization points to achieve the specified accuracy.

When the partial differential equations are written in collocation form using an orthogonal polynomial to represent the trial function a set of ordinary differential equations is obtained which may then be solved by any standard integration algorithm.

In the present study the concentration profile in the fluid phase is approximated by the following trial function based on a nonsymmetric polynomial:

$$C(Z,\tau) = (1-Z)C(0,\tau) + ZC(1,\tau) + Z(1-Z)\sum_{i=1}^{M} a_i(\tau)P_{i-1}(Z) \tag{3.14}$$

where $a_i(\tau)$ are functions of time or constants and P_i are the nonsymmetric polynomials defined by the condition:

$$\int_0^1 w(Z)P_n(Z)P_m(Z)dZ = 0, \quad n = 0,1,\ldots\ldots,m\text{-}1 \tag{3.15}$$

where w(Z) = 1 in the present study.

3.4 RESULTS AND DISCUSSIONS

The dimensionless theoretical model, equations 3.6-3.10, has been solved numerically to study the effect of various parameters on the system. The model parameters are F_j, the fluid flow ratio in section 1 or 2; Pe_j, the Peclet number; $\Phi = 1-\lambda_1-\lambda_2$, the nonlinearity factor; γ_{ij}, ratio of solid down flow to fluid upflow rates; K_i, the equilibrium constants; ψ, ratio of packed solids to voids in bed; α_j, the dimensionless Linear driving force rate parameter; and

λ_i, the individual Langmuir nonlinear factors. For comparison with a real system, the model was solved for the glucose-fructose-Duolite C_2O_4 resin system of Ching and Ruthven [4,5]. This fixes the parameters K_i and Ψ'. The parameter α was considered large as the mass transfer resistance has been reported to be very small for this system.

In the system of Ching and Ruthven the feed and eluent flow rates, and the switch times were varied while the bed length and column diameter were fixed. Their steady state linear local equilibrium model could be described by two parameters for each section, namely Pe_j and γ_i. And they showed that an efficient separation of glucose and fructose occurs for a wide range of operating conditions provided that the condition $\gamma_F > 1.0$, $\gamma_G < 1.0$ are fulfilled in both pre-feed and post-feed sections.

In the present theoretical study, the effects of the feed and eluent flow rates, switch times, bed lengths, diameter, bed configuration and nonlinear equilibrium parameter were investigated. For a particular system, the process parameters affects only the $Pe_j\,(V_j, L_{s_j}, D_{L_j})$, and $\gamma_{ij}\,(K_i, u, V_j)$ for each section.

The model was first solved for the base case of Ching and Ruthven [4,5] , for which the relevant parameter values are given in Table 3.1. The dimensionless concentration profiles are computed at different time intervals representing the transient behavior of the prefeed and postfeed regions for the separation of glucose and fructose and are illustrated in Figure 3.3. In the postfeed section, the glucose concentration profile grows rapidly during initial start up and always exceeds the fructose profile which is zero for the later 40% of the section, whereas in the prefeed section the fructose profile builds up much more slowly and always exceeds the glucose profile which is zero for the first 70% of the section. It takes about 1620 min for the transient profiles to reach the steady state. The experimental results of Ching and Ruthven [4,5] are also shown on the figure, and satisfactory agreement between the model predictions and the experimental data is observed.

To examine the effect of the nonlinear parameter $\Phi = 1-\lambda_1-\lambda_2$, the base case of Ching and Ruthven [4,5] was run with $\lambda_1 = \lambda_2 = 0.4$, (nonlinear) and the steady state results are plotted in Figure 3.4 along with the results for the case where $\lambda_1 = \lambda_2 = 0.0$ (linear). For the linear case ($\lambda = 0.0$), a separation analogous to Figure 3.3 is observed - the difference is attributed to a new set of parameters used for the computation (see Table 3.1). However, for the nonlinear case ($\Phi = 0.2$) poor to no separation may be observed in both sections. Here the adsorbent removes both components equally from fluid resulting in the poor separation as may be observed for the solid phase concentration profiles which are plotted in Figure 3.5. It thus appears that the criterion of Ching and Ruthven [4,5] ($\gamma_F > 1, \gamma_G < 1$ in both sections) is no longer sufficient in the case of nonlinear adsorption. Because of the coupling nature of the isotherms at $\Phi = 0.2$, the adsorption equilibrium curve is a surface rather than lines which is shown in Figure 3.6. If one of the components follow linear isotherm, the system becomes uncoupled. In the present study monoethanolamine (nonlinear) and methanol (linear) is chosen to test the criterion reported by Ching and Ruthven [4,5]. Parameters for this system are adopted from Ching et al. [3] and are given in Table 3.2. Figure 3.7 represents an example of bad separation since it does not follow the criterion of Ching and Ruthven [4,5]. The γ criterion can be fulfilled by reducing the eluent flow rate, however, the separation is not improved in the post feed section, as shown in Figure 3.8.

To improve the separation for coupled nonlinear systems the operating parameters can be adjusted until good separation is achieved. One such possible set for the glucose-fructose system with coupled nonlinear equilibria is shown in Table 3.1. This set of parameters is now considered as the base case for nonlinear system for which the concentration profiles are shown in Figure 3.9, in which the individual bed length, switch time, and feed rate were increased. It should be noted however, that under the revised operating conditions, if the nonlinear parameter is removed such that Φ becomes equal to 1 (the linear case), the separation becomes poorer as may be observed from Figure 3.10. This suggests that the operating conditions are very sensitive to the linearity of the isotherm. It may also be noted that the criterion for the linear case that γ_G should be less than 1 is no longer sufficient for the coupled nonlinear case. In Table 3.3, the effect of change in the process parameters on the various dimensionless groups that have been used in the model are listed. It may be noted that since the mass transfer resistance has been reported to be very low [4], the dimensionless parameter α has no effect on the system performance.

The effect of individual bed length for nonlinear system ($\lambda = 0.4$) can be observed by comparing Figures 3.9 and 3.11. It is evident from these figures, that the separation and the purity of glucose in both post and pre feed sections is getting worse by decreasing the bed length. From Table 3.3 it is clear that except for the Peclet number, the effect of individual bed length on the dimensionless groups is very pronounced. As the length is increased, γs are reduced significantly in both prefeed and postfeed section. Since mass transfer resistance is very low for this system, it can be said that the poor separation can be attributed to the low dimensionless flow ratio.

The effect of eluent rate is shown in Figures 3.12 and 3.13. In the post feed section the concentration profiles of glucose and fructose approaches each other indicating poorer separation, once the eluent rate is either decreased or increased as compared to the base case shown in Figure 3.9. Further, the separation of glucose and fructose in the prefeed section is better at the intermediate eluent rate (E = 179 ml/min). Dimensionless parameter are changed slightly with the increment of eluent flow rate. Peclet numbers in both sections are increased approximately by 20% moving the system toward plug flow but γ_i's are decreased by about 30% in both the sections. As a result the system performance becomes poorer.

Figure 3.14 shows the effect of feed flow rate on the concentration profiles of glucose and fructose in both the prefeed and post feed sections.The concentration profile for fructose drops very sharply in the post feed section with the decrease of feed flow rate. This indicates separation is achieved much earlier in the post feed section. On the other hand the separation of fructose is reduced in the extract phase of the prefeed section. The change in feed flow rate changes the parameters in the postfeed section only and it can be seen that the change in dimensionless parameters favours better separation which leads to an improved system performance.

The effect of switch time on the system performance can be observed from Figure 3.15. Comparison with Figure 3.9 shows that decrease in switch time reduces the separation drastically in post feed section but improves the recovery of fructose in the pre feed section. This may be attributed to the lower residence time at shorter switch times. From Table 3.3 it is clear that the effect of change in switch time is quite significant on the parameters of both prefeed and postfeed sections. Peclet numbers are increased significantly but on the other hand γ_i in both sections are decreased by about 40%. As the system moves toward more plug flow region, the purity of the product becomes worse.

Figure 3.16 shows the effect of column diameter on the separation between glucose and fructose. It is evident that good separation is achieved by increasing the column diameter to 0.4 cm. The separation in the postfeed section is extremely good while the recovery of fructose from the prefeed section is also significant. If the dimensionless parameter values are compared with the base case (Figure 3.9), it is clear that the increase in column diameter has decreased the Peclet numbers by 20% but has increased γ_i quite significantly which results in a better separation.

The effect of number of individual adsorption column in a particular section on the system performance is shown in Figure 3.17. The base case shown in Figure 3.9 is plotted with 5 columns in the post feed and 6 columns in the pre feed section. Keeping the total active number of columns constant, i.e. 11, Figure 3.17 is plotted with 4 and 7 columns in the post and prc feed sections respectively. When the steady state concentration profiles for glucose and fructose for both the sections are compared with that of the base case (Figure 3.9), it can be seen that qualitatively the profiles remain the same. This interesting phenomena can be explained by the dimensionless numbers listed in Table 3.3. Though the Peclet numbers for all sections have changed due to the change in section lengths, the parameter, γs are unaltered in both sections. Therefore, the performance is expected to be qualitatively same.

3.5 CONCLUSIONS

A theoretical study of a more general case, unsteady state with non-linear isotherm, was performed for the continuous counter current adsorption systems. The relevant equations were solved to observe the effects of parameters of practical significance on the performance of the system. The present study reveals that the system performance is very sensitive to the nonlinear parameter λ. Under the same operating conditions while $\lambda = 0.0$ may give good separations, the system would show poorer performance at higher λ and vice versa.

Though γ is important to find out physically the direction of components in each section, γ alone cannot predict good separation. Good separation can be predicted from the relative slopes of the operating line and equilibrium line in both prefeed and postfeed sections for systems with linear isotherm. In case of uncoupled nonlinear isotherm, good separation can also be explained using similar approach. But in case of coupled nonlinear isotherm, such criterion can not be applied because of the complex nature of the equilibrium isotherm.

It can be concluded that as the system moves toward high mixing the separation improves. At ideal plug flow i.e. $Pe \rightarrow \infty$, the system performance decreases drastically. Besides this, it is also evident that good separation occurs only when the γ of fructose is greater than 2.45. On the other hand, bad separation prevails when γ values of fructose are less than 1.86.

The results obtained for the limiting case of linear isotherm ($\lambda = 0.0$) was compared with the experimental data of Ching and Ruthven [10,11] at both unsteady and steady state conditions and were found to agree well.

Although, a Langmuir type of isotherm has been used in the present simulation, any other isotherm can be conveniently used. This makes the present model more general and adaptable for simulation from unsteady to steady state conditions for any type of equilibrium isotherm. Further, the model can be easily extended to simulate the more practical " Sorbex " system.

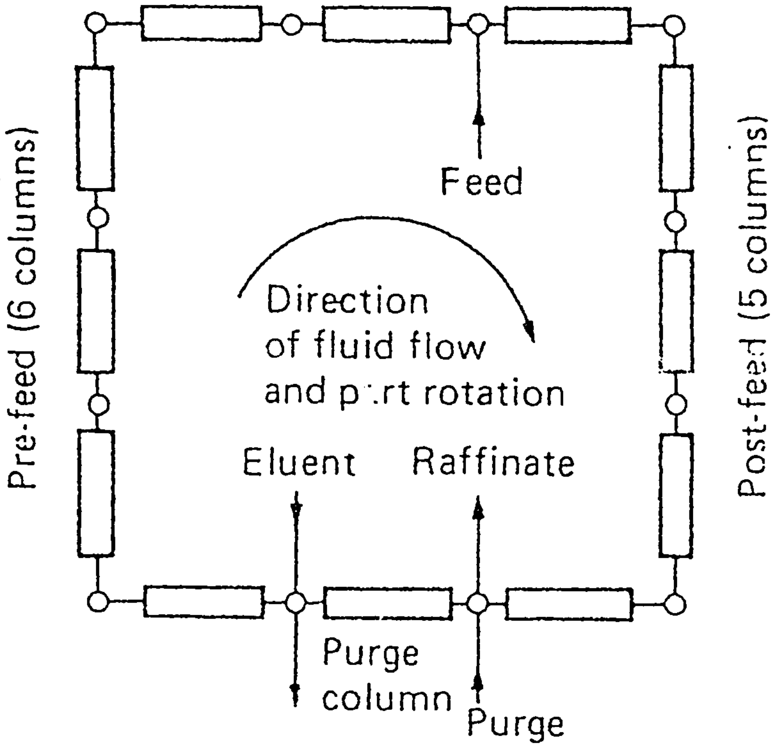

Figure 3.1 Schematic diagram of 2-section simulated moving bed.

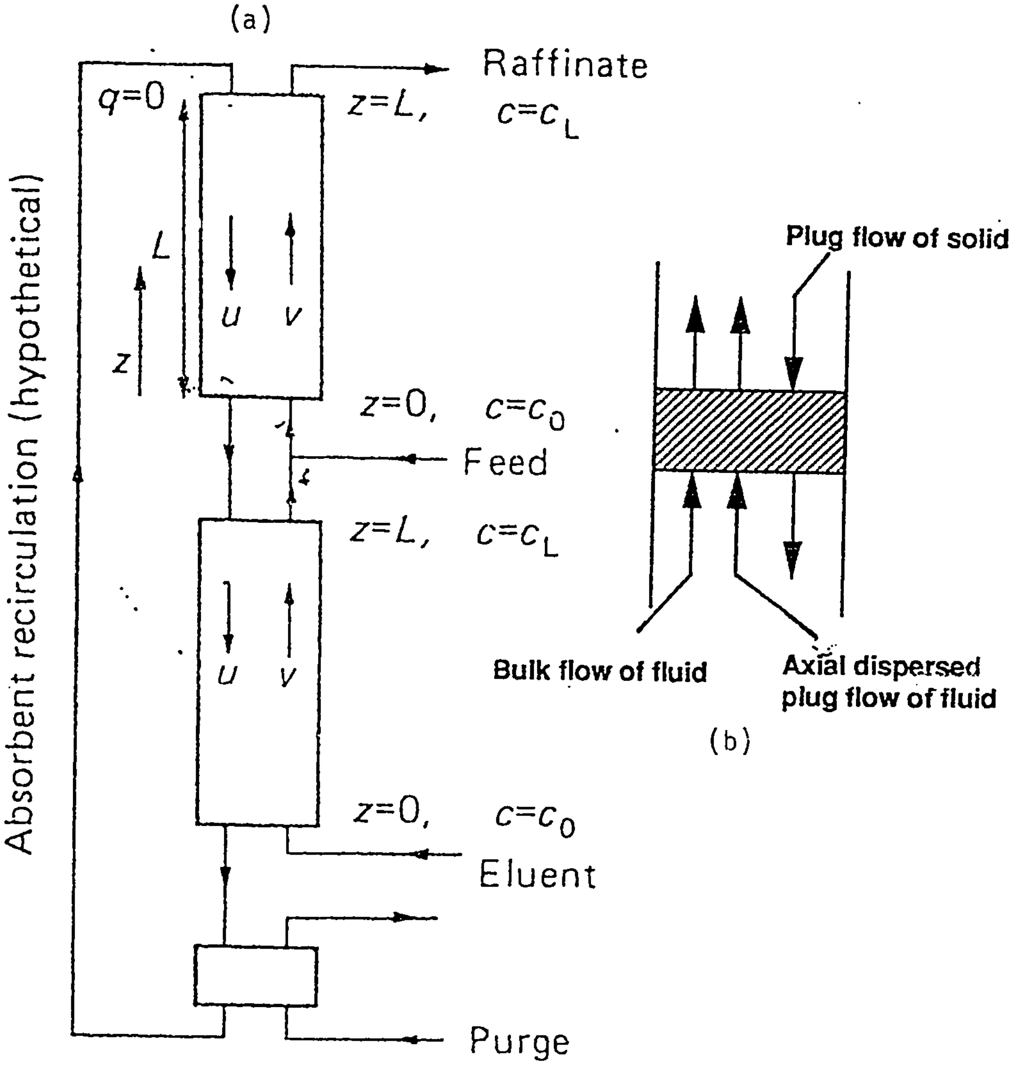

Figure 3.2 (a)Schematic diagram of 2-section equivalent countercurrent system.

(b) Schematic diagram of the mass balance of jth section for 2-section equivalent countercurrent model.

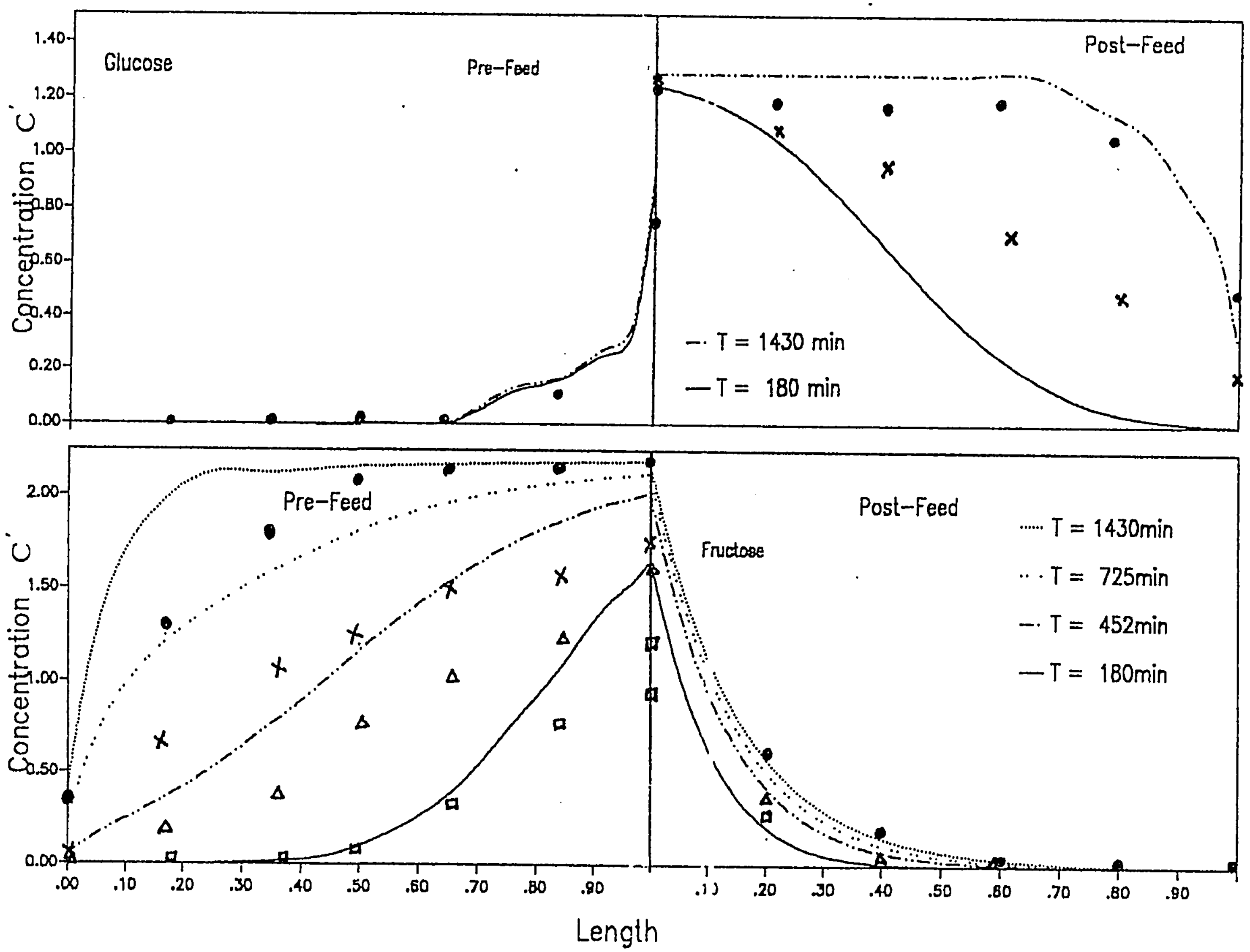

Figure 3.3 Unsteady state concentration profile of glucose and fructose
[Experimental- Glucose: • (1620 mins.), × (270 mins.) Fructose: ◻ (180 mins.), △ (450 mins.), × (720 mins.), • (1620 mins.)]

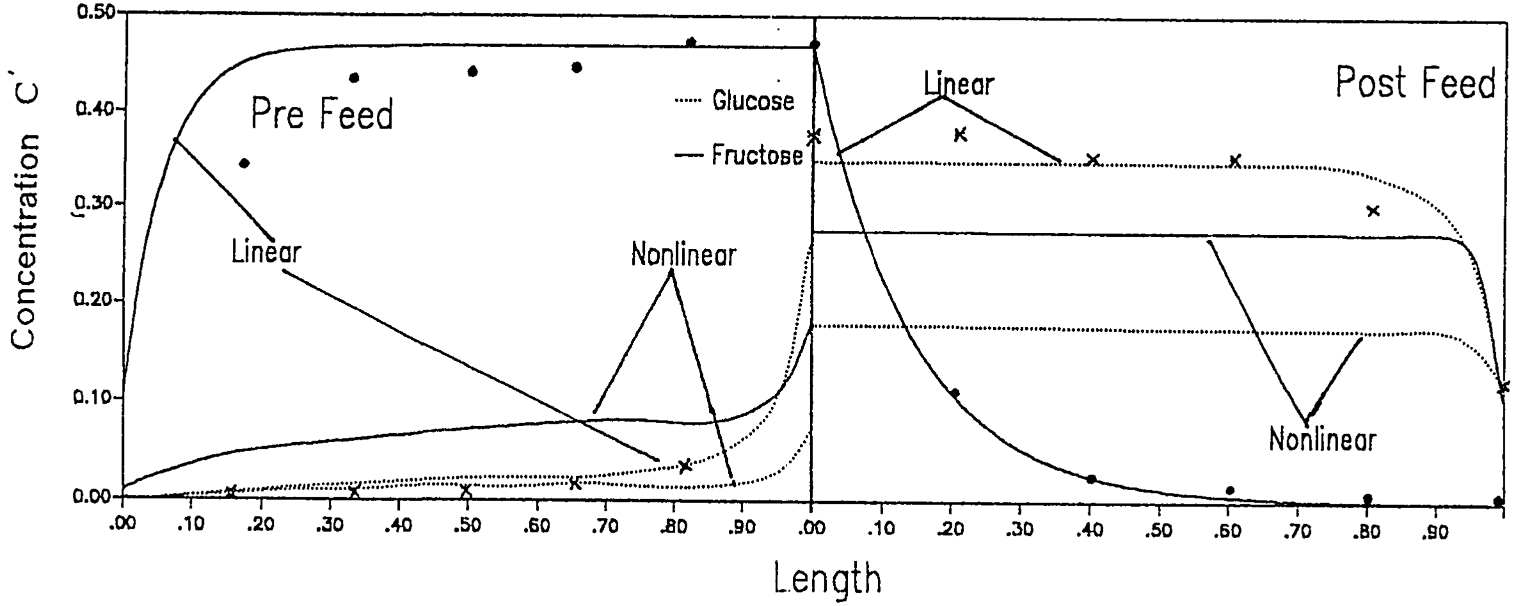

Figure 3.4 Effect of nonlinear parameter, λ on the system performance.

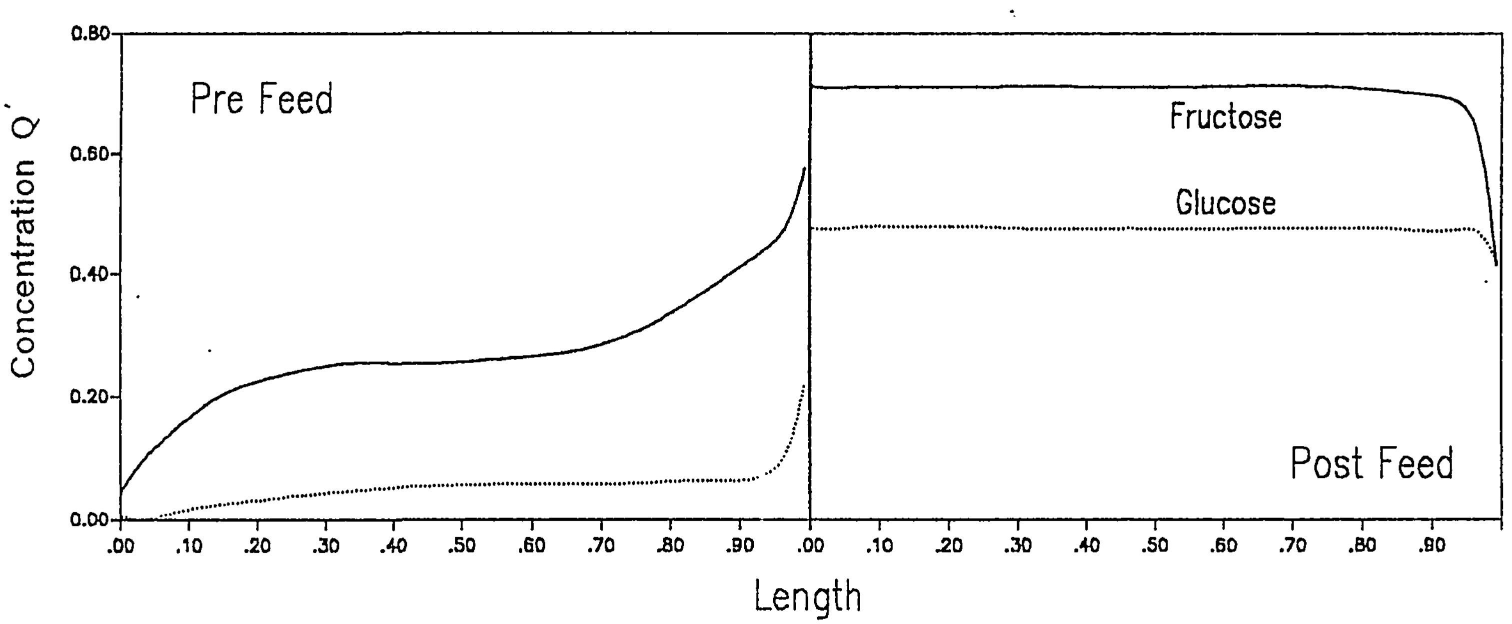

Figure 3.5 Solid phase concentration profile at $\phi = 0.2$.

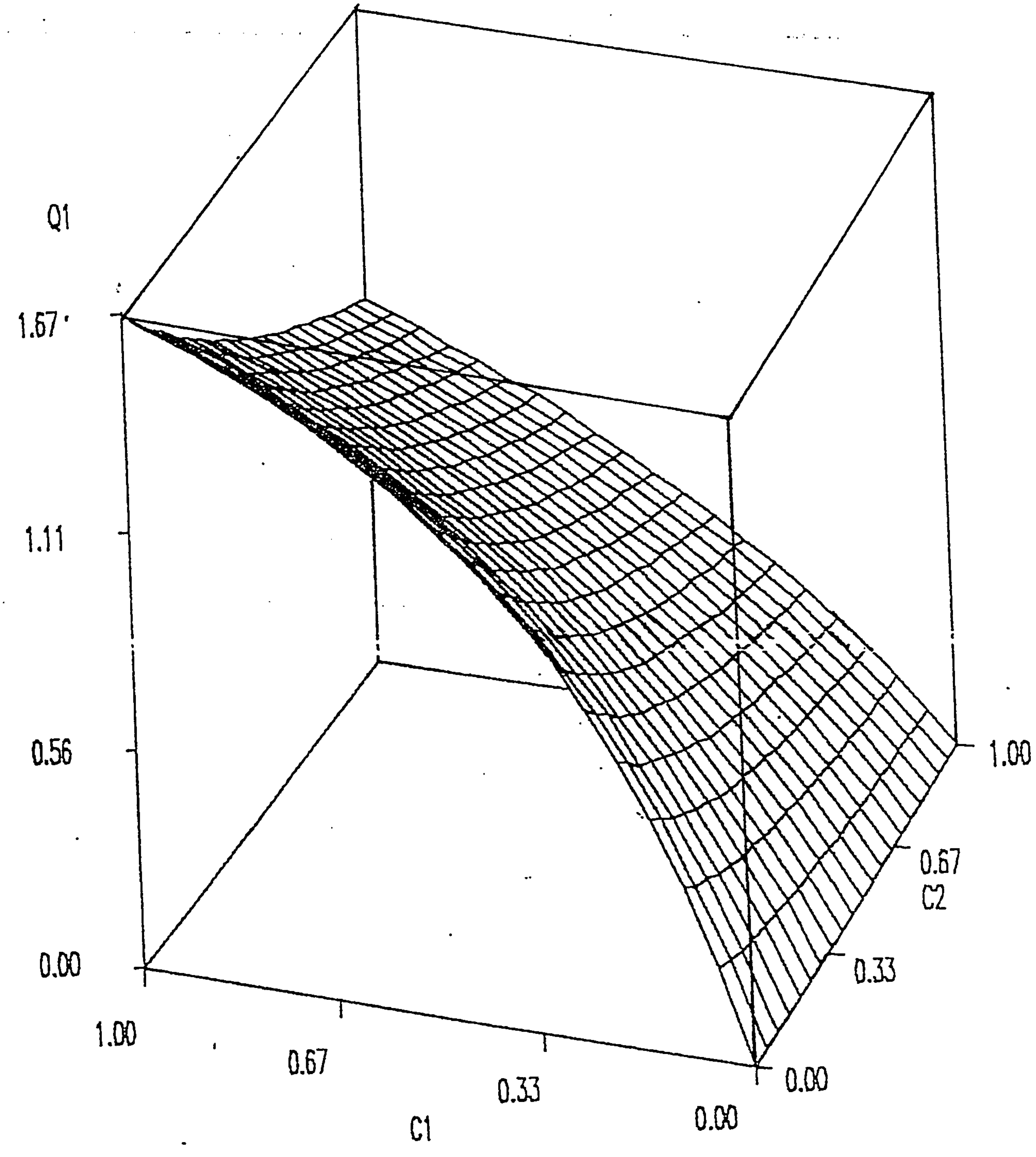

Figure 3.6 Equilibrium diagram of a coupled nonlinear system.

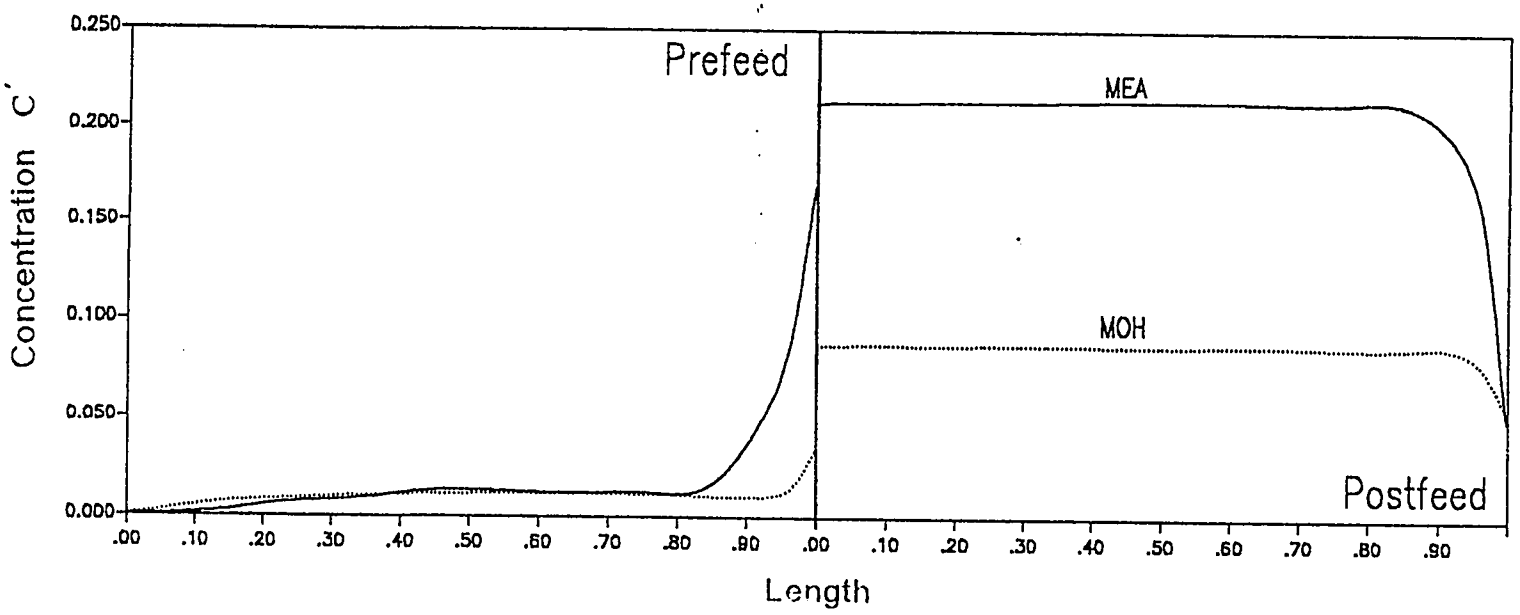

Figure 3.7 Concentration profile of MEA and MOH with the process parameters reported by Ching et al.

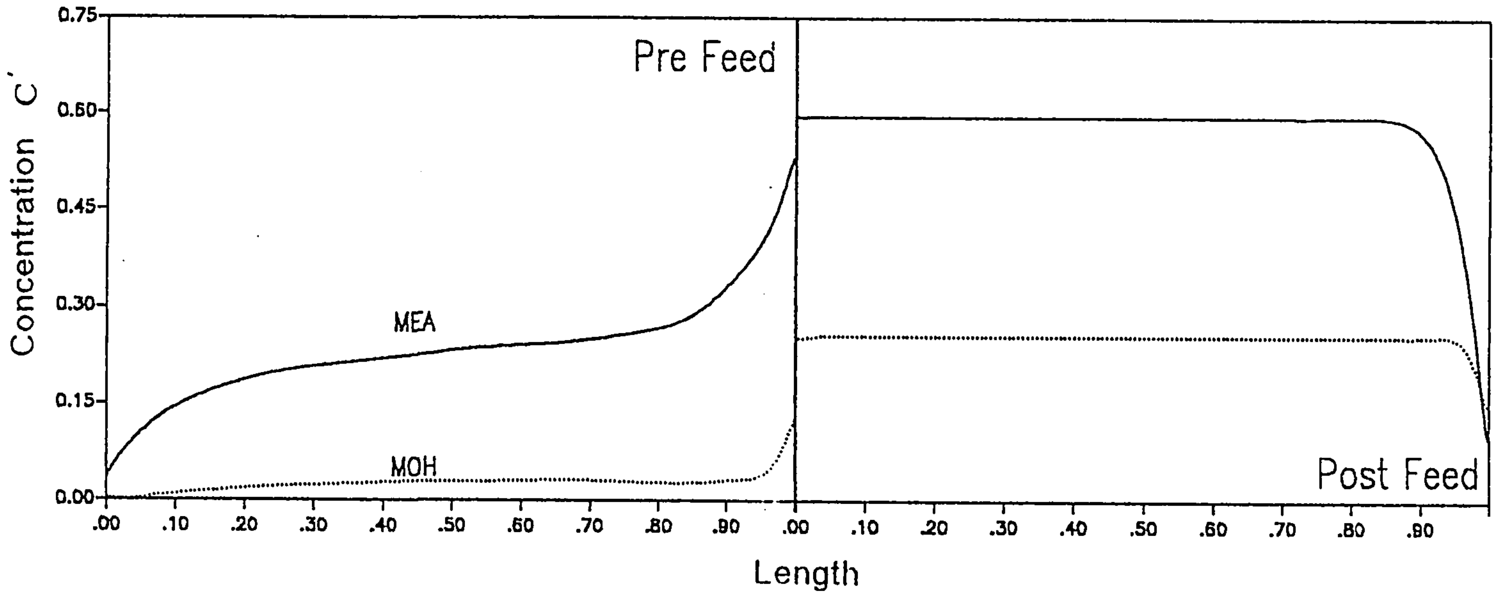

Figure 3.8 Effect of flow ratio on the system performance of an uncoupled nonlinear system.

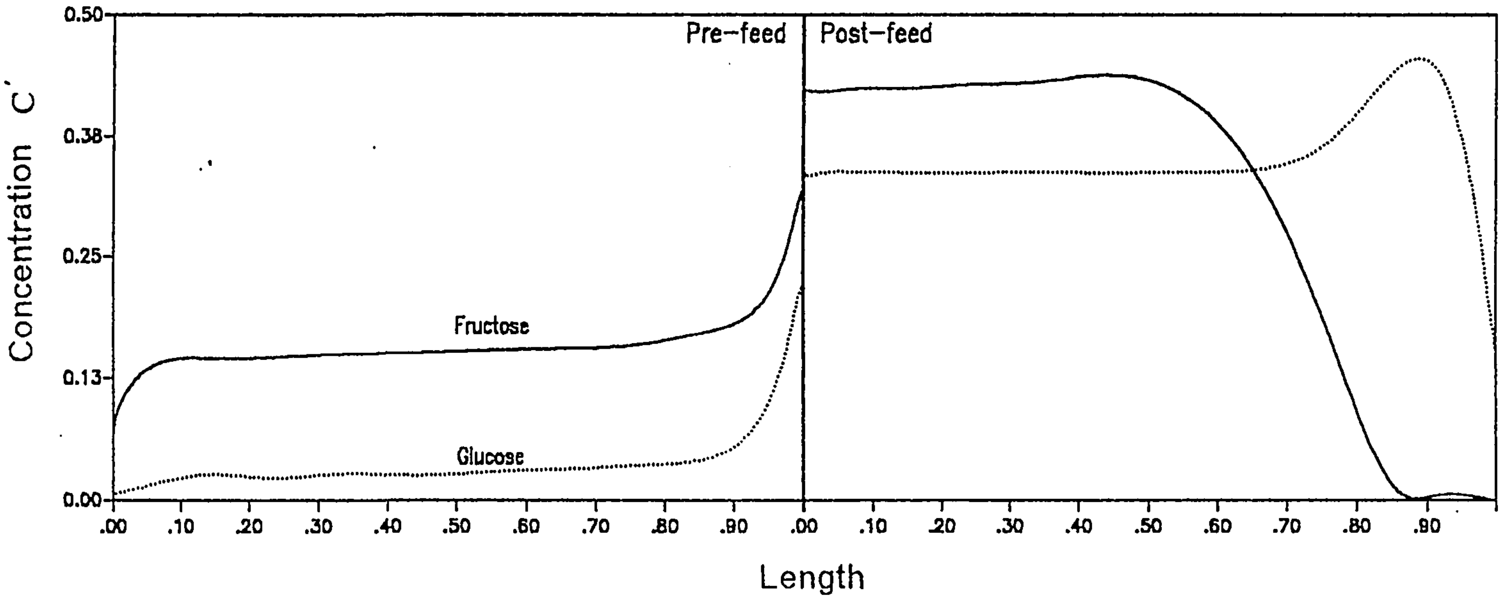

Figure 3.9 Concentration profile of new base case of glucose and fructose with new set of parameters (L = 200 cm, Eluent flowrate = 179.0 ml/min, Feed flow rate = 10 ml/min , Diameter = 5.1 cm, τ = 13.33 mins.)

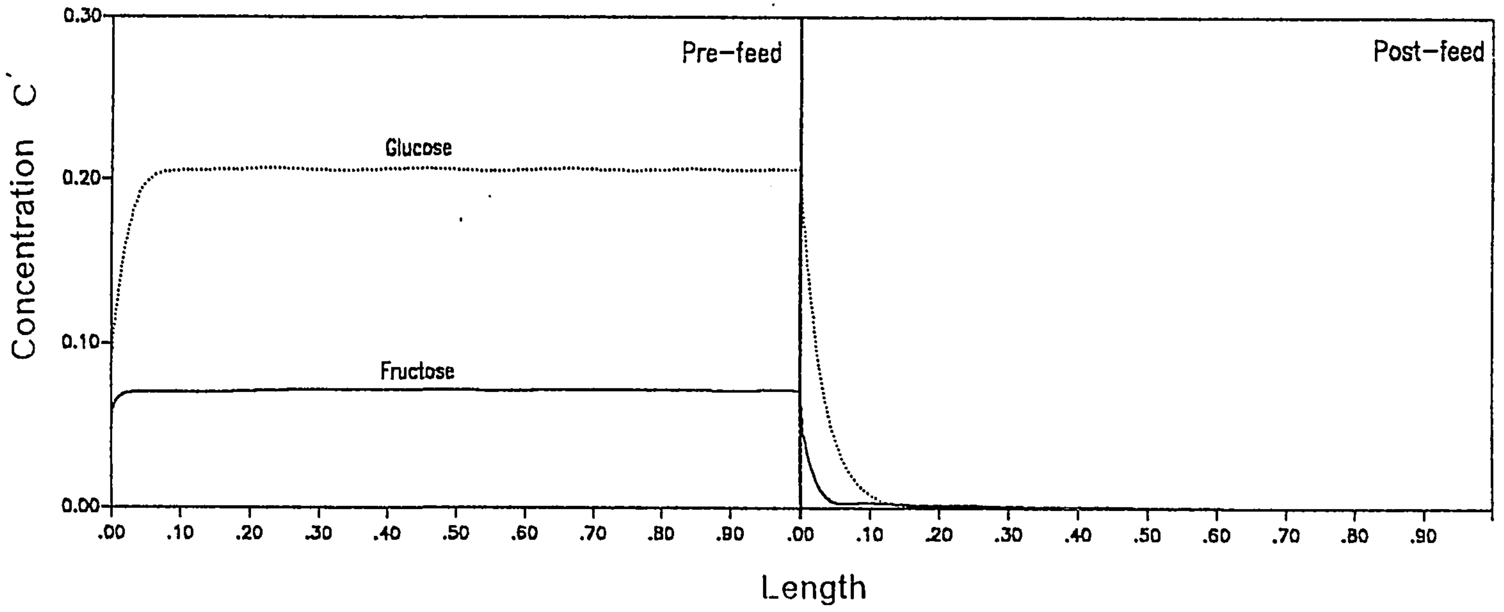

Figure 3.10 Effect of nonlinear parameter λ, on the performance of 2-section equivalent system.

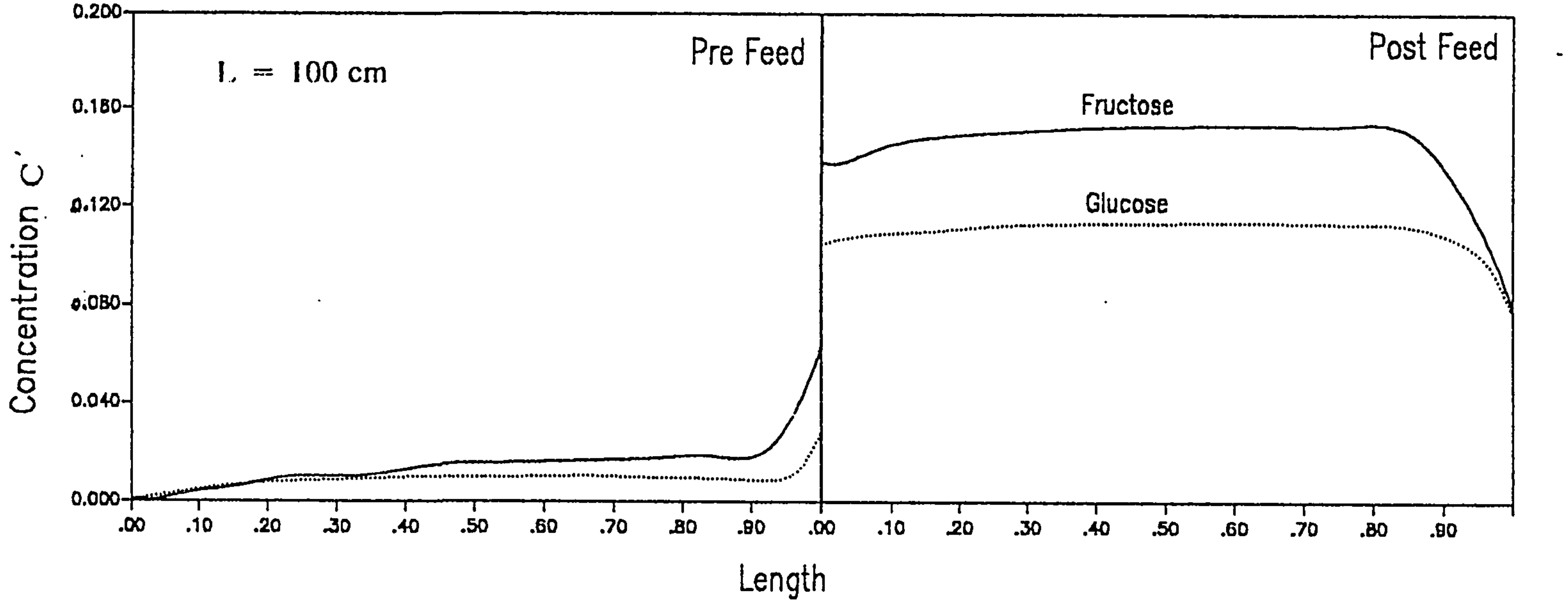

Figure 3.11 Effect of bed length on the performance of 2-section equivalent system.

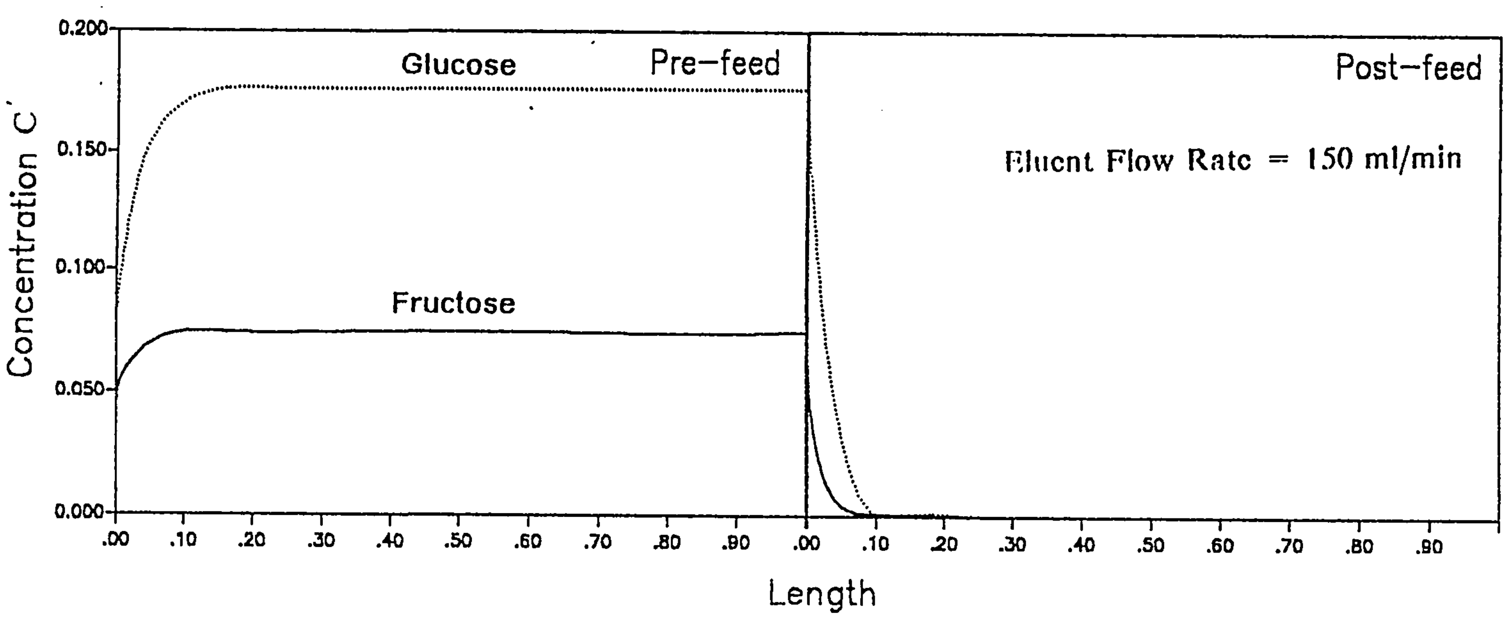

Figure 3.12 Effect of eluent flow rate (low) on the performance of the 2-section equivalent system.

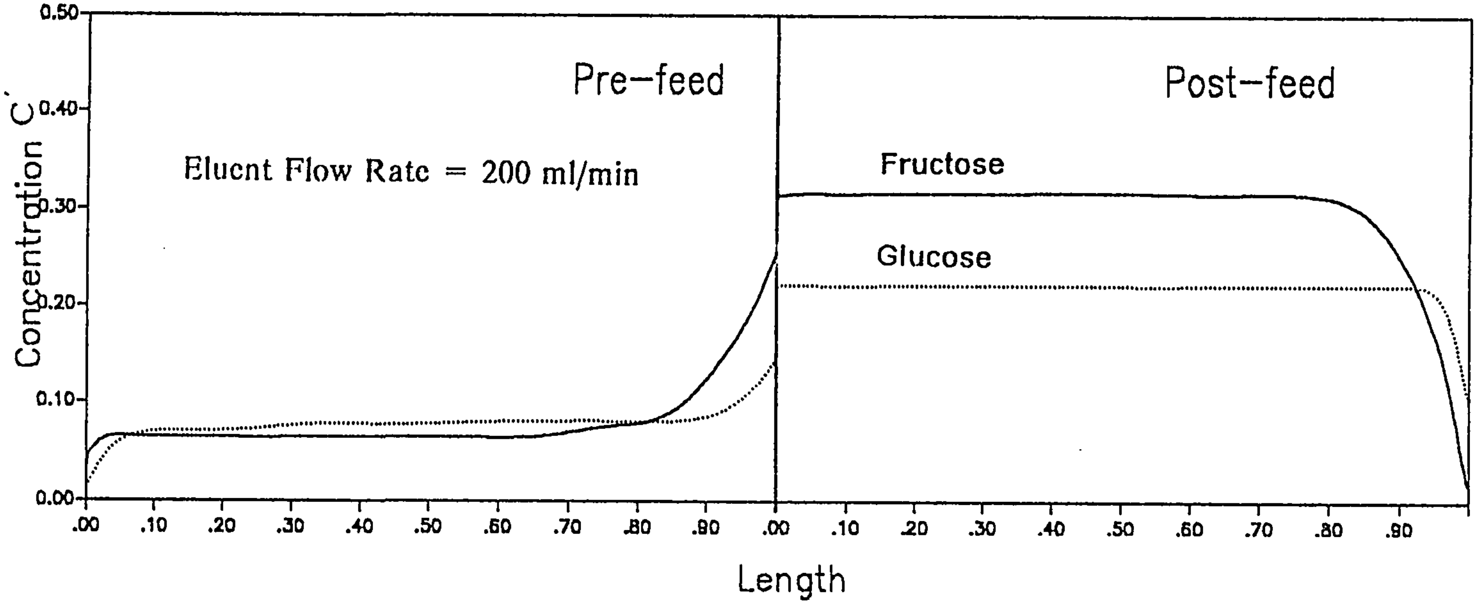

Figure 3.13 Effect of eluent flow rate (high) on the performance of the 2-section equivalent system.

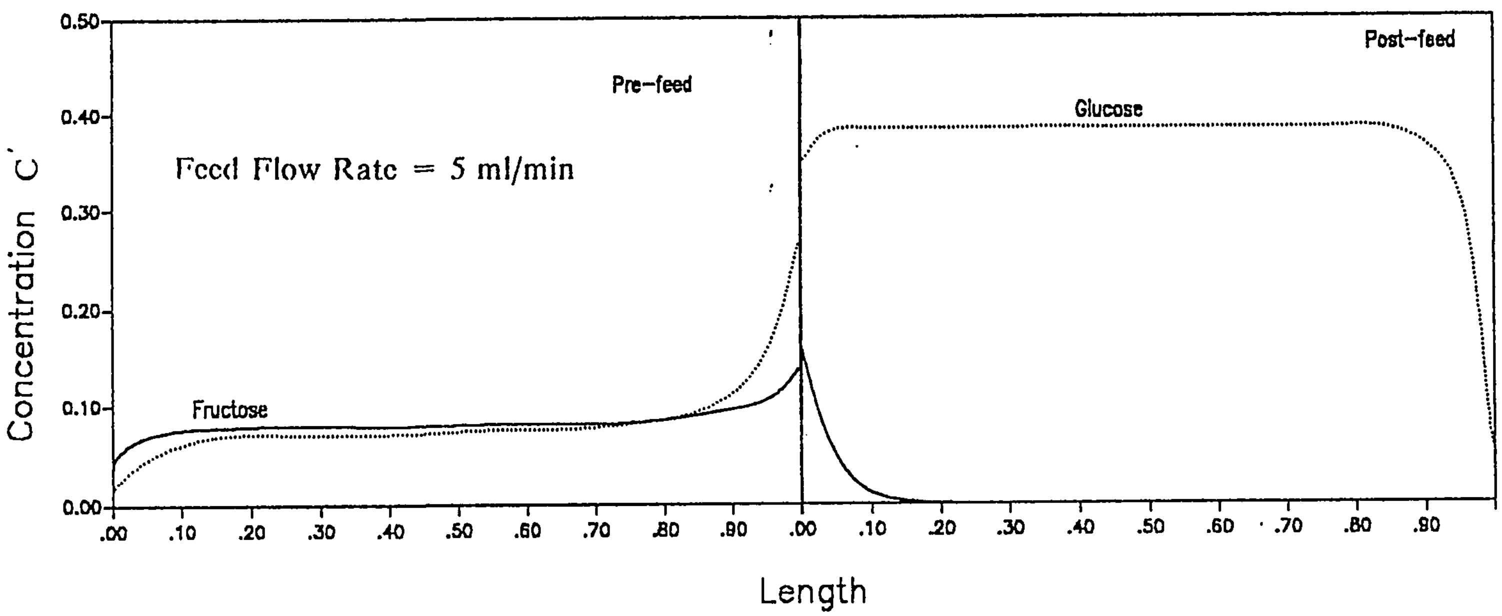

Figure 3.14 Effect of feed flow rate on the performance of the 2-section equivalent system.

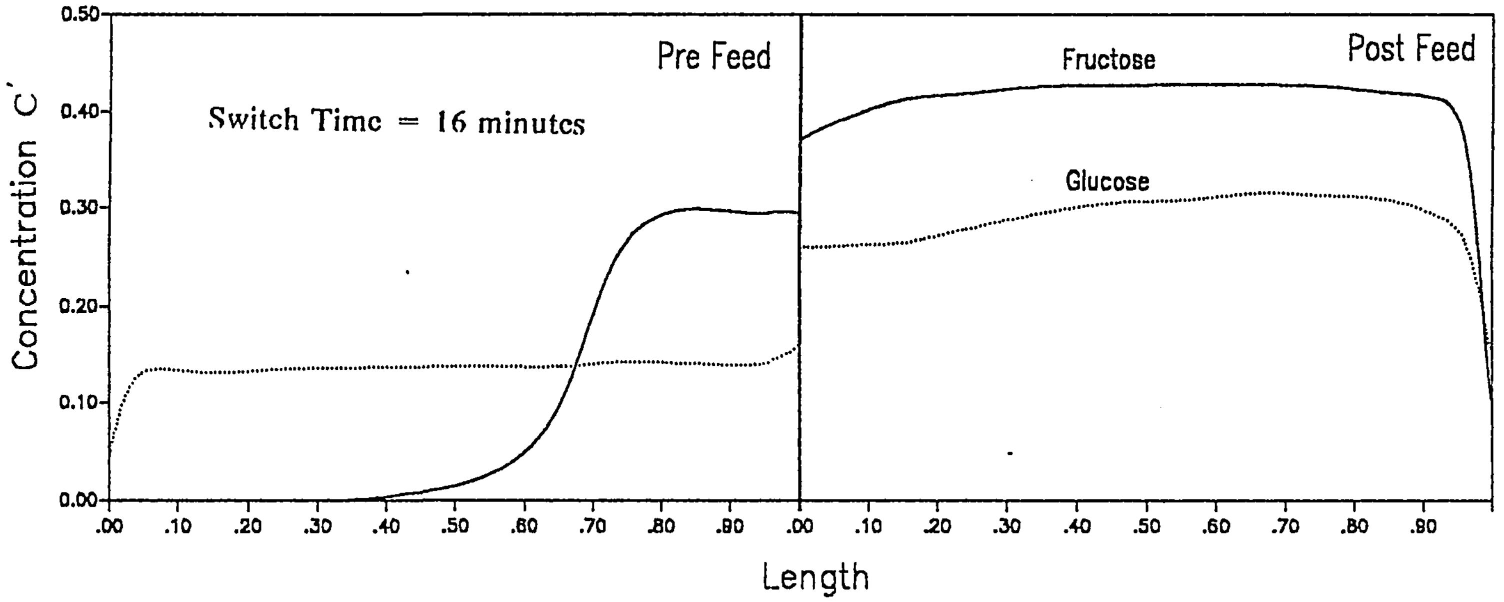

Figure 3.15 Effect of switch time on the performance of the 2-section equivalent system.

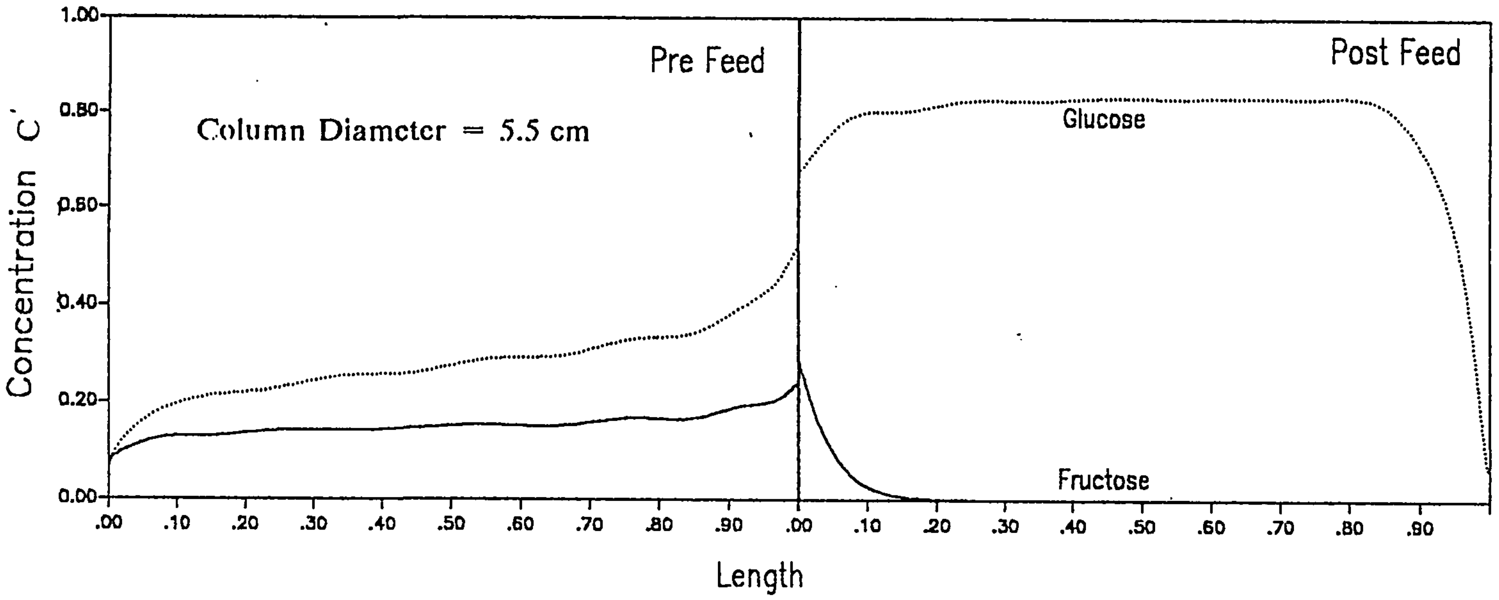

Figure 3.16 Effect of column diameter on the performance of the 2-section equivalent system.

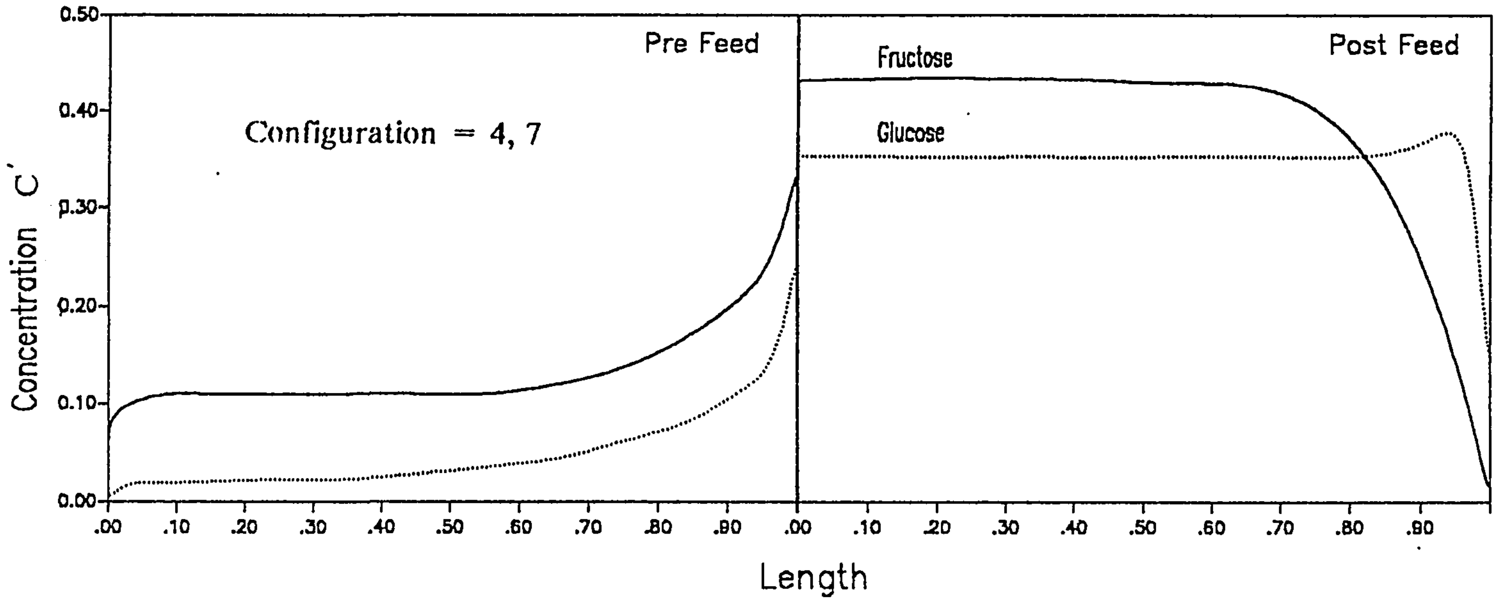

Figure 3.17 Effect of column configuration on the system performance of 2-section equivalent countercurrent system.

Table 3.1 Parameter values for the Glucose-Fructose system

Parameter	Steady state		Unsteady state
	Linear case of Ching and Ruthven [4] Run 4	Nonlinear case (present study)	Linear case of Ching and Ruthven [5]
Feed composition (%Glucose,%Fructose)	5,5	-	5,5
Switch Time,min	15.0	13.33	15.0
Feed flowrate,ml/min	7.5	10.0	6.0
Desorbent rate,ml/min	97.76	179.0	99.76
Bed length,cm	100	200	100
Configuration Prefeed,Postfeed	6,5	6,5	6,5
Column diameter,cm	5.1	5.1	5.1
$\lambda(A,B)$	0.0,0.0	0.4,0.4	0.0,0.0
K_A	0.88	0.88	0.88
K_B	0.50	0.50	0.50

A = Fructose, B = Glucose

Table 3.2 Parameter values for the MEA-MOH system

Parameter	Nonlinear case of Ching et al.[3]
Feed composition (%MEA,%MOH)	20,10
Switch Time,min	30.5
Feed flowrate,ml/min	5.0
Desorbent rate,ml/min	87.4
Bed length,cm	100
Configuration Prefeed,Postfeed	6,5
Column diameter,cm	5.5
$\lambda(A,B)$	0.435,0.0
K_A	1.24
K_B	0.63

A = Monoethanolamine (MEA), B = Methanol (MOH)

Table 3.3 Effect of process parameters on dimensionless groups of coupled nonline
system.

					Post Feed		Pre Feed				
Effect		F_2	Pe_1	Pe_2	γ_1	γ_2	γ_1	γ_2	α_1	α_2	Figure No.
Base Case		0.71	70.25	75.60	2.45	1.42	2.89	1.66	27.20	38.45	3.9
Column Diameter (cm)	(5.5)	0.65	49.10	48.80	4.09	2.37	5.20	3.00	45.10	69.00	3.16
Eluent Flow Rate (ml/min)	(200)	0.74	83.22	92.86	1.86	1.08	2.10	1.22	20.64	27.88	3.13
Eluent Flow Rate (ml/min)	(150)	0.61	46.73	43.81	4.33	2.51	5.91	3.43	48.10	78.80	3.12
Feed Flow rate (ml/min)	(5)	0.77	66.42	75.60	2.65	1.54	2.87	1.67	29.42	38.45	3.14
Individual Bed Length (cm)	(100)	0.77	67.49	78.81	0.64	0.37	0.69	0.40	7.05	9.18	3.11
Configuration	(4,7)	0.48	56.20	88.20	2.45	1.42	2.87	1.67	21.76	44.86	3.17
Switch Time (min)	(16)	0.74	91.90	103.03	1.55	0.9	1.75	1.017	20.70	28.08	3.15

Post Feed and Pre Feed sections are consedered as Section #1 and Section # respectively.

REFERENCES

(1) Berg C., Trans. AICHE, 42, 665 (1956).

(2) Broughton, D. B., and Berg, R. C., Hydrocarbon Processing, 48(6), 115-120 (1969).

(3) Ching, C. B., Ho, C., and Ruthven, D. M., Chem. Eng. Sci., 43, 703-711 (1988).

(4) Ching, C. B., and Ruthven, D. M., Chem. Eng. Sci., 40(6), 877-885 (1985b).

(5) Ching, C. B., and Ruthven, D. M., Chem. Eng. Sci., 40(6), 887-891(1985).

(6) Ching, C. B., Ruthven, D. M., and Hidajat, K., Chem. Eng. Sci., 40, 1411-1417 (1985).

(7) Finlayson, B. A., Non linear analysis in Chemical Eng., McGraw Hill, (1980).

(8) Hidajat, K., and Ching, C. B., Trans I Chem. Eng., 68, 104-108 (1990).

(9) Hidajat, K., and Ching, C. B., and Ruthven, D. M., Chem. Eng. J., 33, B55-B61 (1986).

(10) Kehde, H., Fairfield R. G., Frank J.C., and Zahnstechner, L. W., Chem.

Eng. Prog, 4, 575 (1978).

(11) Lapidus L., and Amundson N. R, Ind. Eng. Chem., 42, 1071 (1950).

(12) Neuzil, R. W., and Jensen, R. A., 85th National Meeting AIChE, Philadelphia, June 1978

(13) de Rosset, A. J., Neuzil, R. W., and Broughton, D. B., Percolation Processes, NATO ASI No. 33, 249-281, Noordhoff, Holland (1981).

(14) de Rosset, A. J., Neuzil, R. W., and Korous, D., Ind. Eng. Chem., Process Des. Dev., 15(2), 261-266 (1976).

(15) Ruthven, D. M., and Ching, C. B., Chem. Eng. Sci., 44(5), 1011-1038 (1989).

(16) Villadsen, J.V., Selected approximation methods for Chemical Engineering problems. Denmarks tehnishe hojskile, Lyngsby (1970).

CHAPTER 4

UNSTEADY STATE SIMULATION OF "SORBEX" SYSTEM WITH NONLINEAR ADSORPTION ISOTHERMS

4.1 INTRODUCTION

In previous work [9] an efficient and general unsteady state model with nonlinear equilibrium isotherm for continuous countercurrent adsorption system represented by two sections was developed. Though, the system proved efficient for separation of fructose from glucose, the concentration of fructose was very low in the extract. A costly evaporation process would be required to achieve the product at a desired concentration level. To overcome this disadvantage, a more practical process called 'SORBEX' system was introduced by UOP [2]. In this process, the countercurrent system is divided into four sections and desorption is achieved by correctly adjusting the flow rates in each section using water (eluent) instead of a separate purge column [2-4].

The first reported application of this process was by Bieser and deRosset [1]. Although some process details have been published both for linear glucose-fructose separation [5,6,12,13] and nonlinear MEA-MOH separation [7,10], only limited efforts have been directed towards modelling and experimental investigation of the dynamics of such systems. A general review of counter current systems has been reported by Ruthven and Ching [14]. The simplest theoretical model of the 'SORBEX' system based on steady state conditions and linear isotherm was presented by Ching et al. [6] and was shown to provide a good representation of their experimental data on the glucose-fructose system. The numerical simulation of the unsteady state case with linear isotherm was published by Hidajat et al. [11]. The system was considered as a cascade of ideal theoretical stages with the number of stages determined from pulse chromatographic experiment, which limits its applicability to linear isotherms. Further, dispersed plug flow was assumed in this study. A steady state model of the 'SORBEX' system has been presented by Ching et al. [7] for the nonlinear isotherm. In most practical systems the concentrations of adsorbable species are large and therefore the effect of nonlinearity of the isotherm becomes very significant in optimizing the operating parameters [9]. The more general case of solving the unsteady state system with plug flow for a nonlinear isotherm needs to be solved to comprehend the effects of various process parameters on the system performance.

In this paper, a general mathematical model of the continuous countercurrent 'SORBEX' system is developed which includes the nonlinear (Langmuir) equilibrium isotherm. The equations developed have been solved from unsteady to cyclic steady state. The effect of various operating parameters (viz. switch time, feed flow rate, eluent flow rate, bed length etc.) on the performance of the system has been investigated. Comparisons of the experimental data for the MEA-MOH [7,10] and glucose-fructose system [6,11] with the present simulation results show good agreement.

4.2 THEORETICAL MODEL

The model is developed for twelve columns with four hypothetical countercurrent sections whose configuration was reported by Ching et al. [6] as shown in Figure 1.3. The system thus may be considered as approximately equivalent to the hypothetical continuous countercurrent arrangement shown in Figure 4.1a. The equivalent solid velocity (u) is given by the ratio of individual column length to switch time.

The theoretical model for the equivalent continuous countercurrent system can be obtained from an overall mass balance around a differential volume of adsorber shown in Figure 4.1b. The following assumptions are adopted to formulate the model.

1) Plug flow of solid.

2) Axially dispersed plug flow of fluid.

3) Isothermal operating conditions.

4) Linear driving force expression for mass transfer rate.

5) Isotherms are of nonlinear Langmuir form.

Adsorbent is considered to be flowing with a downward velocity $u = L/\tau_s$ where L is the individual column length and τ_s is the switch time, while the liquid is flowing upwards with a velocity V.

The basic differential equation describing the system dynamics for ith component and jth section can be written as

$$D_{L_j}\frac{\partial^2 c_{ij}}{\partial z^2_j} - V_j\frac{\partial c_{ij}}{\partial z_j} + (\frac{1-\varepsilon}{\varepsilon})u\frac{\partial q_{ij}}{\partial z_j} = \frac{\partial c_{ij}}{\partial t} + (\frac{1-\varepsilon}{\varepsilon})\frac{\partial q_{ij}}{\partial t} \tag{4.1}$$

For a Langmuir type of equilibrium isotherms, the rate equation can be written as

$$\frac{\partial q_{ij}}{\partial t} = k_i[\frac{b_i q_s c_{ij}}{1 + \sum_{i=1}^{k} b_i c_{ij}} - q_{ij}] \tag{4.2}$$

Initial Conditions

$$c_{ij} = 0.0, \tag{4.3}$$

Boundary Conditions

at $z_j = 0$,

$$D_{L_j}\frac{\partial c_{ij}}{\partial z_j}\Big|_{z_j=0^+} = -V_j\left(c_{ij}\big|_{z_j=0^-} - c_{ij}\big|_{z_j=0^+}\right) \tag{4.4}$$

at $z_j = L_j$,

$$\frac{\partial c_{ij}}{\partial z_j} = 0.0 \tag{4.5}$$

Material Balances

Material balances for each section are given by the following equations

At the inlet of section IV

$$c_{i4}\big|_{z_4=0^-} = c_{i3}\big|_{z_3=L_{s_3}} \tag{4.6}$$

At the inlet of section III

$$c_{i3}\big|_{z_3=0^-} = \frac{V_2 c_{i2}\big|_{z_2=L_{s_2}} + (V_3 - V_2)c_f}{V_3} \tag{4.7}$$

At the inlet of section II

$$c_{i2}\big|_{z_2=0^-} = c_{i1}\big|_{z_1=L_{s_1}} \tag{4.8}$$

At the inlet of section I

$$c_{i1}\big|_{z_1=0^-} = \left(c_{i4}\big|_{z_4=L_{s_4}}\right)\frac{V_4}{V_1} \tag{4.9}$$

Using the following dimensionless variables

$$C' = \frac{c}{c_{f_i}} \quad Q' = \frac{q}{q_{f_i}} \quad \tau = \frac{t}{L_{s_4}/V_4}; \quad Z_j = \frac{z_j}{L_{s_4}}$$

the above equations are written for ith component and jth section as

$$\frac{\partial C'_{ij}}{\partial \tau} = F_j[\frac{1}{Pe_j}\frac{\partial^2 C'_{ij}}{\partial^2 Z_j} - \frac{\partial C'_{ij}}{\partial Z_j} + \gamma_j \Phi \frac{\partial Q'_{ij}}{\partial Z_j} - \Psi' K_i \Phi \frac{\partial Q'_{ij}}{\partial \tau}] \tag{4.10}$$

$$\frac{\partial Q'_{ij}}{\partial \tau} = \alpha_j[\frac{C'_{ij}}{1 + \sum_{i=1}^{k}\lambda_i(C'_{ij} - 1.0)} - Q'_{ij}] \tag{4.11}$$

Initial Conditions

$$C_{ij} = 0.0 \tag{4.12}$$

Boundary Conditions

at $Z_j = 0.0$

$$C'_{ij_o} = Cl'_{ij} + \frac{1}{Pe_j}\frac{dC'_{ij}}{dZ_j}|_{Z_j=0}, \tag{4.13}$$

where Cl'_{ij} is the inlet concentration of i for section j which can be obtained from the material balance equations.

At $Z_j = \frac{z_j}{L_1}$

$$\frac{dC'_{ij}}{dZ_j} = 0.0 \tag{4.14}$$

Material Balances

At the inlet of section IV

$$Cl'_{i4} = C'_{i3}|_{Z_3=1.0} \tag{4.15}$$

At the inlet of section III

$$Cl'_{i3} = \frac{V_2 C'_{i2}|_{Z_2=1.0} + (V_3 - V_2)}{V_3} \tag{4.16}$$

At the inlet of section II

$$Cl'_{i2} = C'_{i1}|_{Z_1=1.0} \tag{4.17}$$

At the inlet of section I

$$Cl'_{i1} = (C'_{i4}|_{Z_4=1.0})\frac{V_4}{V_1} \tag{4.18}$$

The system of coupled differential equations described by equations (4.10) - (4.14) has been solved from transient to steady state conditions by the method of orthogonal collocation. Equations (4.10) and (4.11) with boundary conditions represented by Equations (4.13) and (4.14) may be expressed in the collocation form [8] for component A and section 1 as

$$\frac{dC'_{A,1,j}}{d\tau} = F_1[(\frac{1}{Pe_1}B_{j,1} - A_{j,1})C'_{A,1,1} + \gamma_1 A_{j,1}Q'_{A,1,1} + (\frac{1}{Pe_1}B_{j,M2} - A_{j,M2})C'_{A,1,M2}$$

$$+ \gamma_1\Phi A_{j,M2}Q'_{A,1,M2} + \sum_{i=2}^{M1}(\frac{1}{Pe_1}B_{j,i} - A_{j,i})C'_{A,1,i} + \gamma\Phi\sum_{i=2}^{M1}A_{j,i}Q'_{A,1,i}$$

$$- \Psi K\Phi\alpha_1\{\frac{C'}{1 + \lambda_A(C'_{A,1,i} - 1) + \lambda_B(C'_{B,1,i} - 1)} - Q'_{A,1,i}\}] \tag{4.19}$$

Boundary conditions are written as

$$(C'_{A,1,i} - CHZ) = \frac{1}{Pe_1}(A_{1,1}C'_{1,i} + A_{1,M2}C'_{1,M2} + \sum_{i=2}^{M1}A_{1,i}C'_{1,i}) \tag{4.20}$$

and

$$A_{M2,1}C'_{A,1,1} + \sum_{i=2}^{M1}A_{M2,i}C'_{A,1,i} + A_{M2,M2}C'_{A,1,M2} = 0 \tag{4.21}$$

where $CHZ = Cl'_{A,1}$.

The detailed derivation of equations (4.19), (4.20) and (4.21) is shown in the Appendix. Similar, equations have been developed for all the four sections.

For the system in the present study, two columns in section IV, three columns in sections II and III and four columns in section I have been considered. This system configuration was used by Ching et al. [6], in their experiments. Sixteen collocation points were used for each section which requires solution of 256 simultaneous nonlinear ordinary differential equations. The above sets of differential equations have been solved using the functional iteration method.

4.3 RESULTS AND DISCUSSION

4.3.1 Effects of Process Parameters on Separation

The proposed theoretical model was solved for different cases to observe the effects of various parameters on the performance of the system. In Table 4.1, a set of parameters for the MEA-MOH system is tabulated which was reported by Ching et al. [7] and Hidajat et al. [11] and have been considered to be our base case. The results of the numerical simulation from transient to the steady state conditions for various system parameters are shown in Figures 4.2 to 4.7. The effect of these changes in parameters on the different dimensionless groups are shown in Table 4.2. It may be noted here that the mass transfer resistance for MEA-MOH system has been reported to be very low [6], and therefore the dimensionless parameter α has no effect on the system performance.

The results of the present simulation is analyzed in terms of degree of separation in extract and raffinate, which is defined as $E = \frac{C'_A - C'_B}{C'_A + C'_B}$ and $R = \frac{C'_B - C'_A}{C'_A + C'_B}$ where E and R refers to the extract and raffinate phases and C'_A and C'_B are dimensionless concentrations of MEA and MOH respectively. Using this definition the degree of separation can be represented in a -1 to +1 scale. As the degree of separation approaches towards 1 a better separation is achieved. On the other hand, when degree of separation approaches to -1 it means that E phase is component B rich and in the R phase concentration of component A which is the strongly adsorbed species is high. At degree of separation 0 there is no separation between the components.

From Figure 4.2, it can be seen that for 4,3,3,2 bed configuration, a relatively pure product can be obtained in both extract and raffinate streams. When the sizes of the sections are doubled the separation improves. But when the bed number is reduced by one in each section, the separation becomes relatively poorer in the extract. The steady state concentration shows that both the previous configurations produce relatively pure products.

It is also observed that except the E curve of 3,2,2,1 configuration, all curves reach steady state after about 1000 mins. In case of 3,2,2,1 arrangement the E curve takes about 1500 mins. to attain the steady state. The change in column configuration has a tremendous effect on all of the dimensionless groups of Table 4.2 except for γ. The γ criterion for good separation as described by Ching et al.[6,7] which is

section IV: $\gamma_{IV1} > 1, \gamma_{IV2} > 1$
section III: $\gamma_{III1} > 1, \gamma_{III2} < 1$
section II: $\gamma_{II1} > 1, \gamma_{II2} < 1$
section I: $\gamma_{I1} < 1, \gamma_{I2} < 1$

is followed in all sections. If γ values are compared for both 8,6,6,4 and 3,2,2,1 configurations, it can be seen that they are identical and match exactly with that of the base case. Besides γ, at 8,6,6,4 configuration Peclet numbers for all four sections are increased by about 100%. On the other hand, at 3,2,2,1 arrangement flow ratio Fs are decreased by 30%, while the Peclet numbers are reduced by 100%. Therefore, it can be concluded that the degree of separation is more strongly dependent on γ, rather than other dimensionless numbers.

Figure 4.3 shows the effect of switch time on degree of separation. It is clear that the switch time of 22.1 min gives the best product separation among the three switch times reported here. When the switch time is increased to 30.4 min the degree of separation is reduced both in the extract and raffinate phases. This behavior can be explained by the change in the dimensionless groups. The change in switch time affects the solid phase velocity which eventually changes the Peclet numbers since the dispersion coefficient used in the definition of Peclet number is taken to be a function of equivalent solid phase velocity also. At a 15 min switch time and at a 30.4 min switch time the magnitudes of Peclet numbers are decreased and increased respectively by about 20% and 30%. Since γ is a strong function of solid phase velocity, the effect is quite significant. At a switch time of 30.4 min γ_{1B} is less than 1 and thus fall into the bad separation category. On the other hand, at a 15 min switch time, the magnitude of γ for MOH in section 3 and 2 and γ for MEA in section 1 are greater than 1 which violate conditions of good separation. At lower switch time, though the raffinate produces almost pure MEA instead of MOH, as indicated by degree of separation (-1), low concentration of MOH in extract makes this switch time unacceptable.

The effect of individual bed length while keeping the bed configuration of the base case is shown in Figure 4.4. For bed length of 50 cm, separation in both raffinate and extract has become poorer. In case of bed length of 200 cm raffinate gives pure MEA, however, the difference between MEA and MOH is very low in the extract. Among these bed lengths, only the 100 cm long columns produce concentrated MEA and MOH. Though change in bed length has changed the dimensionless parameters of Table 4.2 moderately, it affects the γ values in all the four sections. It is clear from Table 4.2 that at higher bed length γ values for MOH in sections 2 and 3 and of MEA in section 1 are much higher than 1 and thus fall into the poor separation category. At a bed length of 50 cm γ for MOH in sections 3 and 4 and γ for MEA in sections 2 and 3 are less than 1 while result in a worse separation. The magnitudes of Peclet numbers in all four sections are increased or decreased by 30% when the individual bed length is increased or decreased by a factor of two. At 50 cm bed length curves E and R reach steady state at about 500 and 1500 mins. The E curve shows a peculiar behavior at lower time, the degree of separation drops sharply to -1 level and then slowly increases to its steady state value.

The effect of column diameter is shown in Figure 4.5. At a diameter of 5.5 cm, separation in both extract and raffinate is very good but with the increase or decrease of diameter slightly, the degree of separation decreases both in extract and raffinate streams. The change in column diameter changes the flow rates in each section and thereby changing all the dimensionless parameters except the Fs of Table 4.2. At a diameter of 6 cm which is about 10% more than that of the base case, Peclet numbers are increased by 10%. At a 5.1 cm column diameter, the above mentioned parameters are decreased by the same percentile. At a diameter higher than that of the base case, γ values are following the specified criterion for good separation but in case of lower column diameter, γ values for MOH are not less than 1 in both sections 3 and 2 which is required for better separation.

Figure 4.6 depicts the effect of eluent flow rate on the performance of the system. The degree of separation is largest when the eluent flow rate is 87.4 ml/min. As the eluent rate is increased to 100 ml/min, the degree of separation decreases to 0.5. At an eluent rate of 75.0 ml/min separation becomes zero. This behavior can be explained from the γ values reported in Table 4.2. At higher eluent rate γ of MOH in section 4 is less than 1 and thus violates the criterion of good product purity. On the other hand, at a low flow rate, γs for MOH in section 2 and 3 and γ for MEA in section 1 are much higher than 1 which leads to a poorer separation. Besides γ, other parameters are not significantly affected by change in eluent rates though this change is affecting the fluid phase velocity in all four sections. The concentration profiles in unsteady region for both higher and lower eluent rates are quite interesting. At an eluent rate of 100 ml/min curve R reaches to its steady state value at about 2000 mins. It may be further observed that at lower time up to 1200 mins it produces almost pure MOH in the raffinate stream after which the degree of separation drops to 0.4. At a lower eluent rate the unsteady profiles for both E and R show that both the curves drop to zero separation, which is their steady state value after about 1800 mins of operation.

Figure 4.7 shows the effect of feed flow rate. It can be seen that at feed rates of 5.0 and 3.0 ml/min degree of separation is almost equal and the magnitudes are approximately 1 in both extract and raffinate, which indicates a very efficient separation. At higher feed rates the degree of separation in both the streams declined. As can be seen from Table 4.2, at both at high and low feed flow rates γ values obey the good separation criterion. However in section 4 at high feed flow rate γ for MOH is very close to one which leads to a relatively poorer product composition. The unsteady profiles of both E and R curves for both base case and a feed flow rate of 3 ml/min are quite similar. In both the cases curve R reaches steady state instantly but curve E attains its steady state value after about 1300 mins. At a feed rate of 10 ml/min, curve E reaches to its steady state value at about 1500 mins and curve R at 2300 mins. But up to about 1500 mins. the degree of separation in R stream was +1 and after that it drops down to its steady state degree of separation of 0.6. It may be noted however that the change in feed flow rates have changed only the parameter values of postfeed sections.

4.3.2 Comparison with Experimental Data

4.3.2.1 Linear System

In Figure 4.8, results of the steady state solution of the present model is presented for the limiting case of linear system (glucose-fructose) for which the parameters are taken from the reported values of Ching and Ruthven [6] and are presented in Table 4.2. In this figure results obtained from experimental studies of Ching and Ruthven [6] are also shown. From this figure it can be concluded that the present model, which is a more general one, provides a good representation of the performance of a equivalent continuous countercurrent adsorption system.

4.3.2.2 Nonlinear System

In order to check the validity of the present model for nonlinear system, computations were performed for the MEA-MOH system. Figure 4.9 shows a comparison between the steady state solution of the present model for the MEA-MOH system and the experimental results reported by Ching et al. [7] and Hidajat et al. [11]. This figure shows the profile when only MEA follows a Langmuir type of equilibrium isotherm but MOH follows linear relationship and there is no isotherm dependency between MEA and MOH. All the curves agree very well with the experimental results. Also shown in this figure are the profiles if both isotherms were chosen linear. It is evident that the prediction is not good with linear isotherm assumption.

In Figures 4.10, the performance of the system is shown for the case when a nonlinear binary Langmuir for of isotherm for MEA and linear isotherm for MOH are considered. This would make the isotherms coupled as can be observed from equation 4.11. It can be seen from this figure that concentration and purity of product in both extract and raffinate streams become poorer compared to uncoupled case.

4.4 CONCLUSIONS

A theoretical model of 'SORBEX' system for unsteady state is developed for nonlinear MEA-MOH system. The model equations are solved to investigate the effect of various process parameters on the performance of this widely used countercurrent adsorption system. The present study reveals that the system performance as well as dynamics are very much dependent on some physical parameters of the system, viz. bed length and diameter of the adsorption columns. Other operating parameters like feed flow rate, eluent flow rate and switch time affect the performance of the process considerably. The system is very sensitive to these parameters and should be chosen carefully.

The results obtained for the case of MEA-MOH, when MEA follows nonlinear (Langmuir) and MOH follows linear equilibrium isotherms, were compared with the experimental and theoretical results of Ching et al. [7] and Hidajat et al. [11] at steady state. Also the glucose-fructose systems was investigated and compared with result of Ching et al. [6]. Good agreements are observed with the predictions from the present model for both systems.

The effects of various parameters were obtained for uncoupled isotherm relation between MEA and MOH. The effect of coupling between the isotherms on the system performance was also computed which indicated that the overall performance becomes poorer. The present model can be employed to predict the performance of countercurrent adsorption systems for various combinations of isotherm relationship, viz. linear-linear, linear-nonlinear and nonlinear - nonlinear etc. The above features make the present model more general and versatile for simulation of continuous countercurrent systems from unsteady to steady state conditions for various types of equilibrium isotherms.

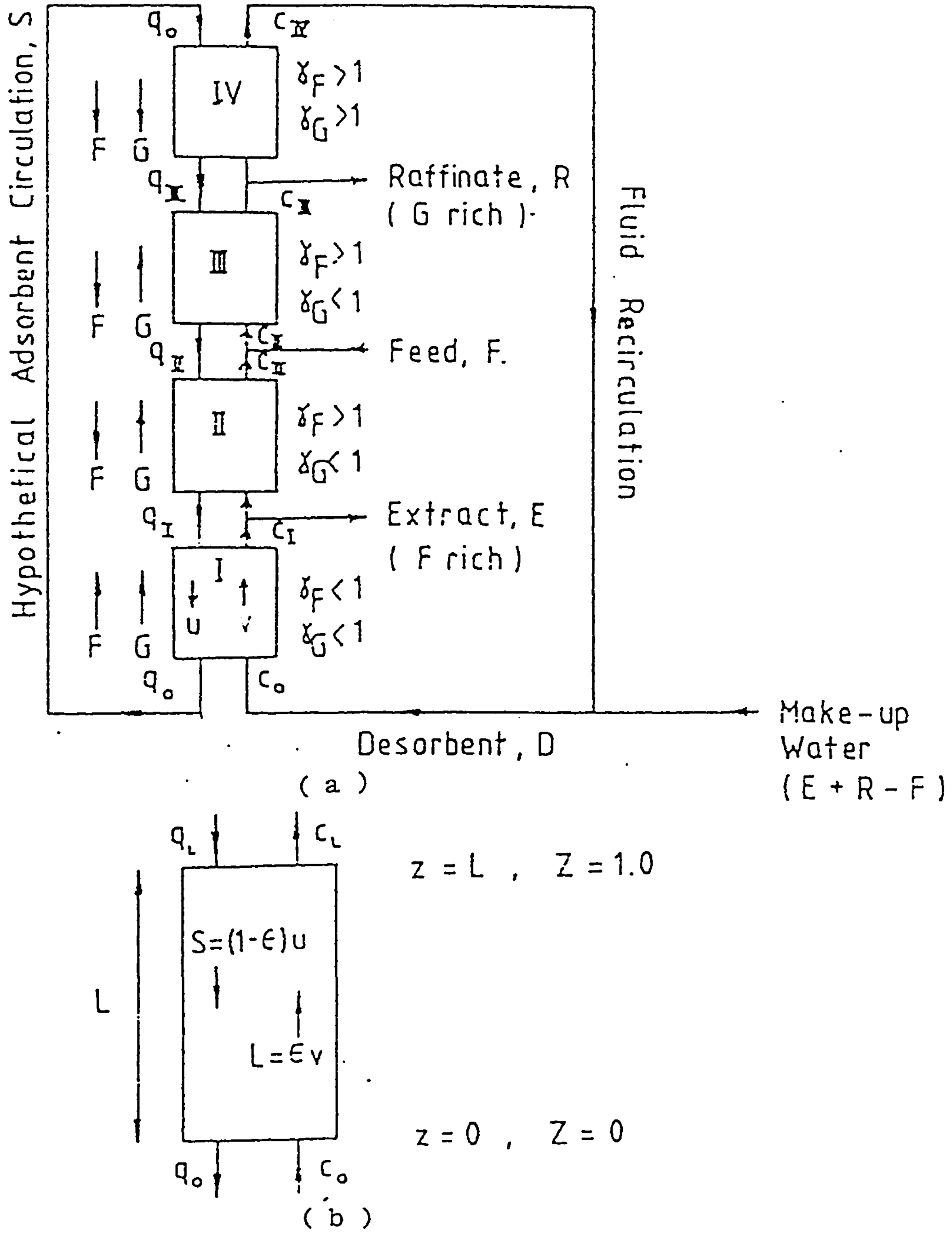

Figure 4.1(a) Schematic diagram of 4-section equivalent countercurrent system.

(b) Schematic diagram of the mass balance of jth section for 4-section equivalent countercurrent model.

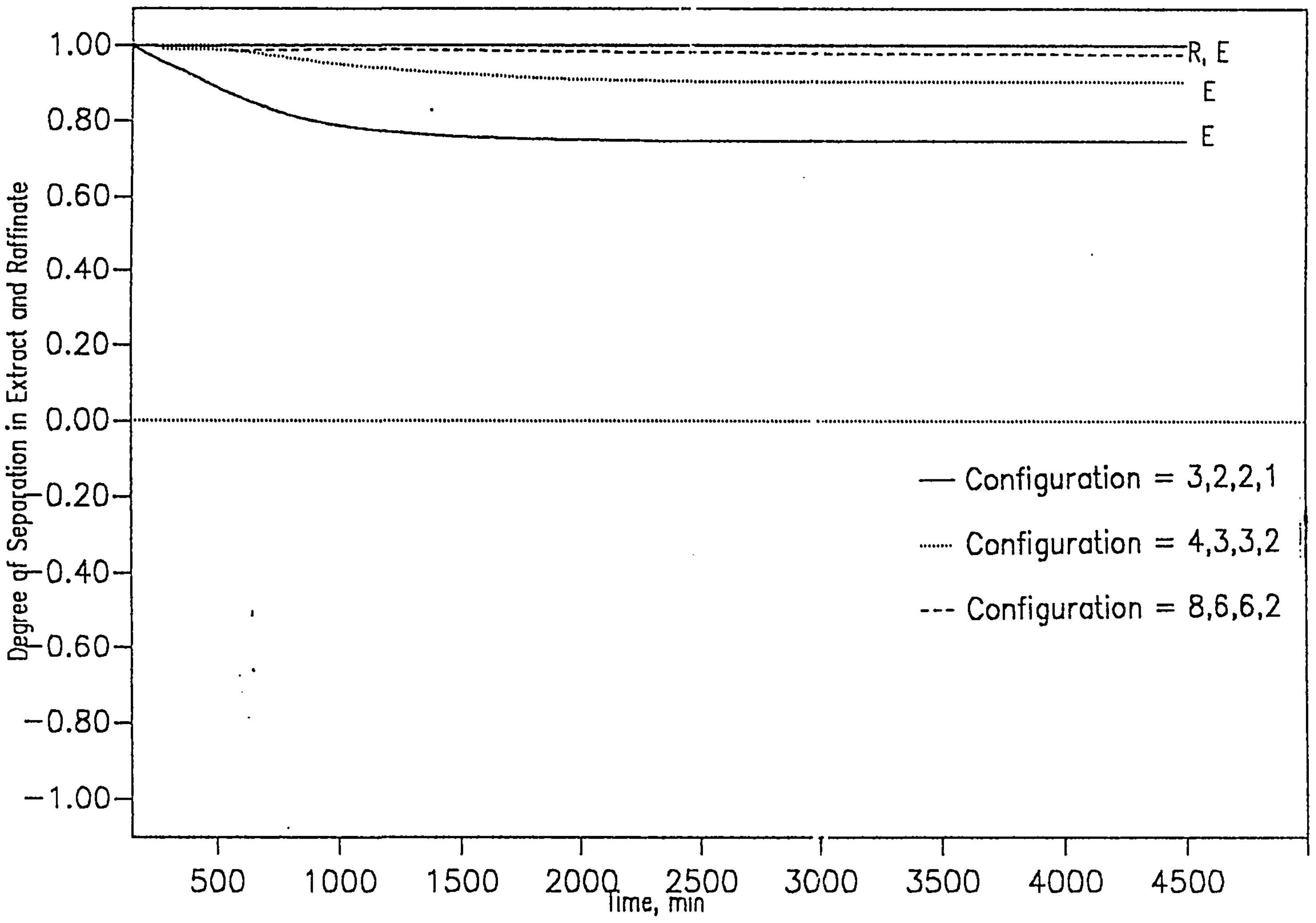

Figure 4.2 Effect of configuration on the performance of the 4-section equivalent system.

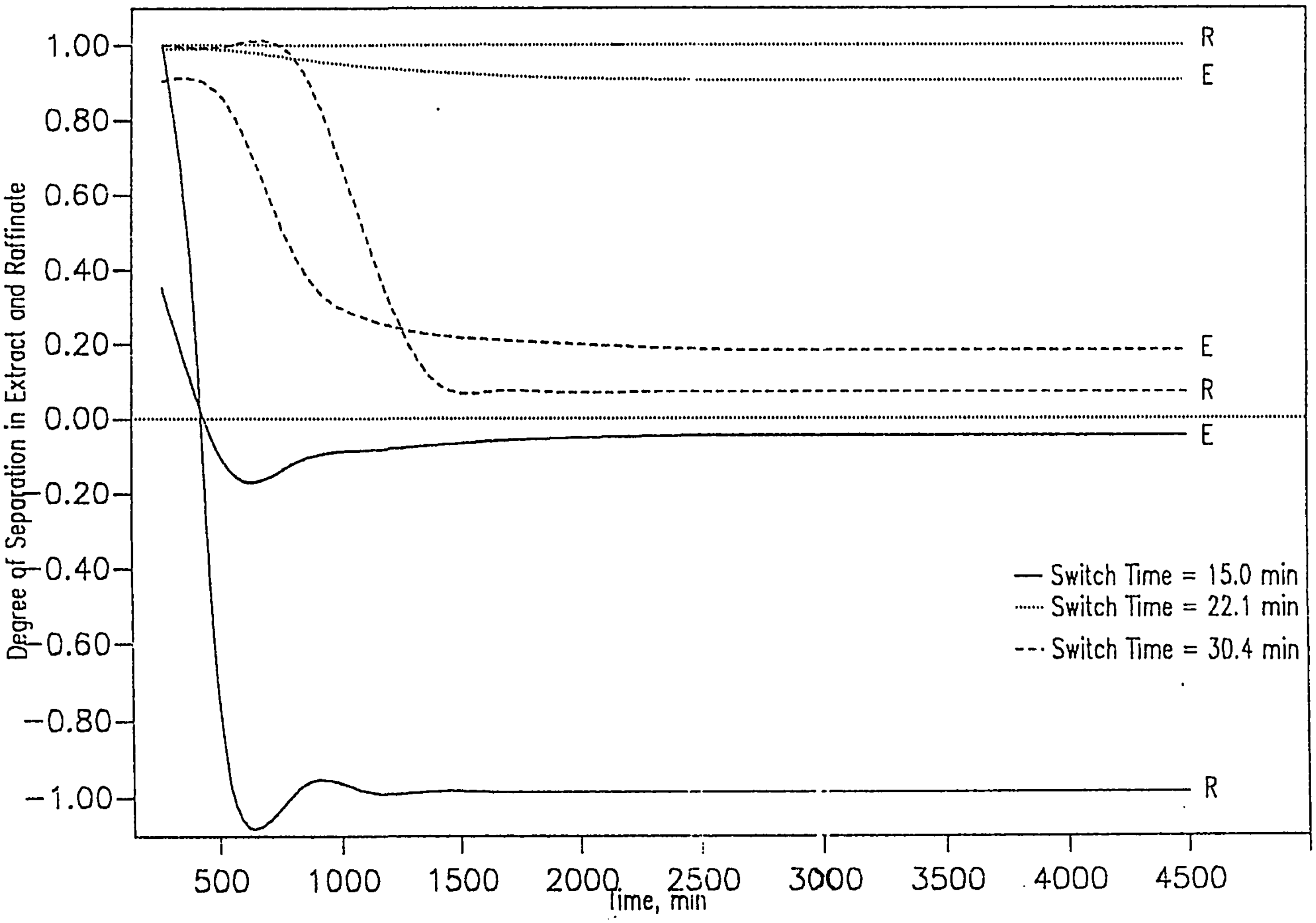

Figure 4.3 Effect of switch time on the performance of the 4-section equivalent system.

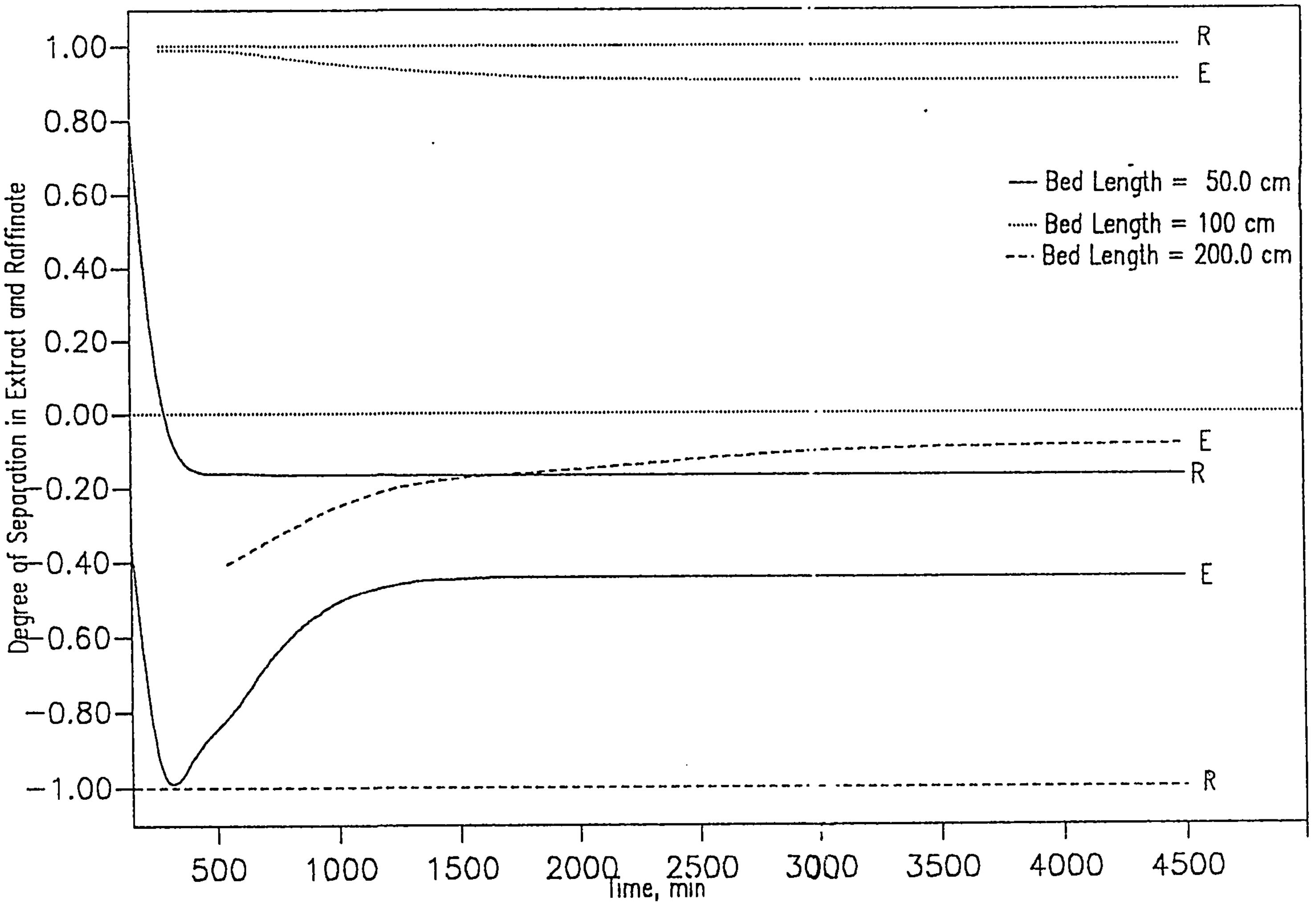

Figure 4.4 Effect of individual bed length on the performance of the 4-section equivalent system.

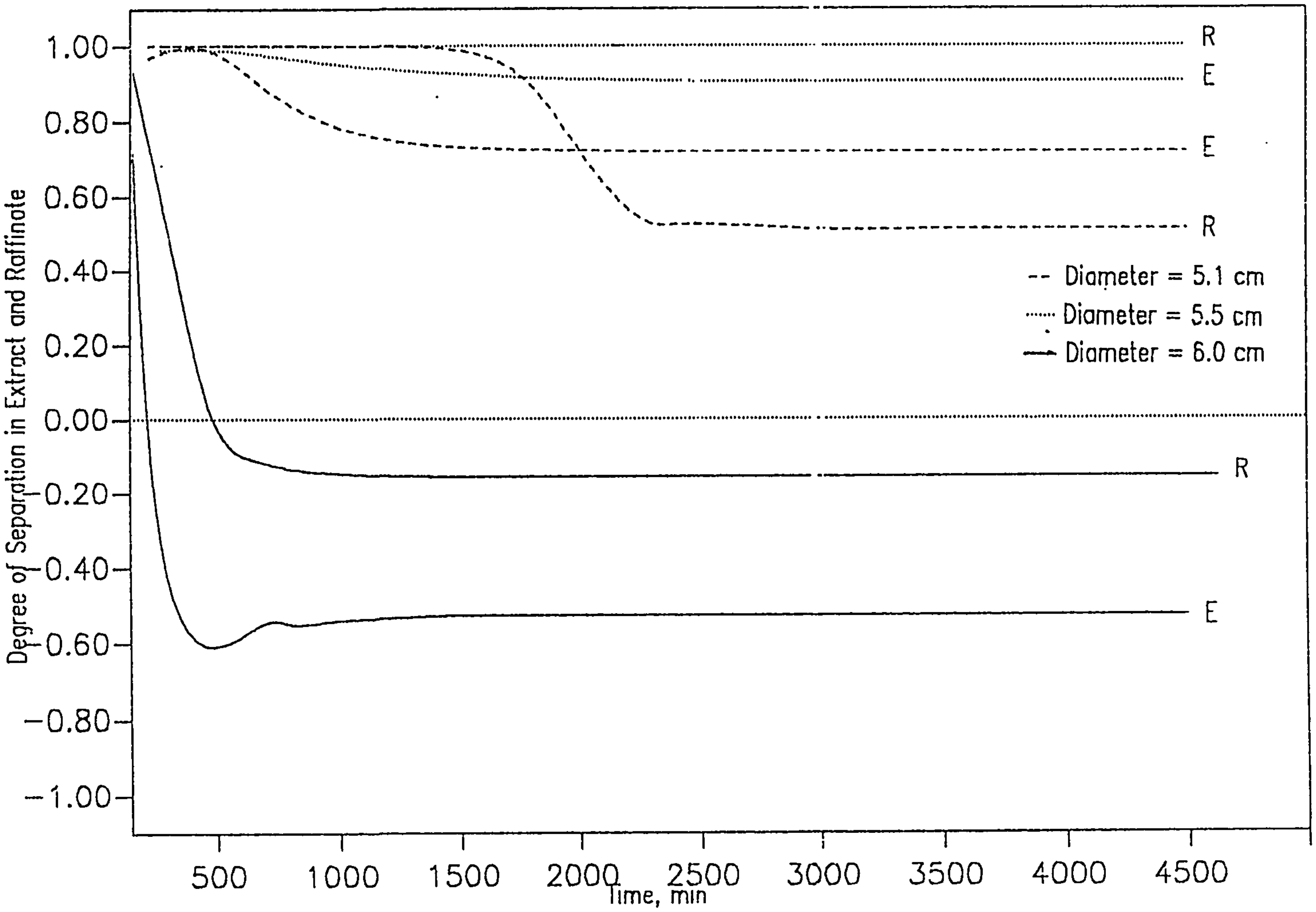

Figure 4.5 Effect of column diameter on the performance of the 4-section equivalent system.

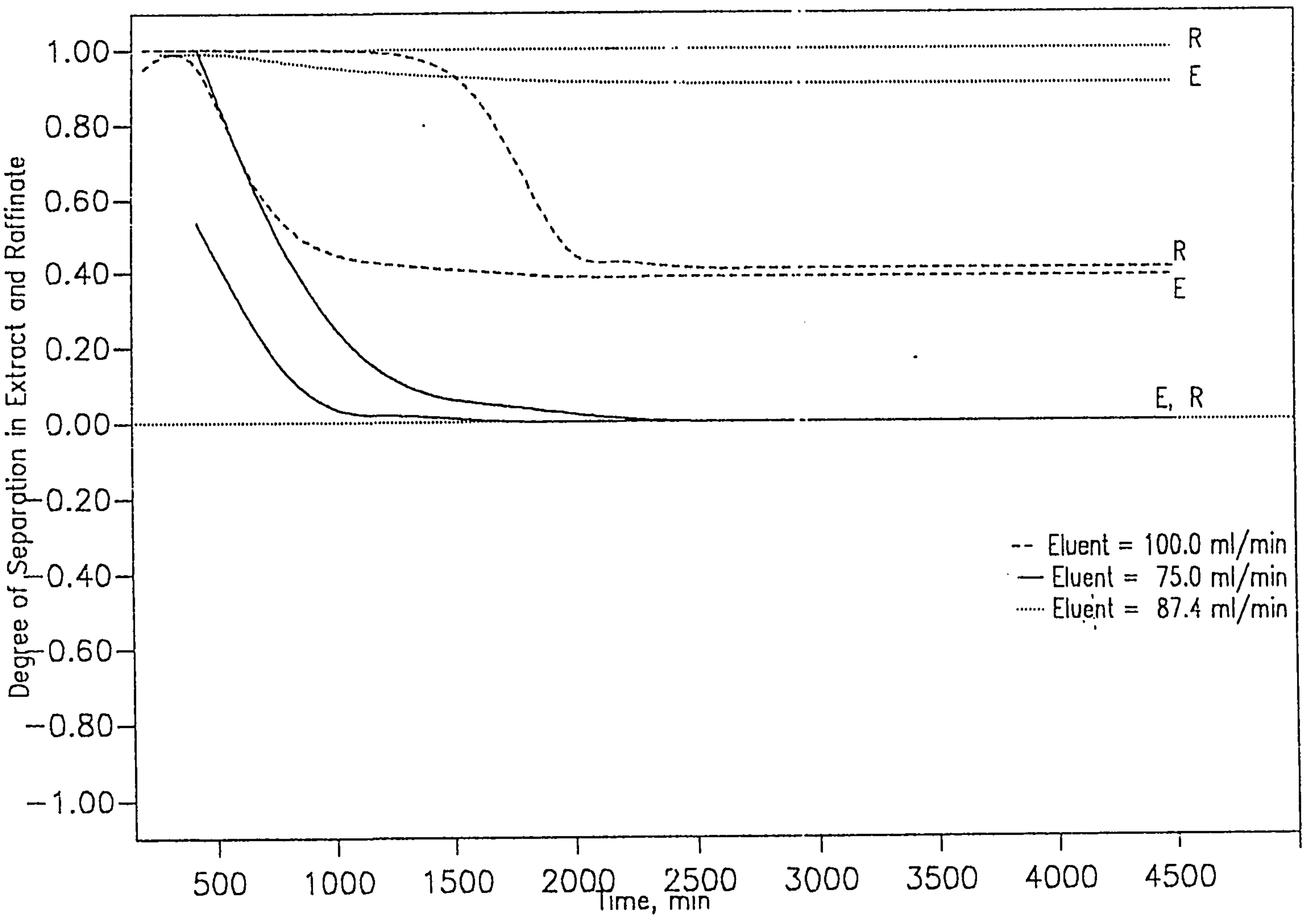

Figure 4.6 Effect of eluent flow rate on the performance of the 4-section equivalent system.

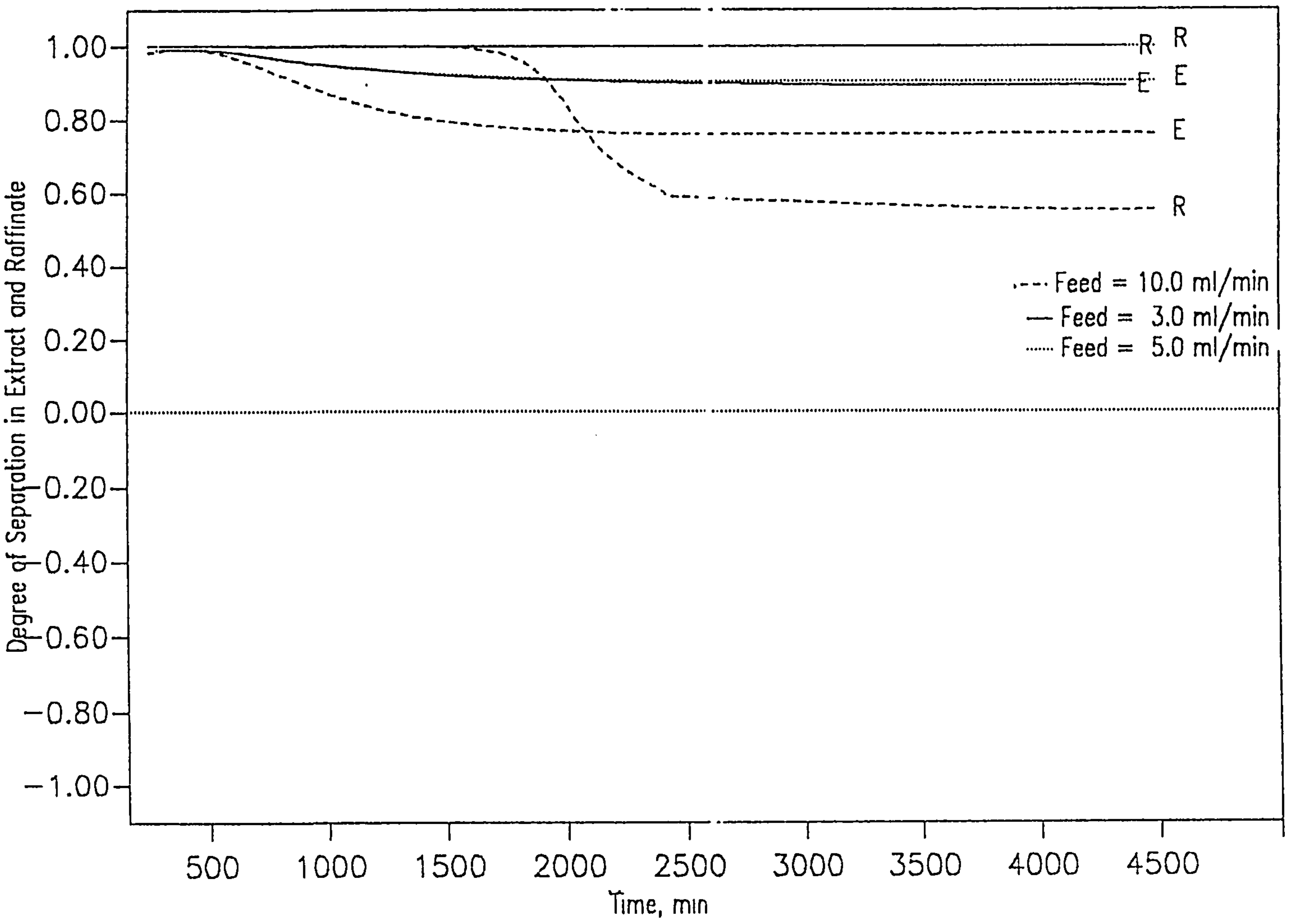

Figure 4.7 Effect of feed flow rate on the performance of the 4-section equivalent system.

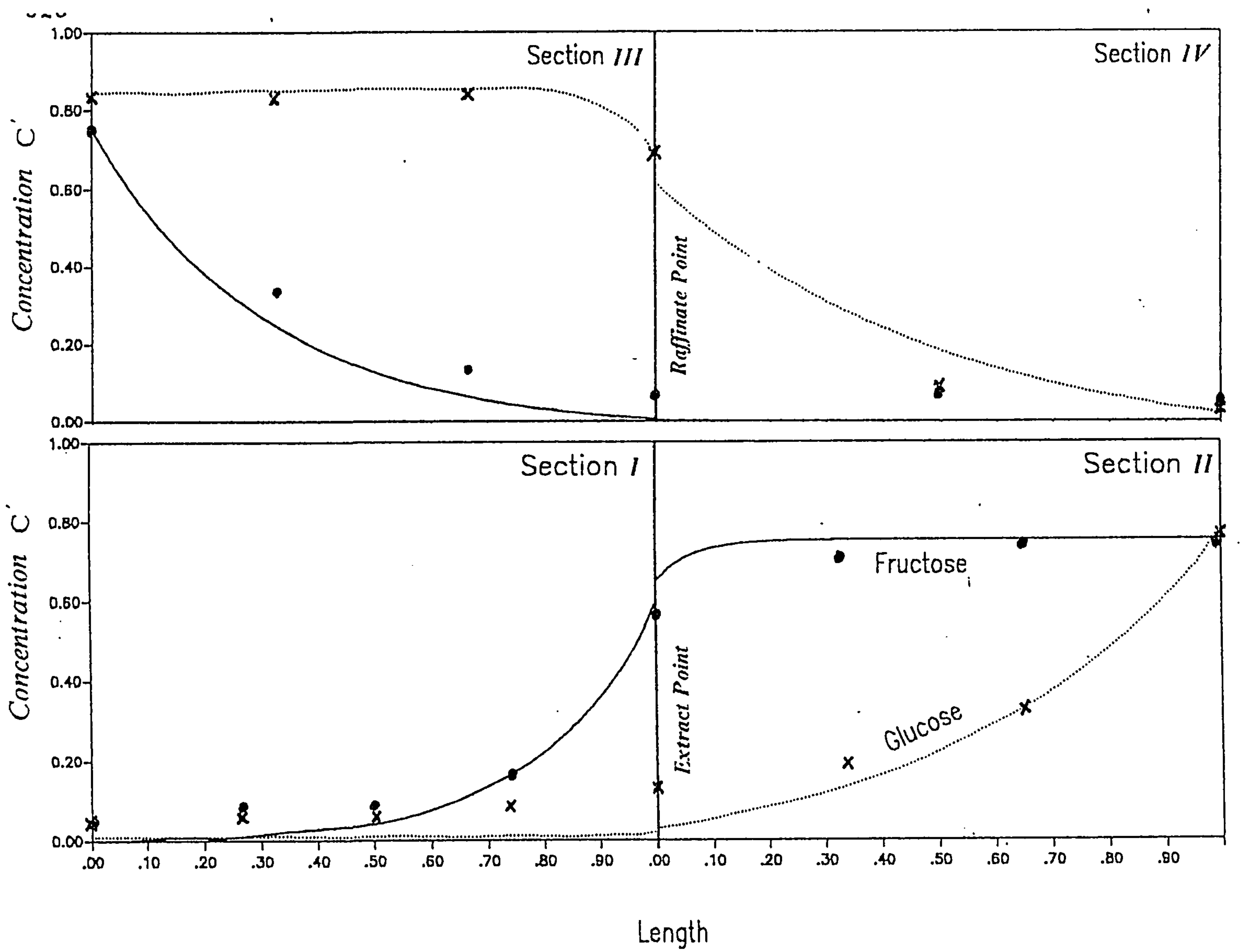

Figure 4.8 Experimental and theoretical concentration profile of glucose and fructose.(Experimental;Glucose x, Fructose •).

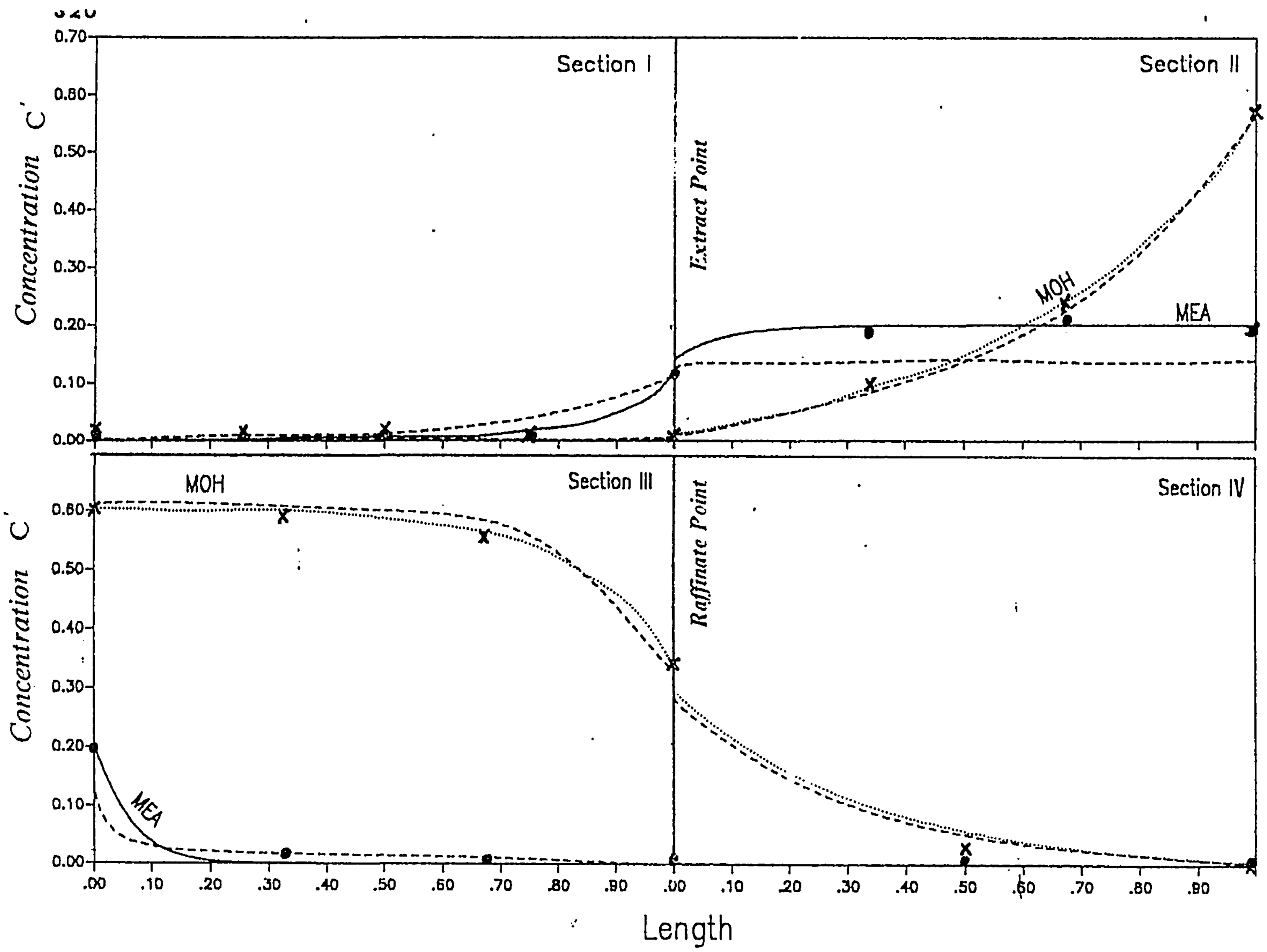

Figure 4.9 Experimental and theoretical concentration profile of monoethanolamine and methanol. (Experimental;MEA• , MOH×).

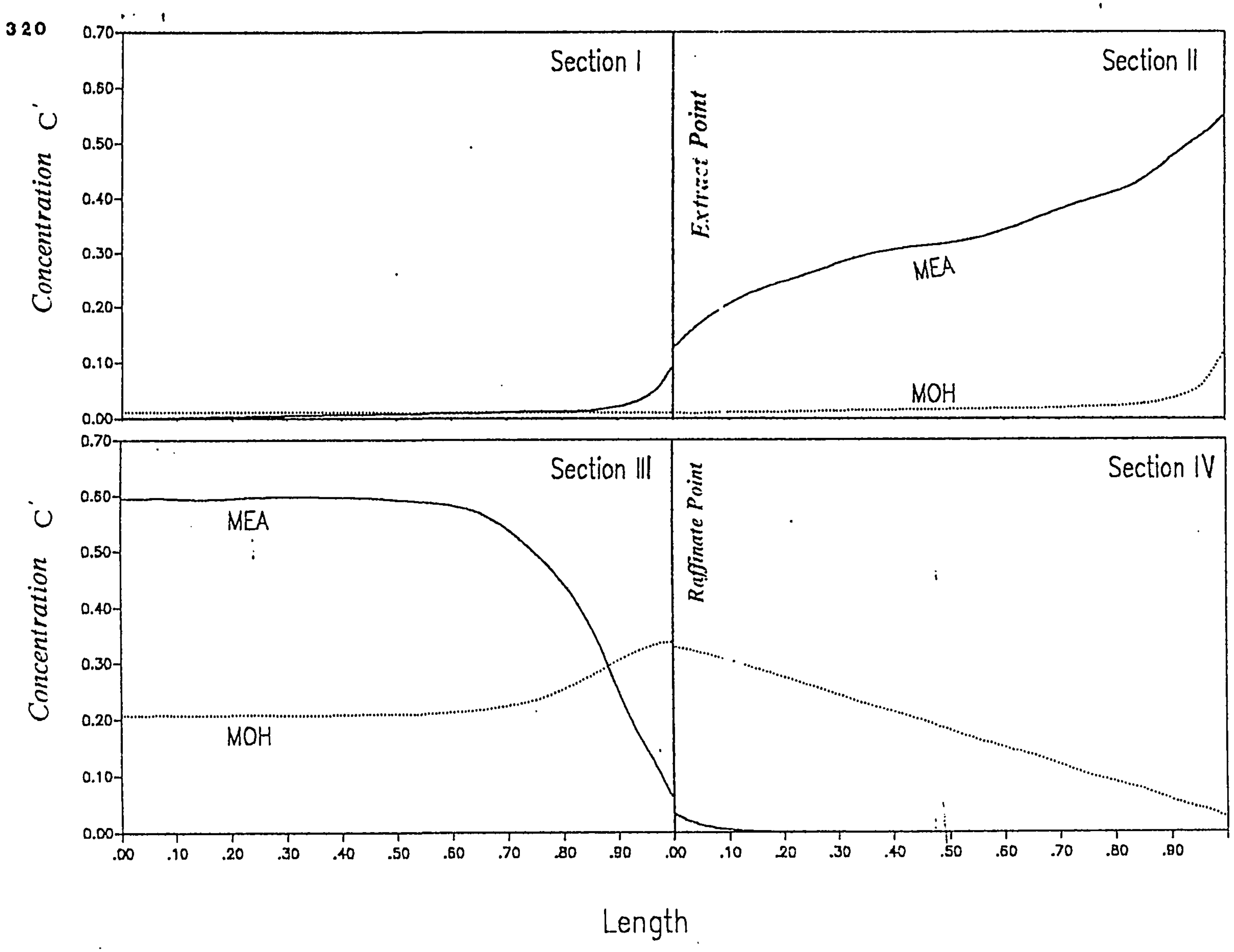

Figure 4.10 Effect of coupling between isotherms on the concentration profile of MEA-MOH system.

Table 4.1 Parameter values for the Glucose-Fructose and MEA-MOH system

Parameter	Linear case of Ching and Ruthven [6]	Nonlinear case of Ching et al.[7]
Feed composition (%A,%B)	5,5	20,10
Switch Time,min	30.5	22.1
Feed flowrate,ml/min	10.0	5.0
Desorbent rate,ml/min	38.8	87.4
Raffinate rate,ml/min	13.8	13.7
Extract rate,ml/min	16.8	44.0
Bed length,cm	100	100
Configuration	4,3,3,2	4,3,3,2
Column diameter,cm	5.1	5.5
$\lambda(A,B)$	0.0, 0.0	0.435,0.0
K_A	0.88	1.24
K_B	0.50	0.63

A = Fructose/MEA, B = Glucose/MOH

Table 4.2 Effect of process parameters on dimensionless groups for nonlinear MEA-MOH system.

													Section 4		Section 3		Section 2		Section 1	
Effect		F_3	F_2	F_1	Pe_4	Pe_3	Pe_2	Pe_1	α_4	α_3	α_2	α_1	γ_1	γ_2	γ_1	γ_2	γ_1	γ_2	γ_1	γ_2
Base		0.93	0.83	1.26	17.9	31.77	30.1	53.62	12.05	12.96	14.45	9.57	2.31	1.17	1.65	0.84	1.84	0.94	0.92	0.465
Diameter	(6)	0.93	0.83	1.26	19.4	34.01	32.4	56.22	10.36	11.14	12.43	8.2	1.98	1.01	1.42	0.722	1.58	0.81	0.79	0.40
cm	(5.1)	0.93	0.83	1.26	16.2	29.16	27.5	50.45	14.34	15.42	17.20	11.39	2.74	1.39	1.97	.999	2.19	1.11	1.09	0.553
Eluent	(100)	0.86	0.79	1.06	21.0	35.19	33.9	55.94	8.84	10.28	11.20	8.36	1.69	0.86	1.31	0.66	1.43	0.73	0.80	0.41
ml/min	(75)	1.08	0.93	1.68	13.7	27.34	25.1	50.84	18.75	17.43	20.24	11.1	3.59	1.82	2.22	1.13	2.58	1.31	1.07	0.542
Feed	(10)	0.90	0.73	1.10	19.20	33.23	30.1	53.62	10.53	11.75	14.45	9.57	2.01	1.02	1.50	0.76	1.84	0.94	0.92	0.465
ml/min	(3)	0.95	0.88	1.34	17.3	31.14	30.1	53.62	12.79	13.52	14.45	9.57	2.45	1.24	1.72	0.876	1.84	0.94	0.94	0.465
Bed Length	(200)	0.93	0.83	1.26	23.0	43.21	40.2	80.64	24.10	25.92	28.91	19.14	4.61	2.34	3.31	1.68	3.69	1.87	1.83	0.93
ml/min	(50)	0.93	0.83	1.26	12.3	20.77	20.1	32.1	6.03	6.48	7.23	4.78	1.15	0.59	0.83	0.42	0.92	0.47	0.46	0.233
Configuration	(8664)	0.93	0.83	1.26	35.7	63.54	60.3	107.23	24.10	25.92	28.91	19.14	2.31	1.17	1.65	0.84	1.84	0.94	0.92	0.465
	(3221)	0.7	0.63	0.84	8.9	21.18	20.1	40.21	6.03	8.64	9.64	7.18	2.31	1.17	1.65	0.84	1.84	0.94	0.92	0.465
Switch Time	(30.4)	0.93	0.83	1.26	21.0	36.45	35.0	59.0	12.05	12.96	14.45	9.57	1.68	0.85	1.20	0.61	1.34	0.68	0.67	0.338
min	(15)	0.93	0.83	1.26	14.2	26.0	14.4	46.38	12.05	12.96	14.45	9.57	3.40	1.73	2.44	1.24	2.72	1.38	1.35	0.685

REFERENCES

(1) Bieser, H.J. and deRosset, A.J., 28th Starch Convention, Detmold, West Germany, 27-29 April (1977)

(2) Broughton, D.B., U.S. Patent 3,291,726, 13 December 1966

(3) Broughton, D.B., Chem. Eng. Prog., 64, 60 (1968)

(4) Broughton, D.B., Euzil, R.W.N, Pharis, J.M. and Brearley, C.S., Chem. Eng. Prog., 66, 70 (1970)

(5) Ching, C. B., Hidajat, K., Ho, C., and Ruthven, D. M., Chem. Eng. Sci., 42, 2547-2555 (1987).

(6) Ching, C. B., Ruthven, D. M., and Hidajat, R., Chem. Eng. Sci., 40, 1411-1417 (1985).

(7) Ching, C. B., Ho, C., and Ruthven, D. M., Chem. Eng. Sci., 43, 703-711 (1988).

(8) Finlayson, B. A., Non linear Analysis in Chemical Eng., McGraw Hill, (1980).

(9) Hassan, M.M., Rahman, A.K.M.S., and Loughlin, K.F., Separation and Purification Methods, (submitted)

(10) Hidajat, K., and Ching, C. B., Trans I Chem. Eng., 68, 104-108 (1990).

(11) Hidajat, K., Ching, C. B., and Ruthven, D. M., Chem. Eng. J., 33, B55-B61 (1986).

(12) Neuzil, R. W., and Jensen, R. A., 85th National Meeting AICHE, Philadelphia, June 1978

(13) de Rosset, A. J., Neuzil, R. W., and Korous, D., Ind. Eng. Chem., Process Des. Dev., 15(2), 261-266 (1976).

(14) Ruthven, D. M., and Ching, C. B., Chem. Eng. Sci., 44(5), 1011-1038 (1989).

CHAPTER 5

A DETAILED MODEL FOR SIMULATED MOVING BED ADSORPTION SYSTEM

5.1 INTRODUCTION

Adsorption separations using simulated countercurrent operations are widely used for systems in which mass transfer resistances are very high. The countercurrent mode of operation is usually accomplished by mechanically moving the two phases in countercurrent directions, which is normally a complex and capital intensive operation. This disadvantage has been recently removed by the use of a simulated moving bed arrangement, in which the fluid inlet and outlet points are switched at intervals through a number of fixed adsorbent beds in order to simulate the effect of continuous countercurrent contacts. A number of important industrial separations which include the separation of glucose and fructose, monoethanolamine and methanol have been developed on the basis of this principle. The subject has been reviewed by deRosset et al. [15], and Ruthven and Ching [16]. Ching et al. in a series of papers[1-10], reported the results of an experimental and theoretical study of a small scale 'Sarex' unit for separating glucose and the experimentally observed behavior could be understood by modelling the system in terms of the equivalent true countercurrent system. Recently, a transient model with a general equilibrium isotherm has been presented on the basis of the same approximation [12,14]. Although such a model provides a useful representation of the actual system, it is based on a rather severe idealization and cannot be expected to account fully for the detailed behavior of the actual system. Therefore, in order to get a better insight to the dynamics in each column, a detailed model is required. Hidajat et al. [13] published their results of experimental and numerical simulation of a semi continuous adsorption unit by considering each column as a cascade of ideal mixing stages. By adopting the plate model, they considered each column to be equivalent to ten theoretical stages which they obtained from pulse chromatographic measurements [7]. Such an equivalence is possible only for a linear system. They developed their model for the linear system of glucose-fructose. But for a nonlinear system the process parameters are strongly coupled thereby making it difficult to develop the model with nonlinear equilibrium isotherms on the basis of the plate model.

In the present study, a more general model is therefore developed by writing the appropriate differential equations and relevant boundary conditions for each column. An axially dispersed plug flow model with linear driving force rate expression for mass transfer and binary Langmuir isotherm for equilibrium are considered. The boundary conditions for each column, which are time dependent have been written, and varied as per the switching operations.

Computations are performed for several cycles till the cyclic steady state is obtained. The effects of various process parameters, viz., eluent to feed ratio, Peclet number, bed length, switch time etc. on the system performance is investigated. The results obtained from the present model have been compared both for the linear glucose-fructose system and for the nonlinear MEA-MOH system with that of the equivalent models and with available experimental data.

5.2 THEORETICAL MODEL

The simulated continuous countercurrent system is described in Figure 5.1. To simulate the solid phase movement, feed input position is switched from one bed to another instead of recirculating the solid phase. This switching depends on the equilibrium and kinetic parameters of the system. Each time, with changing feed point and draw off position, material balance and boundary conditions are changed. After the feed location comes back to its original position at time $t = 0$, the system is considered to have completed one cycle.

The governing equations for the detailed model can be obtained from an overall mass balance around a differential volume of adsorber shown in

Figure 5.2. The following assumptions are adopted to formulate the model:

1) Axially dispersed plug flow of fluid.
2) Isothermal operating conditions.
3) Linear driving force expression for mass transfer rate.
4) Isotherms are of nonlinear Langmuir form.

The basic differential equation describing the system dynamics for ith component and jth bed can be written as

$$D_{L_j}\frac{\partial^2 c_{ij}}{\partial z_j^2} - V_j\frac{\partial c_{ij}}{\partial z_j} = \frac{\partial c_{ij}}{\partial t} + \left(\frac{1-\varepsilon}{\varepsilon}\right)\frac{\partial q_{ij}}{\partial t} \tag{5.1}$$

For Langmuir type of equilibrium isotherms, the rate equation can be written as

$$\frac{\partial q_{ij}}{\partial t} = k_i\left[\frac{b_i q_s c_{ij}}{1 + \sum_{i=1}^{k} b_i c_{ij}} - q_{ij}\right] \tag{5.2}$$

Initial Conditions

Initial condition of a bed at any particular time will be equal to the final condition of that bed at the previous switch time.

Boundary Conditions

at $z_j = 0$,

$$D_{L_j}\frac{\partial c_{ij}}{\partial z_j}\Big|_{z_j=0^+} = -V_j\left(c_{ij}\big|_{z_j=0^-} - c_{ij}\big|_{z_j=0^+}\right) \qquad (5.3)$$

at $z_j = L_j$,

$$\frac{\partial c_{ij}}{\partial z_j} = 0.0 \qquad (5.4)$$

Mass Balances

Material balances at the inlet of each bed except for the beds following the feed point and eluent point are

$$c_{i(j+1)^-} = c_{ij}\big|_{z_{L_j}}, \quad j \neq f \, or \, e$$

i.e. the concentration at the inlet of a bed is equal to the exit concentration of the previous bed.

Material balance for the beds following the feed point and eluent point are :

$$c_{if^-} = \frac{V_{f-1}c_{if-1}\big|_{z_{f-1}=L_{f-1}} + (V_f - V_{f-1})c_{if}}{V_f} \qquad (5.5)$$

$$c_{ie^-} = \left(c_{ie-1}\big|_{z_{e-1}=L_{e-1}}\right)\frac{V_{e-1}}{V_e} \qquad (5.6)$$

Using the following dimensionless variables

$$C'_{ij} = \frac{c_{ij}}{c_f};\ Q' = \frac{q}{q_f};\ \tau = \frac{t}{L_1/V_1};\ Z_j = \frac{z_j}{L_1};$$

the above equations can be written in dimensionless form for ith component and jth bed as

$$\frac{\partial C'_{ij}}{\partial \tau} = F_j\left[\frac{1}{Pe_j}\frac{\partial^2 C'_{ij}}{\partial^2 Z_j} - \frac{\partial C'_{ij}}{\partial Z_j} - \Psi K_i \Phi \frac{\partial Q'_{ij}}{\partial \tau}\right] \tag{5.7}$$

$$\frac{\partial Q'_{ij}}{\partial \tau} = \alpha_j\left[\frac{C'_{ij}}{1 + \sum_{i=1}^{k}\lambda_i(C'_{ij} - 1)} - Q'_{ij}\right] \tag{5.8}$$

Initial Conditions

Initial condition of a bed at any particular time will be equal to the final condition of that bed at the previous switch time.

Boundary Conditions and Mass Balances

Boundary conditions in general for all beds can be given by the following equations:

at $Z_j = 0.0$

$$Cl'_{ij^-} = C'_{ij}\big|_{Z_j=0^+} + \frac{1}{Pe_j}\frac{dC'_{ij}}{dZ_j}\Big|_{Z_j=0^+}, \tag{5.9}$$

at $Z_j = \frac{z_j}{L_1}$

$$\frac{dC'_{ij}}{dZ_j} = 0.0 \tag{5.10}$$

where Cl'_{ij} is the inlet concentration of each bed and can be obtained from the material balance equations.

Material balances at the inlet for each bed except for the beds following the feed point and eluent point can be expressed by :

$$Cl'_{ij+1} = C'_{ij}|_{Z_{L_j}}, \qquad j \neq f \, or \, e \tag{5.11}$$

or in other words, the concentration at the inlet of a bed is equal to the exit concentration of the previous bed.

Material balance for the beds following the feed point and eluent point are as follows:

$$Cl'_{if} = \frac{V_{f-1}C'_{if-1}|_{Z_{f-1}=L_{f-1}} + (V_f - V_{f-1})}{V_f} \tag{5.12}$$

$$Cl'_{ie} = (C'_{ie-1}|_{Z_{e-1}=L_{e-1}})\frac{V_{e-1}}{V_e} \tag{5.13}$$

It may be noted, however, that the flow rates in all beds of a particular section are equal but quite different than that of other sections.

After one switch time, the feed point and draw off position will be moved forward by one bed in clockwise direction and so also the boundary conditions. The system of coupled differential equations as described by equations (5.7) to (5.13) have been solved from transient to steady state conditions by the method of orthogonal collocation. Equations (5.7) and (5.8) with boundary conditions represented by equations (5.9) and (5.10) may be expressed in the collocation form [11] for component A and bed 1 as

$$\frac{dC'_{A,1,j}}{d\tau} = F_1[(\frac{1}{Pe_1}B_{j,1} - A_{j,1})C'_{A,1,1} + (\frac{1}{Pe_1}B_{j,M2} - A_{j,M2})C'_{A,1,M2}$$

$$+ \sum_{i=2}^{M1}(\frac{1}{Pe_1}B_{j,i} - A_{j,i})C'_{A,1,i}$$

$$- \Psi K \Phi \alpha_1 \{\frac{C'}{1 + \lambda_A(C'_{A,1,i} - 1) + \lambda_B(C'_{B,1,i} - 1)} - Q'_{A,1,i}\}]$$

(5.14)

Boundary conditions can be written as

$$(C'_{A,1,i} - CHZ) = \frac{1}{Pe_1}(A_{1,1}C'_{1,i} + A_{1,M2}C'_{1,M2} + \sum_{i=2}^{M1} A_{1,i}C'_{1,i}) \tag{5.15}$$

and

$$A_{M2,1}C'_{A,1,1} + \sum_{i=2}^{M1} A_{M2,i}C'_{A,1,i} + A_{M2,M2}C'_{A,1,M2} = 0 \tag{5.16}$$

where $CHZ = Cl'_{A,1^-}$.

The detailed derivation of equations (5.14), (5.15) and (5.16) are similar to those shown in Appendix A. Equations for all 12 beds can be written accordingly.

For the system in the present study, 12 columns with 4,3,3,2 configuration [9] respectively, have been considered. Five collocation points were used for each bed which requires solution of 240 simultaneous nonlinear ordinary differential equations. The above sets of differential equations have been solved using the functional iteration method.

5.3 RESULTS AND DISCUSSIONS

The present model is solved both for linear and nonlinear systems from transient to steady state using the parameter values reported by Hidajat et al. [13] and Ching et al. [10] which are listed in Table 5.1. The numerical runs are performed and plotted to study the dynamic behavior of these systems. Dimensionless concentrations are plotted with respect to bed number for different cycles. The effect of various process parameters on the performance of the system is investigated for nonlinear MEA-MOH system. Moreover, the steady state results of linear and nonlinear systems are compared with that of the experimental results reported in the literature.

5.3.1 Transient Behavior

Figures 5.3 to 5.6, summarizes the results of the transient concentration profiles for all the twelve beds till the cyclic steady state is achieved. Figures 5.3 and 5.4 represent the concentration profiles of glucose and fructose respectively. From these figures it can be seen that after 5 cycles of operation, i.e. after about 1830 minutes, both fructose and glucose reach their steady state profile. The qualitative concentration profiles after cycle 1 and 3 of both the components are similar to that of the steady state profile. In both Figures 5.3 and 5.4, feed is at 12th bed so according to the configuration, raffinate and extract are collected from the end of bed 2 and 8

With time the concentration of the raffinate product, which is mainly the weakly adsorbed species i.e. glucose, reaches to its steady state value of 0.65 while the concentration of other component, fructose, is about 0.02. The existence of discontinuities in concentrations between beds, as shown in these figures, which is pronounced especially between beds 4 and 5 and between beds 11 and 12 are due to the axially dispersed plug flow boundary conditions. Because of the introduction of eluent and feed, respectively after bed 4 and 11, discontinuities are quite significant at these positions. Figures 5.5 and 5.6 are similar plots of nonlinear MEA-MOH system.

According to the configuration the system can be divided into adsorption and desorption sections upon switching. After each switch a new bed is regenerated and included into the adsorption section, at the same time the first bed of the previous adsorption section arrives in the desorption section. The configuration shown in Figure 5.1, has 5 beds in the adsorption section and 7 beds in the desorption section. As can be seen from Figures 5.3 and 5.4, at 12th switch, bed 12 to bed 4 belong to the adsorption section. So the fluid phase concentration of the strongly adsorbed component, i.e. fructose, starts declining as it gets adsorbed faster onto the active sites of the solid adsorbent than glucose which results in almost pure glucose in the raffinate which is drawn from the end of bed 2. The concentration of glucose starts dropping right after bed 2 and reaches a minimum at bed 5. At this point the concentration of both fructose and glucose are almost zero. The water which is introduced at this point, desorbs the previously adsorbed fructose, is introduced at this point, desorbs the previously adsorbed fructose, therefore increasing the fructose concentration in the fluid phase. As a result almost pure fructose can be obtained in the extract stream which is drawn from the end of bed 8. Therefore due to the difference in degree of adsorption between components, a phase lag in concentration exists between the separable species. At the next switch the location of the feed as well as the location of other ports will be advanced one bed in the direction of fluid flow.

In case of MEA-MOH system, the transient profiles are drawn in Figures 5.5 and 5.6, the concentrations follow the same trend. Since the equilibrium constant of MEA is higher than MOH, it gets adsorbed very quickly after introduction of the feed at 12th bed and the concentration reaches to zero at the 2nd bed. After the introduction of the eluent at bed 5, the concentration front of MEA starts rising and at bed 10 reaches to its steady state values of 0.2. Comparison of Figure 5.5 to Figure 5.6 reveals that for MEA it takes about 3 complete cycles to reach steady state, whereas MOH requires more than 10 cycles.

In Figures 5.7 and 5.8, the change in concentration profiles of fructose and glucose in a particular bed are plotted respectively for twelve switches of a cycle at steady state. The corresponding plots for MEA and MOH are shown in Figures 5.9 and 5.10. These figures display how the concentration is changing with respect to switches.

It is also evident from these figures that there exist a transient concentration profile in each bed which is changing with change in switches, although the overall system has reached a cyclic steady state.

5.3.2 Effect of Process Variables

In order to examine the effects of the process variables viz. Peclet number, eluent to feed ratio, column length, switch time, etc., on the performance of the system several simulation runs were performed by changing only the corresponding parameter for the MEA (nonlinear)-MOH (linear) system. The effects of the process variables in terms of raffinate and extract compositions are tabulated in Table 5.2. It may be noted however that the reported concentrations are taken at the end of the switch time instead of time averaged values. The effect of Peclet number is quite large. As Peclet number increases, separation improves only in the raffinate stream. At a very high Peclet number, concentration of MOH in the raffinate reaches a very high level of 0.57 without losing its purity of 100%. But at this low dispersion, the compositions of both MEA and MOH in extract stream are zero. At high dispersion, i.e., at $Pe \rightarrow 0$, MOH concentration in the raffinate is too low and the purity of the product is also reduced. Though at low Peclet number, MEA concentration in extract is high compared to the moderate Peclet number, presence of high concentration of MOH makes this choice unacceptable. The product yield in both the streams are high and satisfactory at a moderate Peclet number.

The effect of eluent to feed ratio at constant feed flow rate is quite significant. Concentration of MEA in raffinate remains zero up to a ratio of 26 though the MOH concentration increases. At higher eluent flow rate, the MEA concentration increases while the MOH concentration decreases, thereby making the separation worse. In the extract, the concentration of MEA decreases with increase in ratio but concentration of MOH decreases to its minimum value of about zero then increases to 0.044 at a ratio of 52.

The concentration of each component, both in raffinate and extract decrease with increase in eluent to feed ratio at constant eluent flow rate. In raffinate, the concentration of MEA drops very sharply from 0.5 to zero when the feed flow rate is halved. After that,with increase in feed flow rate, the concentration of MEA remains unchanged, but the concentration of MOH decreases very slowly. In the extract stream the picture is quite similar to that of the raffinate; only both concentrations are declining very sluggishly. It can be noted here that at this eluent to feed ratio, the purity of both the component in extract and in raffinate is higher than that of the base case but this higher purity is achieved at the expense of lower concentration of MOH in the raffinate.

With increase of bed length, the MEA concentrations, both in raffinate and in extract first decrease to a minimum at a bed length of 100 cm, which is then followed by a slow rise. The MOH concentration in raffinate stream shows the opposite scenario rising to its maximum at 100 cm bed length. At a bed length higher or lower, the concentration is very low. In extract the profile reverse with the concentration of MOH minimum at 100 cm with a concave upward profile.

From Table 5.2, it is clear that the switch time has also a pronounced effect on the system performance. The MEA concentration in raffinate shows a concave upward profile with the minimum at zero at a 22.1 mins. switch time. Although the concentration drops very slowly between 15 and 22.1 minutes, it rises very sharply when the switch time is longer than 22.1 minutes. On the other hand, MOH concentration in the raffinate is a maximum at 22.1 minutes decreasing very sharply at longer or shorter switch times. In the extract stream, the concentration of MEA slowly decreases from 0.1 to almost zero when the switch time is increased by 100%. Conversely concentration of MOH first drops slowly to zero between 15 and 22.1 minutes, but at a switch time longer than 22.1 minutes, it rises very sharply reaching 0.54 at 30 minutes switch time.

From the above analysis, it may be observed that there exists an optimum combination of eluent to feed ratio, column length and switch time at which the system performance is best. This can be explained in terms of the residence time of each column during adsorption and desorption modes of operation. A longer residence time during the adsorption mode pushes the concentration front towards breakthrough. On the other hand, at shorter residence time, the regeneration of the column becomes inefficient. Therefore, both long and short residence times are unsuitable for best process performance. However, the final choice of the operating conditions for any given system would depend on the product purity and yield desired.

A comparison of the results obtained from the detailed model with that of the equivalent countercurrent model is also shown for the base case in Table 5.2. It is evident that the two models predicts almost the same concentrations in both raffinate and extract streams. However, the present model in addition gives a better insight into the profiles in each beds at all times. Further, due to the numerical nature of the problem, the detailed model simulation requires about one fourth computational time as compared to that of the countercurrent model for the same run. For instance, to solve the nonlinear MEA-MOH system for 10 complete cycles, the equivalent countercurrent model requires about 200 minutes CPU time whereas the detailed model needs only about 50 minutes of CPU time.

5.3.3 Comparison with Experimental Data

The results of the steady state solution of the detailed model is presented for linear and nonlinear systems in Figures 5.11 and 5.12 respectively, for which the parameters are taken from the reported values of Hidajat et al. [14]

and Ching et al. [10] which are given in Table 5.1. In these figures results obtained from the experimental studies of those authors using the same parameter values have also been presented. In both cases initially clean beds were assumed at the start of the first switch of the first cycle, and toward the cyclic steady state profile is reached after about 5 cycles for glucose-fructose system and 10 cycles for MEA-MOH system. The experimental data for glucose-fructose system is taken from the semi continuous countercurrent study of Hidajat et al. [13], which were obtained at the middle of each switch time. In the experimental study the samples were taken at the middle of a switch, while for the present theoretical study the concentrations at the end of each switches are reported. In the case of MEA-MOH system, the comparison with the experimental results of equivalent countercurrent study of Ching et al. [10] is shown in Figure 5.12. In this case the experimental results are also reported at the middle of the switch time. The difference in concentrations between their experimental data and the present theoretical results for both systems are due to the difference in sample analyzing time. This results in the difference of concentrations between the experimental and theoretical studies. From both the figures, it is clear that the locations of the product concentrations have been shifted by one bed due to the difference in the reported sampling time. Nevertheless, the agreement between the present model and experiment is quite satisfactory.

5.4 CONCLUSIONS

A theoretical detailed unsteady state model of continuous countercurrent adsorption system is developed and solved for 12 adsorption columns to examine the dynamics of each column.

The model equations were solved to study the change in concentration profiles in each bed with number of cycles, for the linear glucosefructose system and the nonlinear MEA-MOH system. The results obtained for these systems were compared with the experimental results of Ching et al. [10] and Hidajat et al. [13] respectively. Since the experimental data were reported at the middle of the switch time and the theoretical results are at the end of the switch time, there exists a small difference in concentration at each location. Further, the change in concentration of a particular bed at steady state with number of switches is shown both for linear and nonlinear systems. It can be seen from Figures 5.3 to 5.12 that the present model gives better insight into the transient and steady behavior of each column.

The model equations are also solved to investigate the effect of various process parameters (axial dispersion, eluent to feed ratio, bed length and switch time) on the performance of this extensively used countercurrent adsorption system. It is observed that the system is very sensitive to these parameters and thereby the product purity and yields are very much affected by slight change in any of these variables.

It is also seen that the numerical solution of the detailed model is faster than that of equivalent countercurrent model.

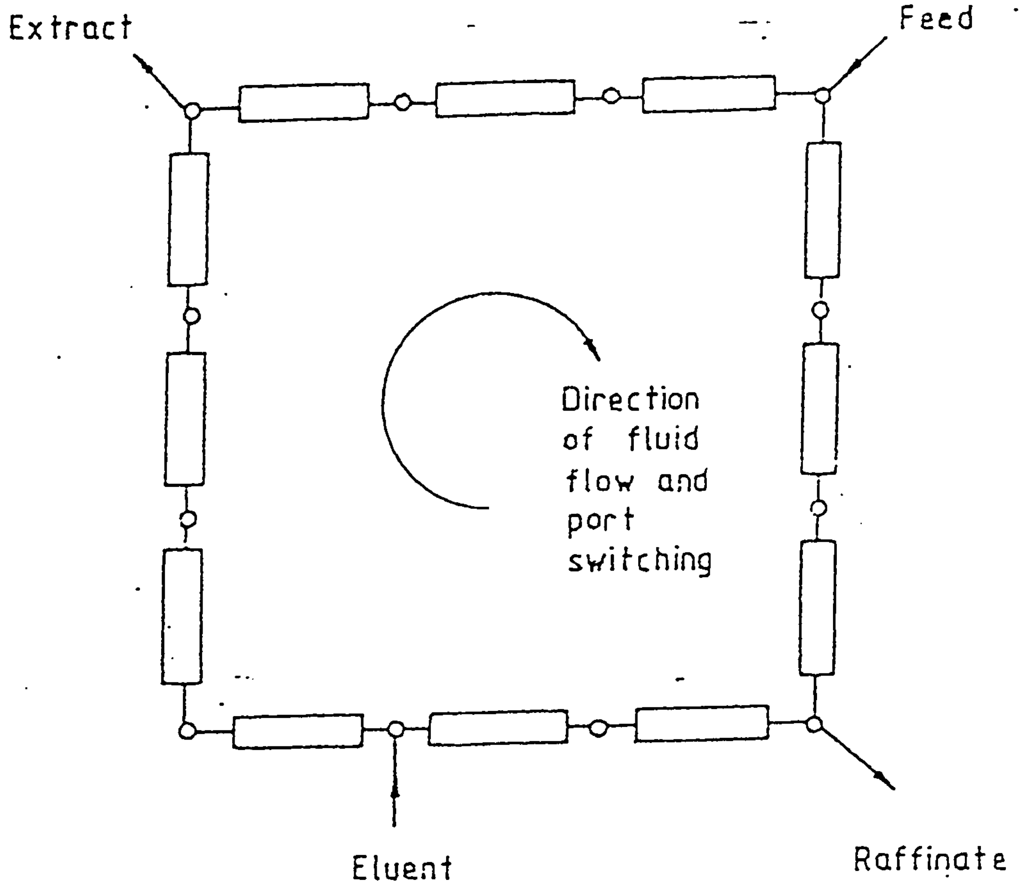

Figure 5.1 Schematic diagram of the physical arrangement of columns and valves for detailed model.

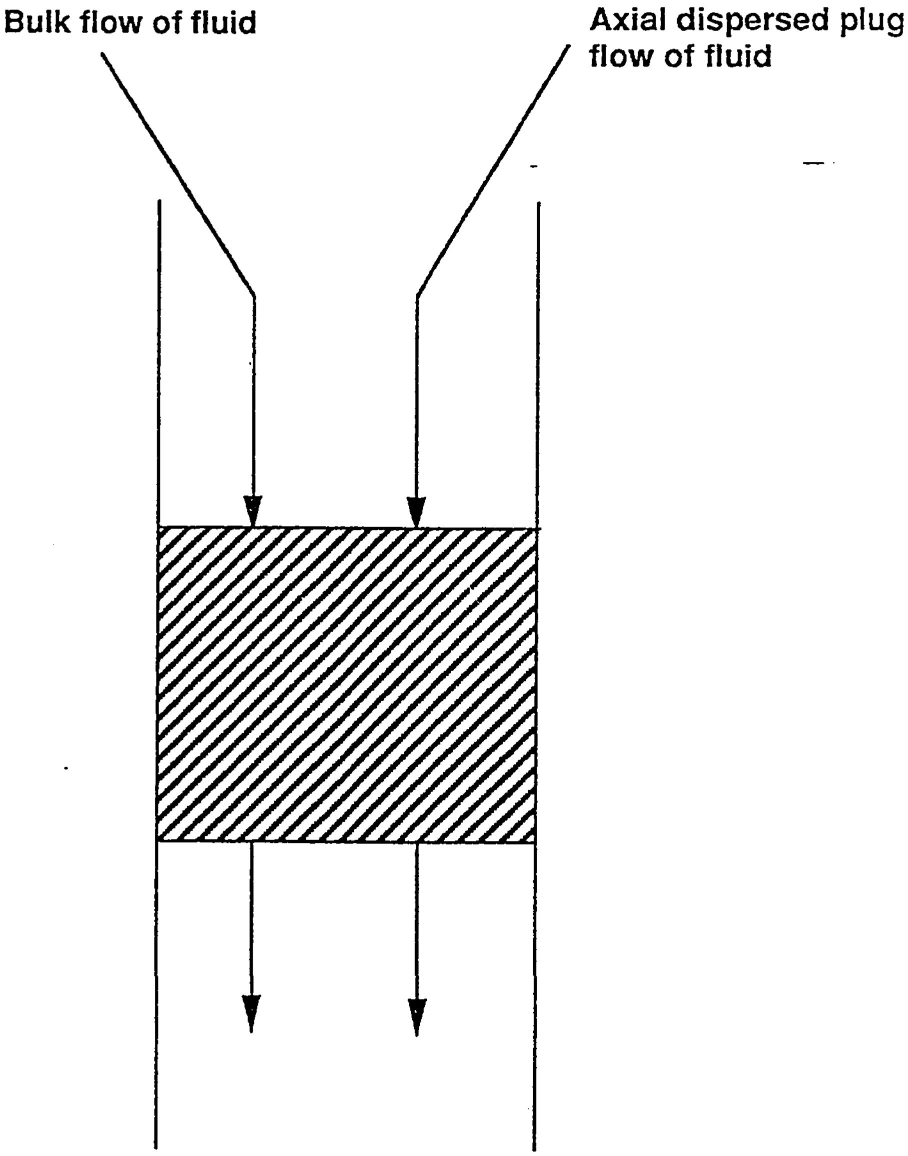

Figure 5.2 Schematic diagram of the mass balance of jth bed for detailed model.

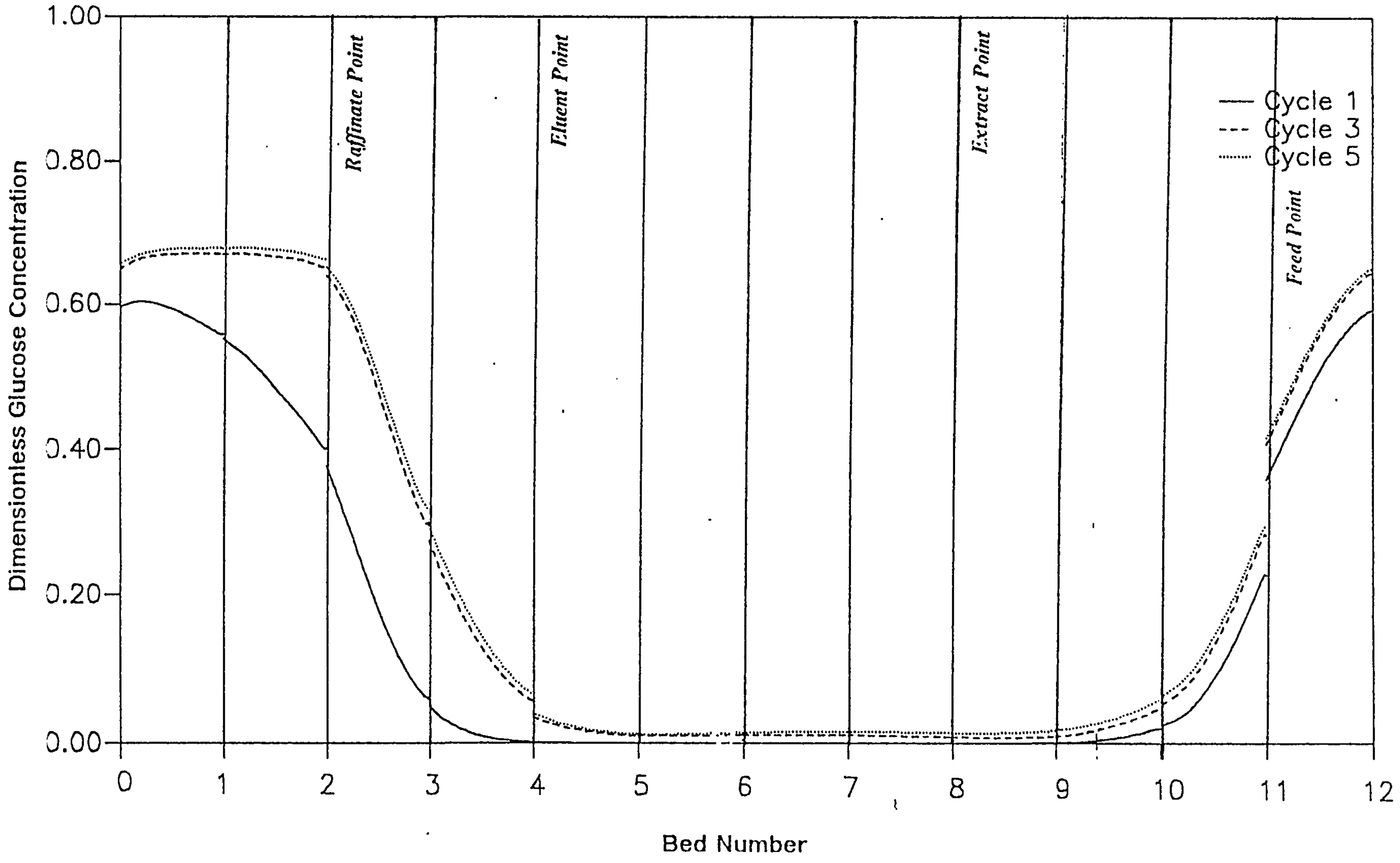

Figure 5.3 Change in concentration profile of glucose with cycle number.

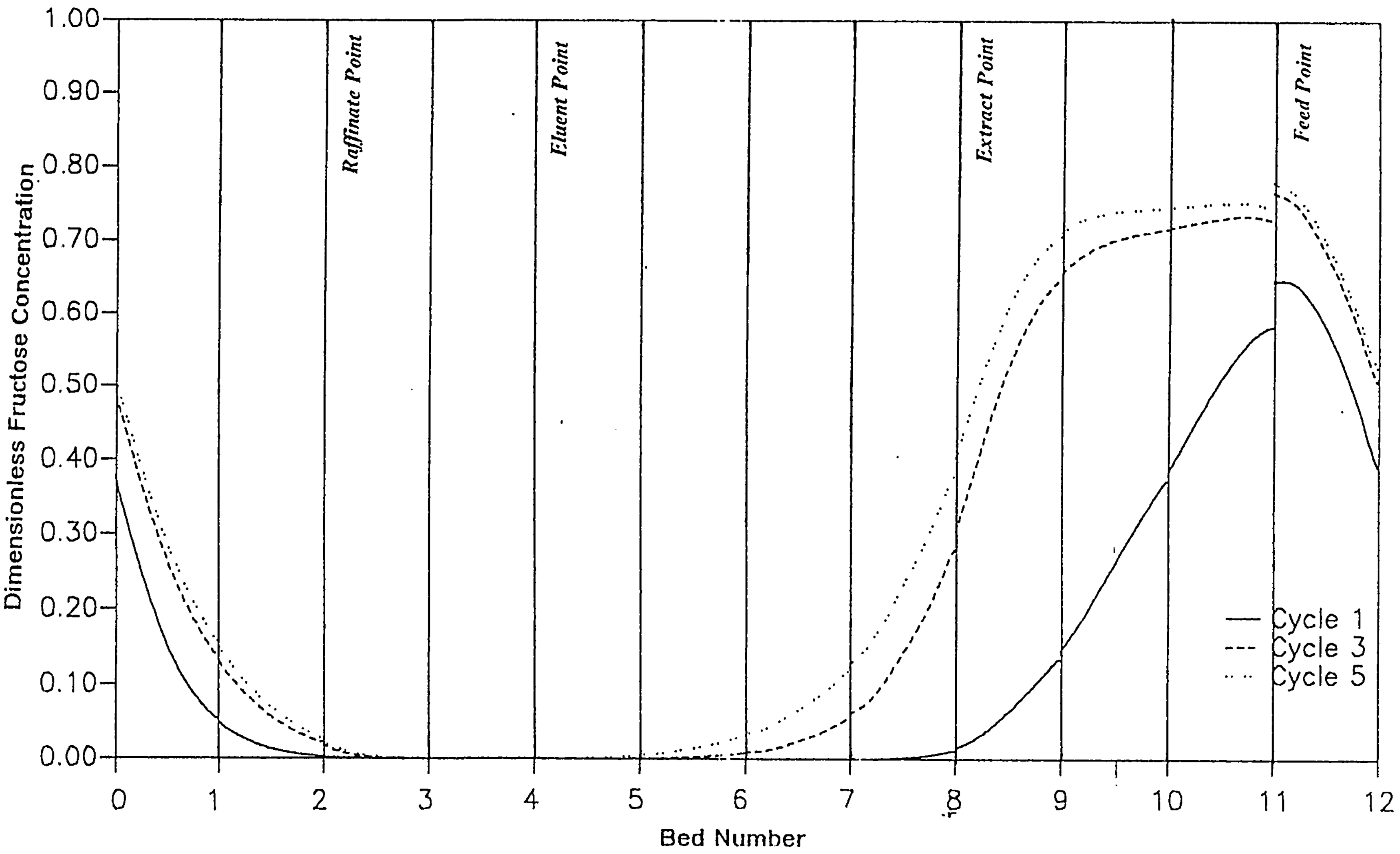

Figure 5.4 Change in concentration profile of fructose with cycle number.

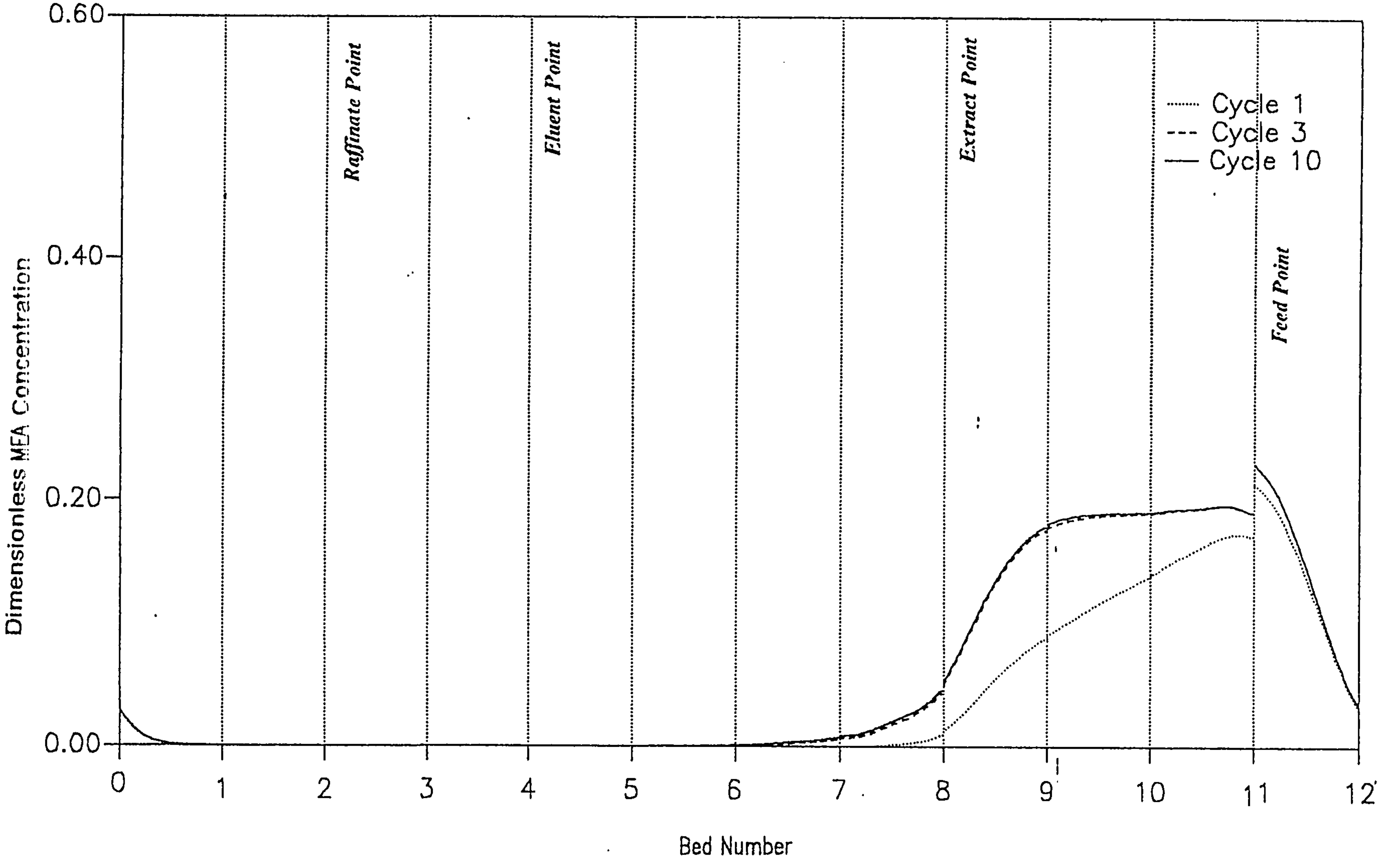

Figure 5.5 Change in concentration profile of MEA with cycle number.

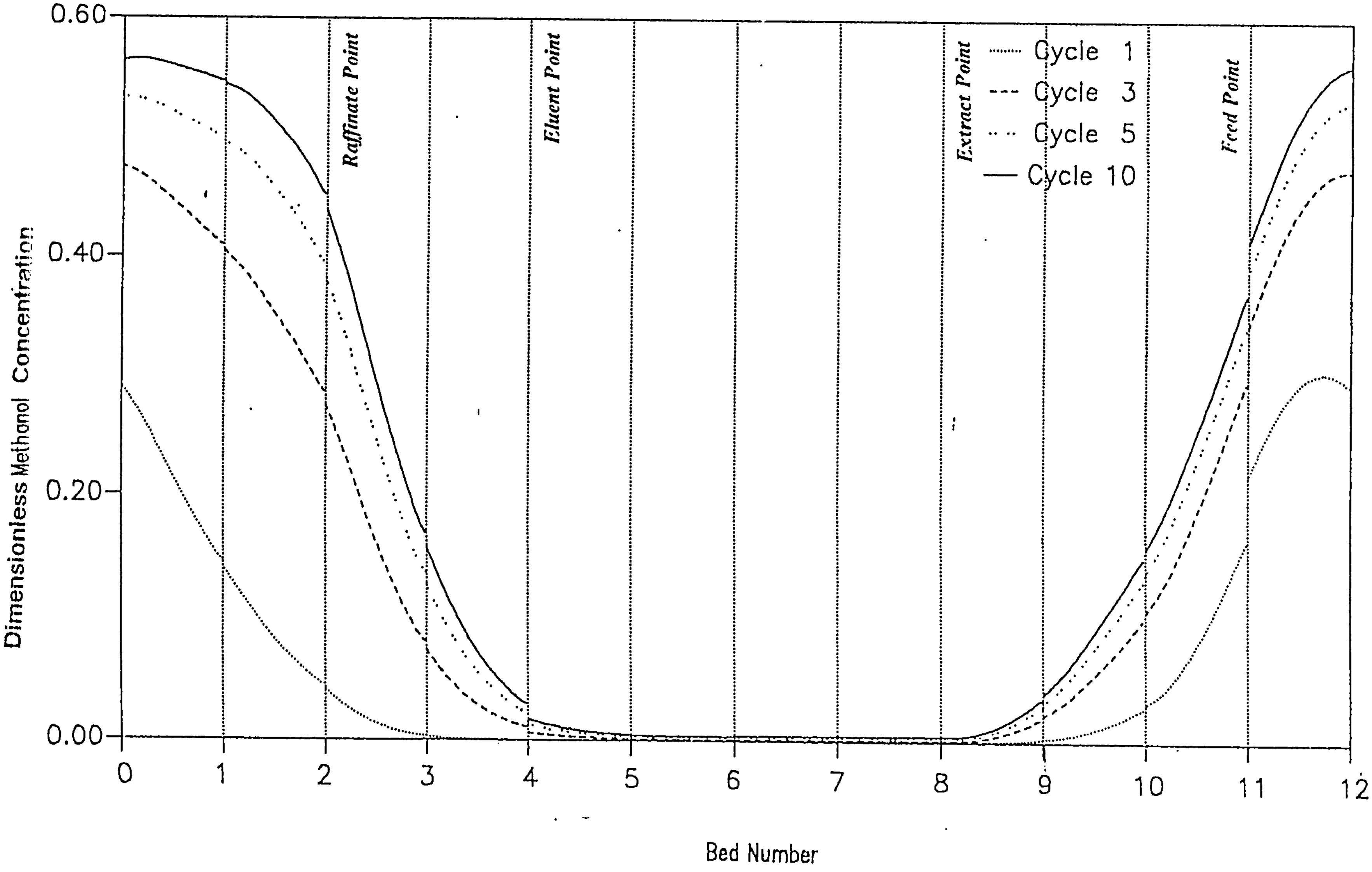

Figure 5.6 Change in concentration profile of MOH with cycle number.

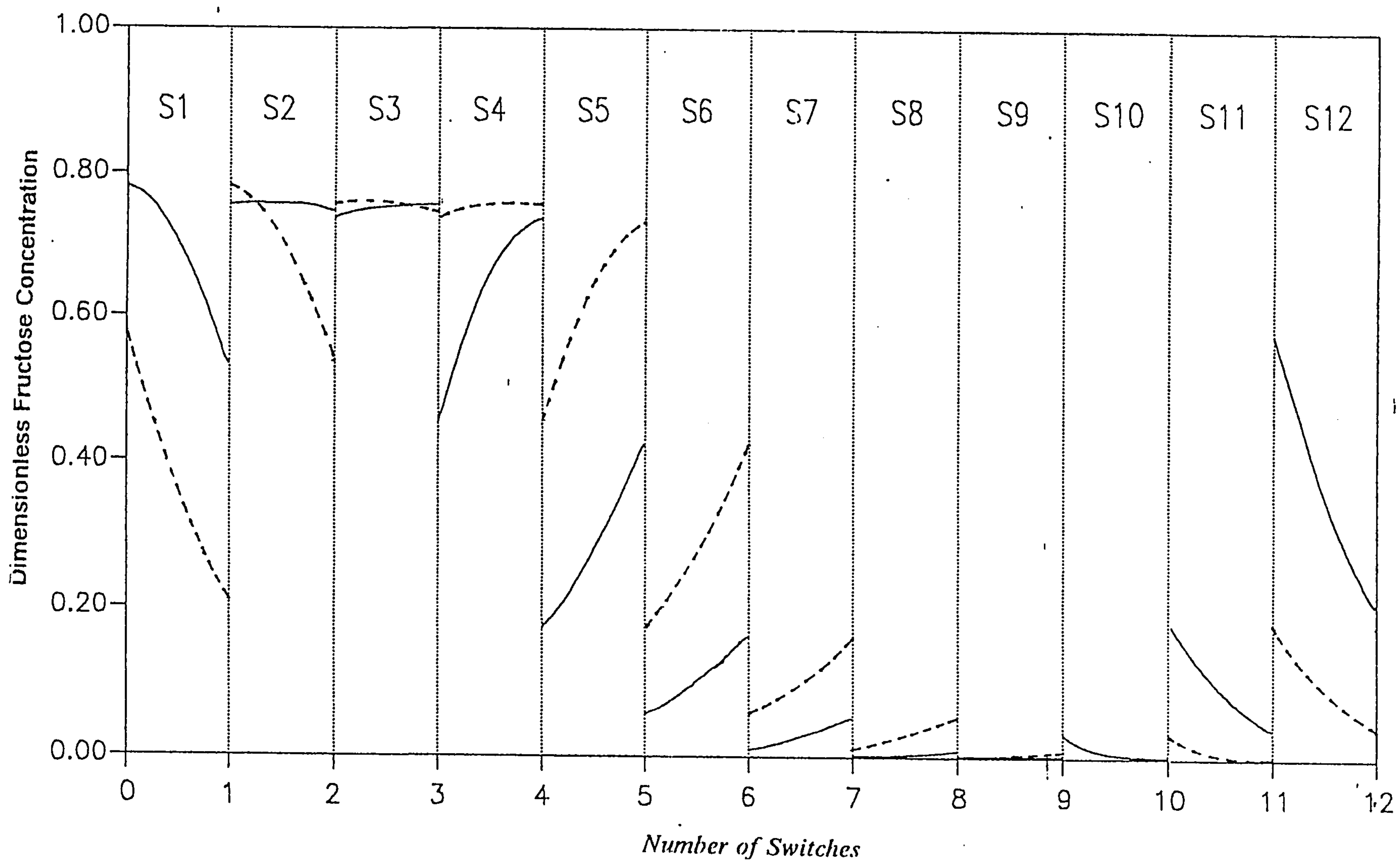

Figure 5.7 Concentration profile of fructose in bed #1 at steady state for 12 consecutive switches (- - - - at the start of switch, ——— at the end of switch).

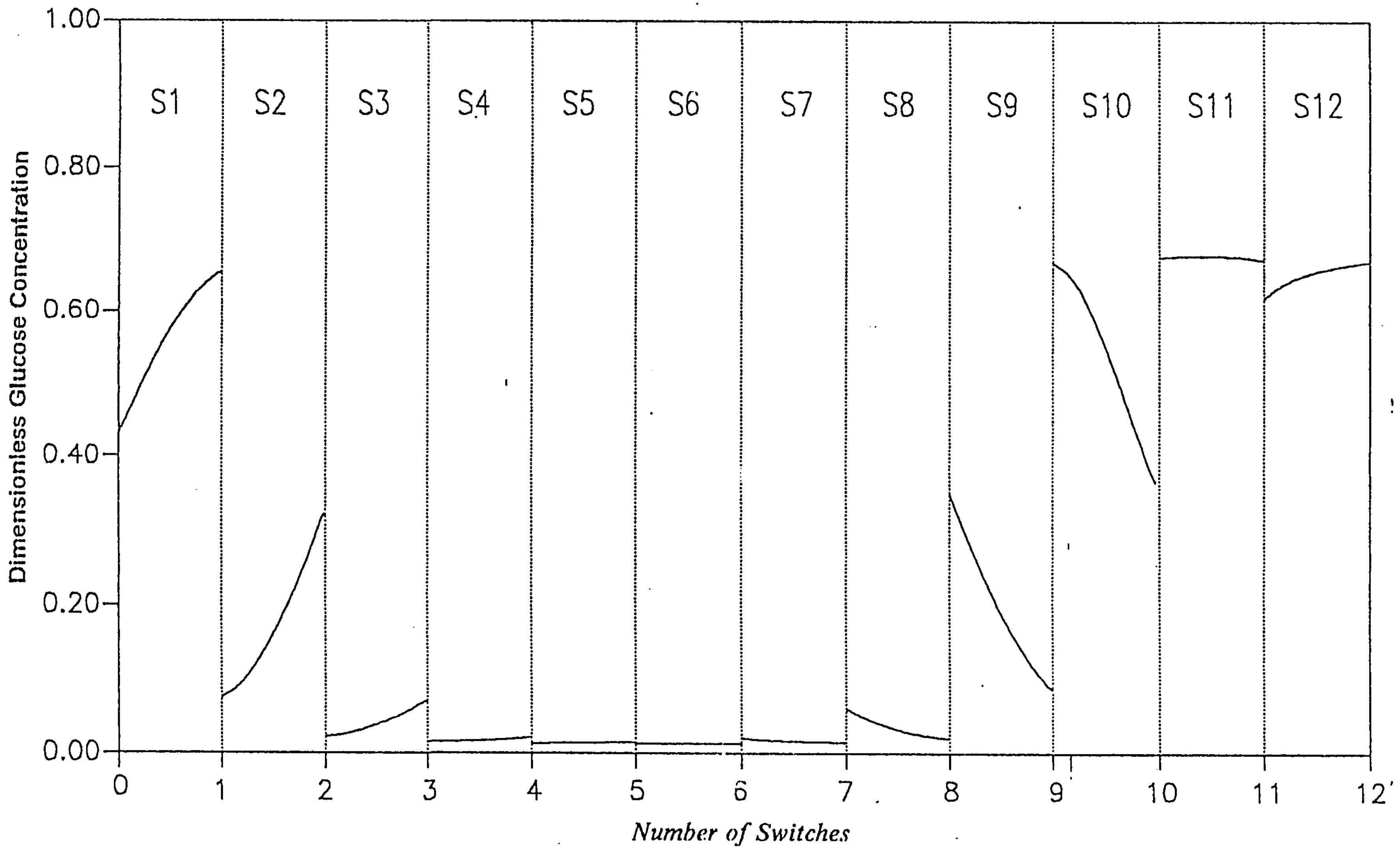

Figure 5.8 Concentration profile of glucose in bed #1 at steady state for 12 consecutive switches.

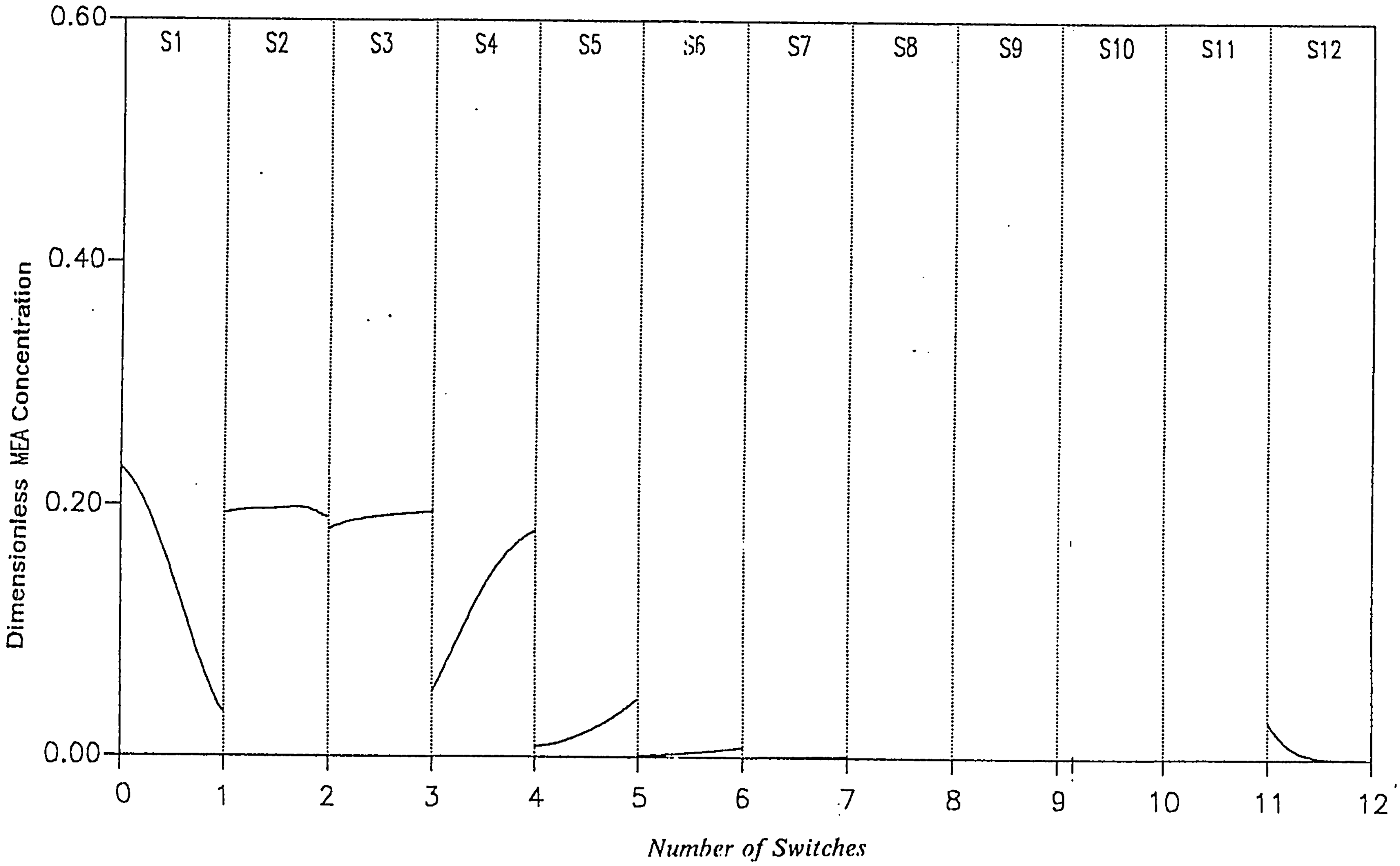

Figure 5.9 Concentration profile of MEA in bed #1 at steady state for 12 consecutive switches.

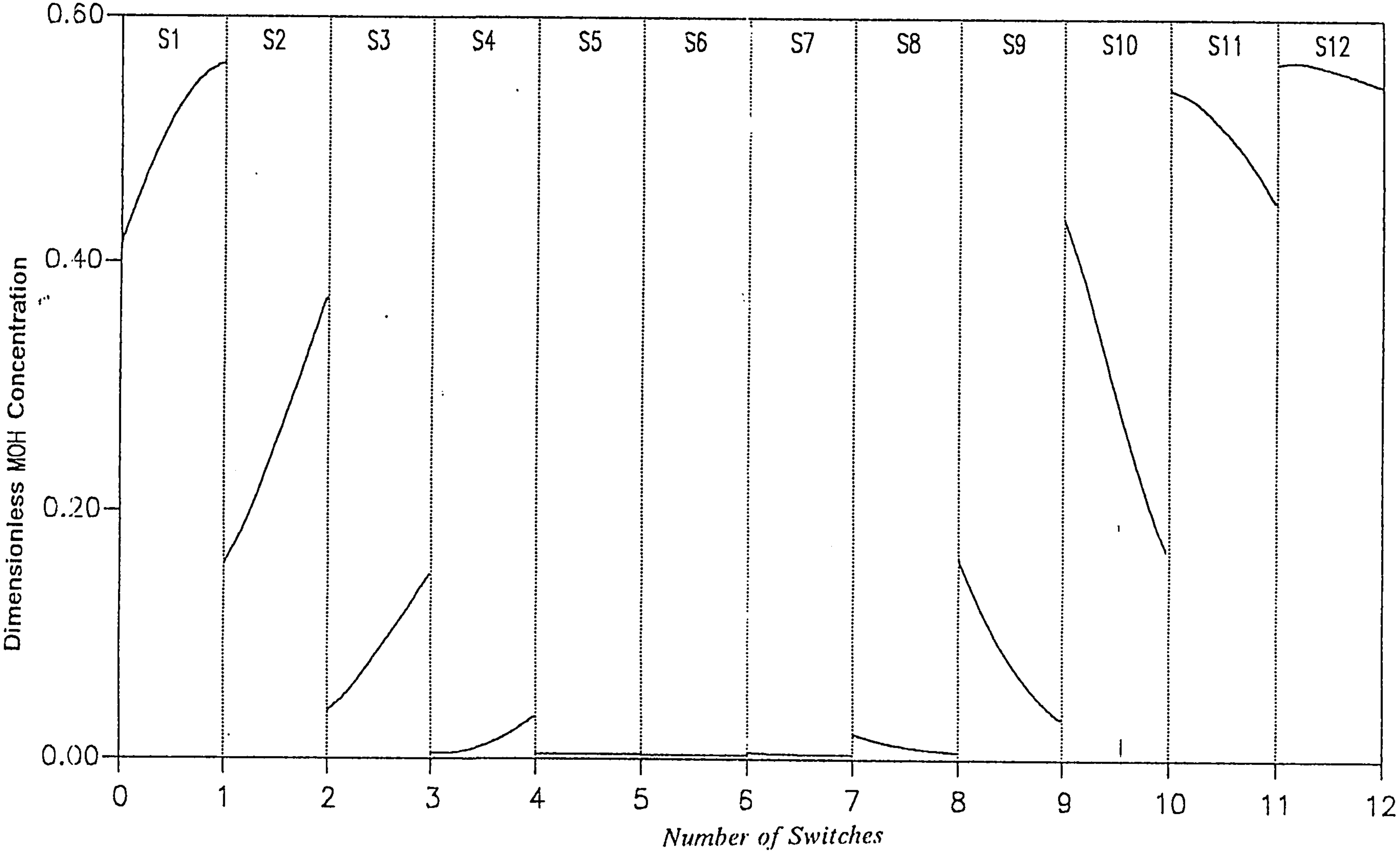

Figure 5.10 Concentration profile of MOH in bed #1 at steady state for 12 consecutive switches.

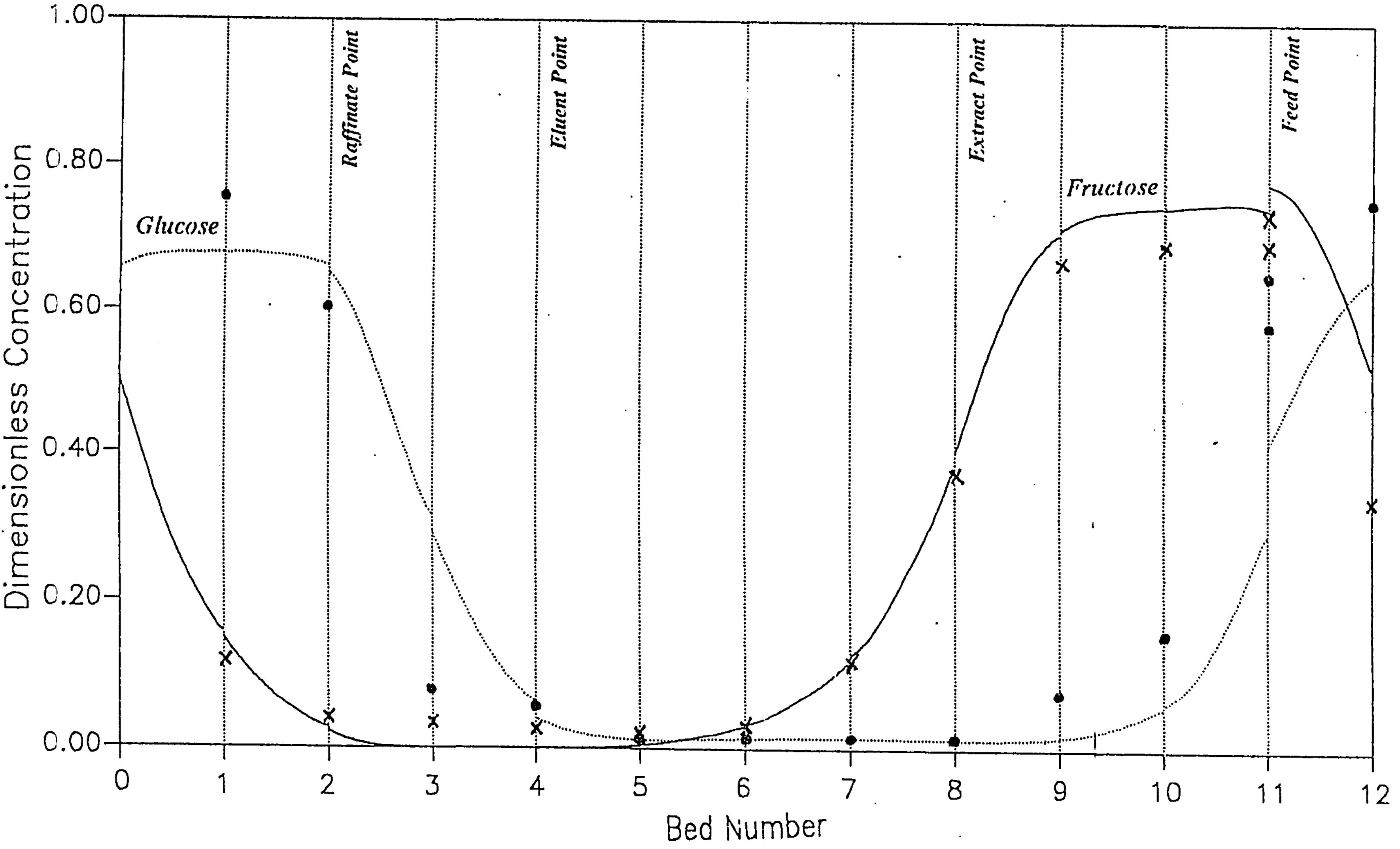

Figure 5.11 Comparison between experimental and theoretical data at steady state for glucose-fructose system. (Experimental;(Glucose •,Fructose ×).

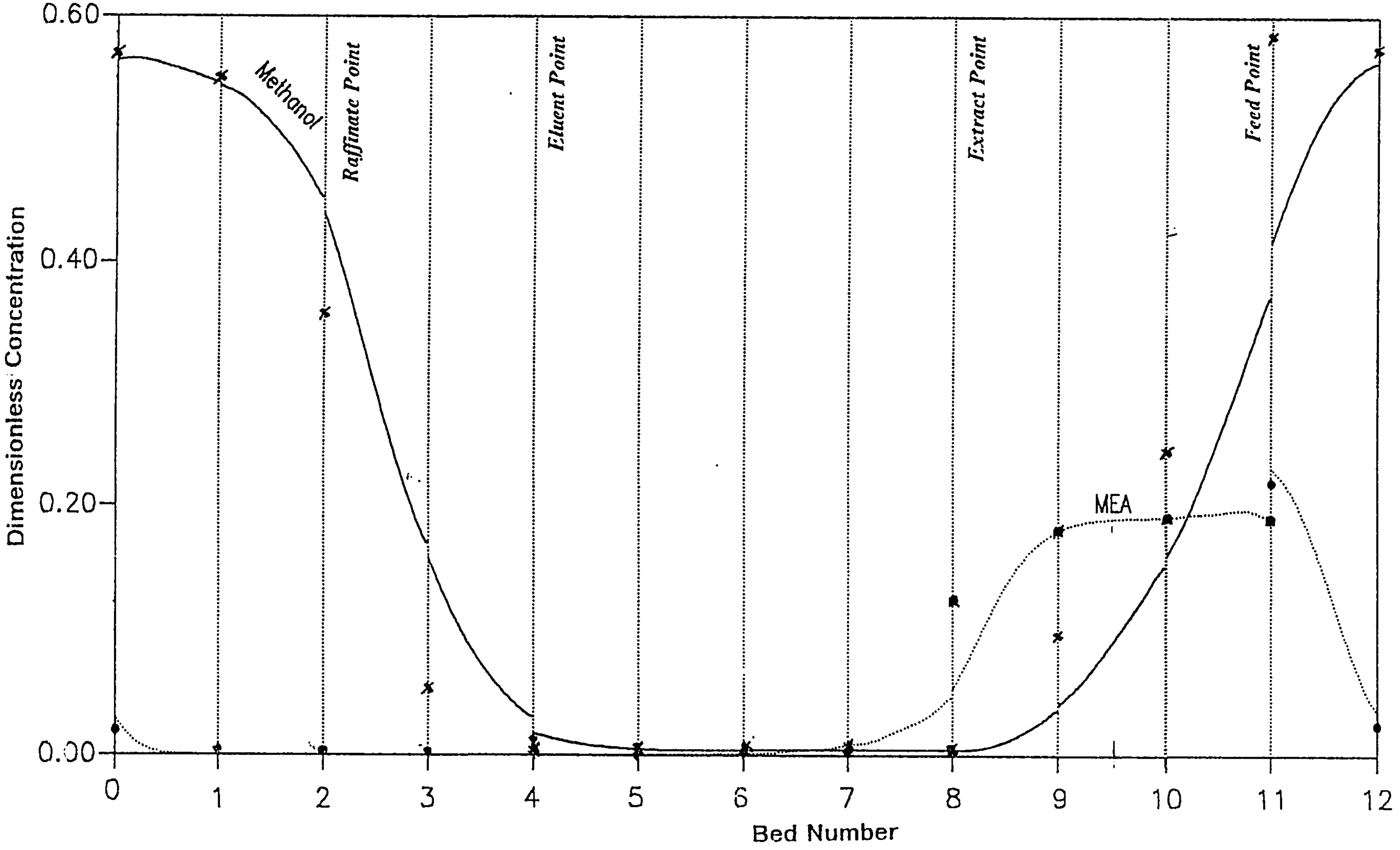

Figure 5.12 Comparison between experimental and theoretical data at steady state for MEA-MOH system. (Experimental;MEA×,MOH•).

Table 5.1 Parameter values for the Glucose-Fructose and MEA-MOH system

Parameter	Linear case of Hidajat et al.[14]	Nonlinear case of Ching et al. [10]
Feed composition (%A,%B)	5,5	20,10
Switch Time,min	30.5	22.1
Feed flowrate,ml/min	9.0	5.0
Desorbent rate,ml/min	65.0	130.4
Raffinate rate,ml/min	13.8	13.7
Extract rate,ml/min	16.8	44.0
Bed length,cm	100	100
Configuration	4,3,3,2	4,3,3,2
Column diameter,cm	5.1	5.5
$\lambda(A,B)$	0.0, 0.0	0.435,0.0
K_A	0.88	1.24
K_B	0.50	0.63

A = Fructose/MEA
B = Glucose/MOH

Table 5.2 Comparison of dimensionless product concentrations at steady state

Variable Effect	Variable Parameter	Raffinate		Extract	
		A	B	A	B
Effect of Axial Dispersion	$Pe \to 0$	0.05	0.2	0.08	0.04
	$Pe = 25$	0.00(0.0)	0.45(0.36)	0.045(0.10)	0.004(0.002)
	$Pe \to \infty$	0.0	0.57	0.0	0.0
Effect of Eluent to Feed ratio(Feed const)	13.0	0.0	0.021	0.10	0.02
	26.0	0.0	0.45	0.045	0.004
	52.0	0.385	0.21	0.004	0.044
Effect of Eluent to Feed ratio(Eluent const)	13.0	0.50	0.70	0.06	0.03
	26.0	0.00	0.45	0.045	0.004
	52.0	0.0	0.24	0.027	0.001
Effect of Bed Length	$L = 50$	0.18	0.156	0.055	0.066
	$L = 100$	0.00	0.45	0.045	0.004
	$L = 200$	0.05	0.035	0.084	0.093
Effect of Switch Time	$\tau = 15.0$	0.038	0.00	0.10	0.07
	$\tau = 22.1$	0.00	0.45	0.045	0.004
	$\tau = 30.0$	0.33	0.2	0.0076	0.536

Base case is $Pe = 25$, Eluent to feed ratio = 26, Bed length = 100 cm and Switch time = 22.1 minutes

Numbers in parenthesis represents the corresponding concentration of MEA and MOH from equivalent continuous countercurrent model [14].

A = Monoethanolamine (MEA), B = Methanol (MOH)

REFERENCES

(1) Ching, C. B., Hidajat, K., Ho, C., and Ruthven, D. M., Chem. Eng. Sci., 42, 2547-2555 (1987).

(2) Ching, C. B., Hidajat, K., Ho, C., and Ruthven, D. M., Reactive Polym., 6, 15-20 (1987).

(3) Ching, C. B., Hidajat, K., Ho, C., and Ruthven, D. M., AICHE, 32,1876-1880 (1986).

(4) Ching, C. B., and Ruthven, D. M., Can. J. Chem. Eng., 62,398-403 (1984).

(5) Ching, C. B., and Ruthven, D. M., AICHE Symp. Ser., 81 (242), 1-8 (1985).

(6) Ching, C. B., and Ruthven, D. M., Chem. Eng. Sci., 41 3063-3071 (1986).

(7) Ching, C. B., and Ruthven, D. M., Chem. Eng. Sci., 40 (6) 877-885 (1985).

(8) Ching, C. B., and Ruthven, D. M., Chem. Eng. Sci., 40 (6) 887-891

(1985).

(9) Ching, C. B., Ruthven, D. M., and Hidajat, R., Chem. Eng. Sci., 40, 1411-1417 (1985).

(10) Ching, C. B., Ho, C., and Ruthven, D. M., Chem. Eng. Sci., 43, 703-711 (1988).

(11) Finlayson, B. A., Non linear Analysis in Chemical Eng., McGraw Hill, (1980).

(12) Hassan, M.M., Rahman, A.K.M.S., and Loughlin, K.F., Separation and Purification Methods, (submitted)

(13) Hidajat, K., Ching, C.B., and Ruthven, D.M., Chem. Eng. J., 33, B55-B61 (1986)

(14) Rahman, A.K.M.S., Hassan, M.M., and Loughlin, K.F., Separation and Purification Methods, (submitted)

(15) de Rosset, A. J., Neuzil, R. W., and Broughton, D.B., Percolation Processes: Theory and Applications, NATO ASI No. 3, 249 (1981).

(16) Ruthven, D. M., and Ching, C. B., Chem. Eng. Sci., 44(5), 1011-1038 (1989).

CHAPTER 6

CONCLUSIONS AND RECOMMENDATIONS

6.1 CONCLUSIONS

6.1.1 Equivalent Countercurrent Model

1) System performance is very sensitive to the nonlinear parameter λ. While operating conditions with $\lambda = 0.0$ may give good separations, the same system may show poorer performance at higher λ and vice versa.

2) The flow ratio γ, is important to find out physically the direction of components in each section, however, γ alone cannot predict good separation.

3) Good separation can be determined by the relative slope of the operating and equilibrium lines in both pre feed and post feed sections which is very straightforward with linear isotherms.

4) In case of uncoupled nonlinear isotherms, good separation can also be predicted from a similar approach with little difficulties but in case of coupled nonlinear isotherms, it is proven very complicated to develop any such criterion because of the complex nature of the equilibrium isotherms.

5) The results of both two-section and four-section equivalent models are compared with corresponding experimental data for limiting cases of linear isotherm (glucose-fructose) and uncoupled nonlinear isotherm (MEA-MOH) at steady state and found to agree well. In case of linear glucose-fructose system, results of unsteady solution match very well with that of the experimental data.

6) The present model therefore, can be used to predict the performance of countercurrent adsorption systems for any type of equilibrium isotherm for both steady and unsteady state.

6) In case of nonlinear system, the effect of coupling between the isotherms is very pronounced and reduces the yield. Also, this coupling makes the numerical prediction and calculations very complex.

6.1.2 Detailed Countercurrent Model

1) This model gives better insight into each adsorption column, which is very helpful in investigating column dynamics.

2) This model is based on less idealization and therefore represent the actual system quite well.

3) The numerical simulation of the detailed model is much more stable and faster than the equivalent model. To get results free of numerical oscillation,

only 5-point collocation scheme is needed whereas for same level of accuracy in equivalent model, 14-point collocation scheme is required.

4) Because of the lower number of collocation points, the detailed model needs only about 50 mins. of CPU time to solve 10 complete cycles for the uncoupled nonlinear case whose parameters are given in Table 5.1. However to solve the four-section model for the same system with same parameter values requires about 200 mins. of CPU time.

6.2 RECOMMENDATIONS FOR FURTHER STUDY

On the basis of results obtained from the present study, the following recommendations can be made for future work:

(1) In the present study, the equilibrium constants are considered to be independent of temperature. But in some cases, due to high concentrations, the heat effects may become quite significant and therefore the assumption of isothermal column condition may not be appropriate. It is therefore recommended that the model be extended to the nonisothermal case.

(2) A linear driving force rate expression was used for solid phase mass transfer in simulating both equivalent countercurrent models and detailed model. However, in order to check the validity of this assumption, it would be desirable to compare directly the results of the present models with that from

the same models extended to include diffusional rate expression for the mass transfer equation.

(3) Since the theoretical models developed provide a good representation of the experimental results and since the model is very general, an optimization program may be included in order to arrive at an optimal combination of operating variables for any countercurrent adsorption system.

(4) As continuous countercurrent adsorption systems are very complicated both in design and operation, the model should be extended to include the process control aspects of these systems.

NOMENCLATURE

b	Langmuir equilibrium constant
c_f	sorbate concentration in feed stream
c_i	sorbate concentration in fluid phase of component i
c_{ij}	sorbate concentration in fluid phase for component i in bed j
C'_{ij}	dimensionless sorbate concentration in fluid phase for component i in bed j
Cf'_{ij},	inlet concentration of fluid phase for component i at bed j
c_o	initial ($t < 0$) steady state values of c
$D_L(D_{L_j})$	axial dispersion coefficient (for flow in bed j)
F_j	dimensionless factor, $(V_jL_4)/(V_4L_j)$
$K(K_A,K_B)$	adsorption equilibrium constant (for A, B)
k	overall effective mass transfer coefficient
L	length of adsorption bed.
L_f	length of adsorption bed following the feed point
L_s	length of adsorption section
q_f	average solid phase concentration which is in equilibrium with fluid phase concentration of feed stream
q_{ij}	average solid phase concentration (of component i in bed j)
Q'_{ij}	dimensionless solid phase concentration of component i at bed j

q_s	saturated solid phase concentration
q^*	equilibrium solid phase concentration
t	time
u	linear velocity of solid
V_j	velocity of fluid at section/bed j
V_f	velocity of fluid at the bed following the feed point
V_e	velocity of fluid at the bed following the eluent point
X_i	mole fraction of component i
z	axial distance coordinate
Z_j	dimensionless distance $\frac{z_j}{L_{s_1}}$ (3), $\frac{z_j}{L_{s_4}}$ (4), $\frac{z_j}{L_1}$ (5)

GREEK LETTERS

Ψ'	ratio of packed to void ratio, $(1-\varepsilon)/\varepsilon$
Φ	non-linear factor, $1-\sum_{i=1}^{N}\lambda_i$
α_j	dimensionless mass transfer parameter $k\frac{L_j}{V_4}$
α_{AB}	separation factor
γ_j	ratio of downflow to upflow rates $=(1-\varepsilon)Ku/\varepsilon V_j$
ε	bed porosity
λ	nonlinearity parameter, $\frac{q_0}{q_s}$
τ	switch time

DIMENSIONLESS GROUP

Pe_j	axial Peclet number for bed/section j V_jL_j/D_j

APPENDIX A

DERIVATION OF THE COLLOCATION EQUATIONS

The partial differential equation in chapters 3, 4 and 5 is repeated here for convenience -

$$\frac{\partial C'_{A,1}}{\partial \tau} = F_1\left[\frac{1}{Pe_1}\frac{\partial^2 C'_{A,1}}{\partial Z^2_1} - \frac{\partial C'_{A,1}}{\partial Z_1} + \gamma_1 \Phi \frac{\partial Q'_{A,1}}{\partial Z_1}\right.$$

$$\left. - \Psi K \Phi \alpha_1 \left\{\frac{C'_{A,1}}{1 + \lambda_A(C'_{A,1} - 1) + \lambda_B(C'_{B,1} - 1)} - Q'_{A,1}\right\}\right] \qquad (A1)$$

at $Z_1 = 0$

$$C'_{A,1} = CHZ + \frac{1}{Pe_1}\frac{dC'_{A,1}}{dZ_1} \qquad (A2)$$

at $Z_1 = 1$

$$\frac{dC'_{A,1}}{dZ_1} = 0 \qquad (A3)$$

and can be reduced to sets of ordinary differential equations by the method of orthogonal collocation.

Equation (A1) becomes

$$\frac{dC'_{A,1,j}}{d\tau} = F_1[\frac{1}{Pe_1}\sum_{i=1}^{M2} B_{j,i}C'_{A,1,i} - \sum_{i=1}^{M2} A_{j,i}C'_{A,1,i} + \gamma_1\Phi\sum_{i=1}^{M2} A_{j,i}Q'_{A,1,i}$$

$$- \Psi K\Phi\alpha_1\{\frac{C'_{A,1,j}}{1 + \lambda_A(C'_{A,1,j} - 1) + \lambda_B(C'_{B,1,j} - 1)} - Q'_{A,1,j}\}]$$

(A4)

$$= F_1[\frac{1}{Pe_1}B_{j,1}C'_{A,1,1} + \frac{1}{Pe_1}\sum_{i=2}^{M1} B_{j,i}C'_{A,1,i} + \frac{1}{Pe_1}B_{j,M2}C'_{A,1,M2}$$

$$- A_{j,1}C'_{A,1,1} - \sum_{i=2}^{M1} A_{j,i}C'_{A,1,i} - A_{j,M2}C'_{A,1,M2}$$

$$+ \gamma_1\Phi(A_{j,1}Q'_{A,1,1} + \sum_{i=2}^{M1} A_{j,i}Q'_{A,1,i} + A_{j,M2}Q'_{A,1,M2})$$

$$- \Psi K\Phi\alpha_1\{\frac{C'_{A,1,j}}{1 + \lambda_A(C'_{A,1,j} - 1) + \lambda_B(C'_{B,1,j} - 1)} - Q'_{A,1,j}\}]$$

(A5)

$$\frac{dC'_{A,1,j}}{d\tau} = F_1[(\frac{1}{Pe_1}B_{j,1} - A_{j,1})C'_{A,1,1} + \gamma_1 A_{j,1}Q'_{A,1,1} + (\frac{1}{Pe_1}B_{j,M2} - A_{j,M2})C'_{A,1,M2}$$

$$+ \gamma_1 \Phi A_{j,M2}Q'_{A,1,M2} + \sum_{i=2}^{M1}(\frac{1}{Pe_1}B_{j,i} - A_{j,i})C'_{A,1,i} + \gamma_1 \Phi \sum_{i=2}^{M1} A_{j,i}Q'_{A,1,i}$$

$$- \Psi' K \Phi \alpha_1 \{\frac{C'_{A,1,j}}{1 + \lambda_A(C'_{A,1,j} - 1) + \lambda_B(C'_{B,1,j} - 1)} - Q'_{A,1,j}\}] \tag{A6}$$

where,

M2 = M + 2,

M1 = M + 1,

M = number of internal collocation points

and j = time interval

Equations (A2) and (A3) are written as

$$(C'_{A,1,1} - CHZ) = \frac{1}{Pe_1}A_{1,1}C'_{A,1,1} = \frac{1}{Pe_1}A_{1,M2}C'_{A,1,M2} + \frac{1}{Pe_1}\sum_{i=2}^{M1}A_{1,i}C'_{A,1,i} \tag{A7}$$

and

$$A_{M2,1}C'_{A,1,1} + \sum_{i=2}^{M1} A_{M2,i}C'_{A,1,i} + A_{M2,M2}C'_{A,1,M2} = 0 \qquad \text{(A8)}$$

From equations (A7) and (A8), $C'_{A,1,1}$ and $C'_{A,1,M2}$ can be expressed in terms of internal collocation points,

$$C'_{A,1,1} = \frac{A_{1,M2}Pe_1CHZ}{(A_{1,1} - Pe_1)\{A_{1,M2} - A_{M2,M2}(\frac{A_{1,1} - Pe_1}{A_{M2,1}})\}} - \frac{\sum_{i=2}^{M1} A_{1,i}C'_{A,1,i}}{A_{1,1} - Pe_1}$$

$$- \frac{A_{1,M2}\sum_{i=2}^{M1}\{A_{M2,i}(\frac{A_{1,1} - Pe_1}{A_{M2,1}}) - A_{1,i}\}C'_{A,1,i}}{(A_{1,1} - Pe_1)\{A_{1,M2} - A_{M2,M2}(\frac{A_{1,1} - Pe_1}{A_{M2,1}})\}} - \frac{Pe_1CHZ}{A_{1,1} - Pe_1}$$

(A9)

$$C'_{A,1,M2} = \frac{\sum_{i=2}^{M1}\{A_{M2,i}(\frac{A_{1,1} - Pe_1}{A_{M2,1}}) - A_{1,i}\}C'_{A,1,i} - Pe_1CHZ}{A_{1,M2} - A_{M2,M2}(\frac{A_{1,1} - Pe_1}{A_{M2,1}})} \qquad \text{(A10)}$$

Solid phase boundary conditions :

$at\ Z_1 = 0, \qquad Q'_{A,1,1} = 1$ (A11)

$at\ Z_1 = 1, \qquad Q'_{A,1,M2} = 0$ (A12)

From equations (A6), (A10), (A11) and (A12)

$$\frac{dC'_{A,1,j}}{d\tau} = F_1[(\frac{1}{Pe_1}B_{j,1} - A_{j,1})C'_{A,1,1} + \gamma_1\Phi A_{j,1} + (\frac{1}{Pe_1}B_{j,M2} - A_{j,M2})C'_{A,1,M2}$$

$$+ \sum_{i=2}^{M1}(\frac{1}{Pe_1}B_{j,i} - A_{j,i})C'_{A,1,i} + \gamma_1\Phi\sum_{i=2}^{M1}A_{j,i}Q'_{A,1,i}$$

$$- \Psi K\Phi\alpha_1\{\frac{C'_{A,1,j}}{1 + \lambda_A(C'_{A,1,j} - 1) + \lambda_B(C'_{B,1,j} - 1)} - Q'_{A,1,j}\}] \tag{A13}$$

After substituting $C'_{A,1,1}$, $C'_{A,1,M2}$, in equation (A13)

$$\frac{dC'_{A,1,j}}{d\tau} = F_1[- \frac{(\frac{1}{Pe_1}B_{j,1} - A_{j,1})}{A_{1,1} - Pe_1}\sum_{i=2}^{M1}A_{1,i}C'_{A,1,i} - \frac{A_{1,M2}(\frac{1}{Pe_1}B_{j,1} - A_{j,1})}{A_{1,1} - Pe_1}$$

$$\{\frac{A_{M2,i}(\frac{A_{1,1} - Pe_1}{A_{M2,1}}) - A_{1,i}}{A_{1,M2} - A_{M2,M2}(\frac{A_{1,1} - Pe_1}{A_{M2,1}})}\}C'_{A,1,i} + \frac{Pe_1 CHZ}{A_{1,1} - Pe_1}(\frac{1}{Pe_1}B_{j,1} - A_{j,1})$$

$$\{\frac{A_{1,M2}}{A_{1,M2} - A_{M2,M2}(\frac{A_{1,1} - Pe_1}{A_{M2,1}})} - 1\} + \sum_{i=2}^{M1}(\frac{1}{Pe_1}B_{j,i} - A_{j,i})C'_{A,1,i}$$

$$+ \left(\frac{1}{Pe_1} B_{j,M2} - A_{j,M2}\right) \frac{\sum_{i=2}^{M1} \left(A_{M2,i}\left(\frac{A_{1,1} - Pe_1}{A_{M2,1}}\right) - A_{1,i}\right) C'_{A,1,i}}{A_{1,M2} - A_{M2,M2}\left(\frac{A_{1,1} - Pe_1}{A_{M2,1}}\right)} \frac{Pe_1 CHZ\left(\frac{1}{Pe_1} B_{j,M2} - A_{j,M2}\right)}{A_{1,M2} - A_{M2,M2}\left(\frac{A_{1,1} - Pe_1}{A_{M2,1}}\right)}$$

$$+ \gamma_1 \Phi\left(A_{j,1} + \sum_{i=2}^{M1} A_{j,i} Q'_{A,1,i}\right) - \Psi K \Phi \alpha_1 \left\{ \frac{C'_{A,1,j}}{1 + \lambda_A (C'_{A,1,j} - 1) + \lambda_B (C'_{B,1,j} - 1)} - Q'_{A,1,j} \right\} \Big]$$

(A14)

Equation (A14) can be rearranged as

$$\frac{dC'_{A,1,j}}{d\tau} = F_1 \Big[\Big[\sum_{i=2}^{M1} \left(\frac{1}{Pe_1} B_{j,i} - A_{j,i}\right) - \left\{ \left(\frac{1}{Pe_1} B_{j,i} - A_{j,i}\right) \frac{A_{M2,i} \frac{A_{1,1} - Pe_1}{A_{1,M2}} A_{1,M2}}{(A_{1,1} - Pe_1)\left(A_{1,M2} - A_{M2,M2} \frac{A_{1,1} - Pe_1}{A_{M2,1}}\right)} \right\}$$

$$+ \left\{ \left(\frac{1}{Pe_1} B_{j,i} - A_{j,i}\right) \frac{A_{1,M2} A_{1,i}}{(A_{1,1} - Pe_1)\left(A_{1,M2} - A_{M2,M2} \frac{A_{1,1} - Pe_1}{A_{M2,1}}\right)} \right\}$$

$$+ \left\{ \left(\frac{1}{Pe_1} B_{j,M2} - A_{j,M2}\right) \frac{A_{M2,i} \frac{A_{1,1} - Pe_1}{A_{1,M2}}}{A_{1,M2} - A_{M2,M2} \frac{A_{1,1} - Pe_1}{A_{M2,1}}} \right\}$$

$$- \{(\frac{1}{Pe_1} B_{j,M2} - A_{j,M2}) \frac{\frac{A_{1,i}}{A_{1,M2}}}{(A_{1,M2} - A_{M2,M2} \frac{A_{1,1} - Pe_1}{A_{M2,1}})}\} - (\frac{1}{Pe_1} B_{j,1} - A_{j,1}) \frac{A_{1,i}}{A_{1,1} - Pe_1}] C'_{A,1,i}$$

$$- \frac{Pe_1 CHZ}{A_{1,1} - Pe_1} (\frac{1}{Pe_1} B_{j,1} - A_{j,1}) + (\frac{1}{Pe_1} B_{j,1} - A_{j,1}) \{ \frac{Pe_1 CHZ}{A_{1,1} - Pe_1} \frac{A_{1,M2}}{A_{1,M2} - A_{M2,M2} \frac{A_{1,1} - Pe_1}{A_{M2,1}}} \}$$

$$- \{(\frac{1}{Pe_1} B_{j,M2} - A_{j,M2}) \frac{Pe_1 CHZ}{A_{1,M2} - A_{M2,M2} \frac{A_{1,1} - Pe_1}{A_{M2,1}}}\} + \gamma_1 (A_{j,i} + \sum_{i=2}^{M1} A_{j,i} Q'_{A,1,i})$$

$$- \Psi K \Phi \alpha_1 \{ \frac{C'_{A,1,j}}{1 + \lambda_A (C'_{A,1,j} - 1) + \lambda_B (C'_{B,1,j} - 1)} - Q'_{A,1,j} \}] \qquad \text{(A15)}$$

Equation (A14) consists of a total of M nonlinear ordinary differential equations for single component and single section continuous countercurrent adsorption system and can be solved by Gear's or AdamMoulton's method along with Functional Iteration method.

VITA

Name	A.K.M. Shamsur Rahman
Father's Name	Abdus Sattar
Date of Birth	December 01, 1964
Place of Birth	Dhaka, Bangladesh
Permanent Address	140 Shantinagar Road Dhaka 1217, Bangladesh

Educational Background:

1980-1982	Notre Dame College (H.S.C.) Dhaka, Bangladesh
1983-1988	Bangladesh University of Engineering & Technology (B.Sc.), Dhaka, Bangladesh
1990-1992	King Fahd University of Petroleum & Minerals (M.S.), Dhaharan, Saudi Arabia

Work Experiance:

1988-1989	A.M. ComputerWays. Worked as a Programmer and participated in developing various computer softwares.